EVALUATION OF SELF-HEALING ABILITY OF CONCRETE PRODUCED WITH SUPPLEMENTARY CEMENTITIOUS MATERIALS AND SUPERABSORBENT POLYMER

セメント系混和材と高吸水性樹脂を混入したコンクリートの
自己治癒能力の評価

CHINDASIRIPHAN Pattharaphon

A THESIS SUBMITTED IN PARTIAL FULFILLMENT OF THE REQUIREMENTS FOR THE DEGREE OF DOCTOR OF PHILOSOPHY

Division of Engineering and Policy for Sustainable Environment
Graduate School of Engineering, Hokkaido University
September 2020

ABSTRACT

Concrete is the most common material for civil engineering constructions. Because of its cost-effective and excellent performance, concrete is reported to be the most general man-made construction material on earth with the annual average production amount of 2.5 tons/person. Structures made of concrete will lose their structural integrity and durability as time elapses, especially those intact with severe environments. Concrete structures are susceptible to cracking during their design service life. Cracks are developed with various reasons, such as shrinkage, hazardous chemical ingress, fatigue induced by mechanical loads, freeze and thawing cycles, and thermal effect. A crack is prominent to increase concrete permeability by generating a pathway allowing harmful chemical agents to infiltrate and exacerbate steel rebar corrosion. It has been reported that a large amount of budget is allocated annually for concrete structural maintenance. Still, periodic inspection and comprehensive maintenance are usually overlooked and insufficient especially for large scale structures requiring to the huge amount of capitals and extensive man powers to carry out. This evidence emphasizes that budgetary constraints are now a global issue, which jeopardizes their structural integrity and serviceability, including safety of the people. Self-healing concrete incorporated with cementitious materials has been developed as a sustainable innovative product. It achieves sustainable development goals by prolonging service life of structures, which allows construction sector to minimize labor resources and reduce a global carbon footprint. Self-healing concrete exhibits excellent results for crack closure, permeability reduction and recovery of mechanical properties. However, most of the self-healing applications depend upon prolonging moisture source to activate healing mechanism. This study investigates the benefits of using different types of supplementary cementitious materials (SCMs) and superabsorbent polymer (SAP) to promote concrete self-healing ability.

In the first stage, the effects of fly ash, rice husk ash (RHA) and SAP were experimentally investigated their self-healing performance using thirteen mix proportions with varying supplementary cementitious materials and SAP replacement ratio. Fly ash with high calcium oxide content was selected to control an initial swelling of SAP and to enhance rheological properties of SAP containing concrete. Two types of RHA with high amorphous silica content were selected because their possession of highly reactive pozzolanic properties. The cylindrical cement mortar specimens were prepared with a pre-crack of approximately 0.2 mm wide. The pre-cracked specimens were healed either by continuous water immersion or exposure to wet-dry conditions. Self-healing performance was evaluated through the changes in physical properties such as the progressive decrease in water discharge through the pre-crack, crack closure and the recovery of ultrasonic pulse velocity. Whereas physiochemical and microstructure development associated with self-healing activities were investigated using stereomicroscopy, scanning electron microscopy (SEM), thermogravimetric/differential thermal analysis (TG/DTA), and energy-dispersive X-ray spectroscopy (EDS). The results show that permeability recovery is significantly improved with increase in fly ash and SAP replacement ratio. At the early age, SAP containing specimens showed a significant water-flow reduction through the pre-crack, which was contributed by the sealant effect of swollen SAP. The results suggested that the coupling of fly ash and SAP in combination achieved a maximum crack closure and permeability restoration of 100% at 28 days of healing which was found to be associated with the development of self-healing materials such as pore-filling ettringite, the precipitation of calcium carbonate and C-S-H. Despite the coupling effects, rice husk ash and SAP showed slightly lower improvement in water-flow reduction, but they exhibited better results on ultrasonic pulse velocity transmitting time recovery compared to that of fly ash containing specimens, which implies that the specimens in RHA series possess higher self-healing ability in terms of compressive strength recovery and microstructure changes associated with autogenous crack repair due to the formation of denser hydrated products such as C-S-H.

The specimens showed an inconsistence trend in self-healing performance in wet-dry exposure caused by insufficient water supply. The uncertainty is mitigated through the existence of either RHAs or SAP due to their application to discharge theirs absorbed moisture and liquid providing for unhydrate-particles. Thus, self-healing activities can be continued in low relative humidity and subsequently promotes permeability reduction by the development of permanent self-healing products emerging to seal the crack. In contrast, the usage of SAP is responsible to increase in total porosity through its initial swelling. This evidence suggested that initial swelling should be minimized at a minimal extent. In contrast, RHAs showed lower disadvantage effects on pore structure distribution because mesopores at their ITZ were filled with calcium and the products of pozzolanic reaction.

In the second stage, the experimental program was designed to evaluate the risk-benefit of using fly ash and SAP as self-healing additives, though it has been proven that SAP is an ideal material to be used in self-healing concrete. Despite of its benefits, mixing of SAP in concrete might come with downside if the mix design is not well implemented. Particularly, the development of SAP pores during their initial swelling which may generate a bypass allowing harmful agents to penetrate concrete. This problem is usually found to be associated with a disability to control SAP's initial swelling. Owing to pozzolanic reaction, concrete alkalinity is reduced in present of fly ash. In this stage, the experimental program investigated the risk of carbonation of self-healed mortar specimens made with fly ash and SAP. Self-healed specimens (from stage 1) was stored in air for 2 years. Carbonation resistance was assessed using carbonation depth measured by spraying phenolphthalein. Portlandite and calcite contents were determined using thermal analysis. The results showed that the fly ash containing specimens has lower portlandite content than the non-fly ash containing series resulted by the pozzolanic reaction. Although the average surface carbonation depths show no noteworthy systematic difference between the reference and specimens solely mixed with SAP, the presence of SAP accounts for approximately 4% higher in calcite content formation which may be encountered either by the progress of chemical reaction or the accelerating effect due to the possession of a suitable relative humidity. In contrast, it is worth mentioning that the carbonation rate is not significant in terms of carbonation depth as none of specimens suffered with a severe carbonation depth confirmed by phenolphthalein spray test. In conclusion, although fly ash and SAP consume portlandite, but the carbonation depth is limited at the low penetration depth while crack closure shows a positive effect on carbonation depth mitigation.

ACKNOWLEDGEMENTS

I would like to honorably express my deepest appreciation and sincere gratitude to my supervisor Professor YOKOTA Hiroshi of the Faculty of Engineering, Hokkaido University. For his always support, his compassionate supervision and patience, motivated me to push myself in the right direction. This research will never be possible without his precious guidance and supports. I could not have imagined having a better advisor and mentor for my Ph.D. study.

My sincere gratitude is extended to all esteemed members of the doctoral evaluation committee, Prof. SENBU Osamu and Prof. MATSUMOTO Takashi for their encouragement and valuable comments which inspired me to refine and fulfill my research from many perspectives.

I would like to send my sincere gratitude to Professor KUNIEDA Minoru of Gifu University and his team for all their supports and collaborations. Their contributions enable and guide my research into the right direction. This appreciation must be extended to Mr. SUZUKI Keita of Laboratory of XPS analysis and Dr. KAWABATA Yuichiro of Port and Airport Research Institute (PARI) for their guidance during the experiment.

A portion of this work was conducted at Thin Section Laboratory, Faculty of Science of Hokkaido University and the XPS Analysis Laboratory, a joint-use facility of Hokkaido University, supported by the Material Analysis and Structure Analysis Open Unit (MASAOU).

A deepest appreciation goes to Hokkaido University for giving me an opportunity to receive a highly prestigious MEXT Scholarship without this support I would not be able to pursue my dream.

I am grateful to thank all my fellows in Lifetime Engineering Laboratory for all their help, comments, cooperation and most of all our lifetime-friendship. My appreciation is extended to my lab partner Mr. PIMPAKAN Paponpat for all his great supports, excellent encouragements and super enthusiasm without his efforts I might not be able to complete my degree.

Most of all, I would like to send my sincere gratitude to my family for being on my side and being all my inspiration for my whole life. Without their great supports, encouragements and scarifications, none of the accomplishment would come true. May my success in life have awarded them with joy and happiness.

LIST OF PUBLICATIONS

International Journals

1. P. Chindasiriphan, H. Yokota, P. Pimpakan, Effect of fly ash and superabsorbent polymer on concrete self-healing ability, Constr. Build. Mater. 233 (2020) 116975. doi:10.1016/j.conbuildmat.2019.116975.

2. P. Chindasiriphan, H. Yokota, P. Pimpakan, Application of rice husk ash and superabsorbent polymer as additive for producing sustainable self-healing concrete, (to be submitted).

International Conferences

1. P. Chindasiriphan, H. Yokota, Self-healing ability of concrete made with fly ash and superabsorbent polymer, in: 2nd ACF Symp. 2017 Innovation of Sustainable Concrete Structures, Chiang Mai, Thailand, 2017.

2. P. Chindasiriphan, H. Yokota, P. Pimpakan, Effect of fly ash and superabsorbent polymer optimization on self-healing capability of concrete, in: SynerCrete'18 International Conference on Interdisciplinary Approaches for Cement-based Materials and Structural Concrete, Funchal, Portugal, 2018: pp. 1071–1076.

3. P. Chindasiriphan, H. Yokota, P. Pimpakan, Effect of fly ash and superabsorbent polymers replacement ratios on development of self-healing products, in: 3rd ACF Symp. 2019 Assessment and Intervention of Existing Structures, Sapporo, Japan, 2019.

4. P. Pimpakan, H. Yokota, P. Chindasiriphan, Effect of water reducing agent on self-healing capability of concrete made with fly ash and superabsorbent polymer, in: 3rd ACF Symp. 2019 Assessment and Intervention of Existing Structures, Sapporo, Japan, 2019.

5. P. Chindasiriphan, H. Yokota, Effect of fly asha and superabsorbent polymer on concrete carbonation, in: 16th East Asia-Pacific Conference on Structural Engineering & Construction, Brisbane, Australia, 2019.

TABLE OF CONTENTS

LIST OF FIGURES

LIST OF TABLES

CHAPTER 1

INTRODUCTION

- General background
- Research motivation
- Research concept

GENERAL BACKGROUND

Construction and its related industries have dominated quintessential roles to the growth and prosperity of the global economy and social development. It is an investment-led sector where government shows high interest. Government contracts with construction industry are related to the development of infrastructures in health care, transportation, city planning as well as energy securities. According to World Bank national accounts data, construction industry accounts for 29.1% of GDP in Japan and approximately 25.4% of global GDP in FY2017. By far concrete has been used as one of the main construction materials in the modern civil engineering works due to its versatility, durability, and cost effective. Concrete is a composite material which consist of water, cement and aggregate bonded together by hydration reaction. It is reported that the current rate of concrete annual production is approximately 10 billion ton [1]. To match with the increasing demand, it is predicted that the total annual cement production has to be increased up to 18 billion tons by FY2050 [2].

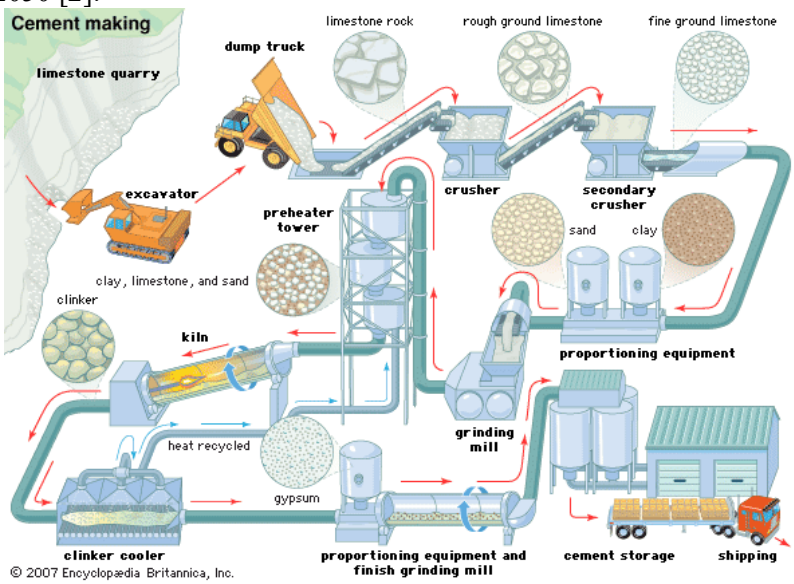

Fig. 1.1: Cement production process

1.1 RESEARCH MOTIVATIONS

The principle of three pillars of sustainability is adopted, considering social, economic and environment. Sustainable considerations are a powerful tool to ensure that natural resources we have today can be used without compromising the ability of future generations to meet their needs. This research has been attempted to establish a framework resolving challenges of construction and its related industries which may be able to reduce negative impacts toward the environments.

i. Engineering & economic aspects

Although concrete is strong in compression, it is weak in tension. It is generally found that concrete structures deteriorate during the service life due to shrinkage, excessive loading and exposure to severe environmental conditions. Cracked concrete is prone to deterioration, as the cracks allow harmful agents to infiltrate and cause steel corrosion. Once a crack start to propagate, it generally shortens service life of concrete structures. Without an immediate and proper actions, cracked concrete becomes more vulnerable, and leads to structure failure. In the European countries, it was reported that around £40 billion is spent annually for structural maintenance in the UK, a significant share of which is used to repair deteriorated concrete structures [3]. Garder et al. [4] reported that about a half of the infrastructure budget in the EU

goes to the repair, maintenance and replacement of damaged concrete structures. Zhang and Wang [5] reported that according to the Federal Highway Administration's 2013 National Bridge Inventory Database (NBI), about 25% of USA national bridges are suffering with structural deteriorations which require more than $12 billions of budget for structural maintenance and retrofit. The report of Ministry of Land, Infrastructure and Tourism, Japan [6] recorded that the approximate budget of 1.9 trillion JPY was used for maintenance and replacement of road infrastructures in FY2018. These evidences suggest that budgetary constraints are a global matter, with infrastructure construction outpacing maintenance. Proper maintenance is neglected for some structures, thereby jeopardizing their structural soundness, serviceability and safety.

ii. Environmental aspects

Despite the benefit, concrete production comes with a significant price as it is considered as an intensive energy consumption process including the consumption of the vast amounts of natural resources. The process generates enormous impacts to the environment. Jonkers et al. [7] emphasizes that the cement industry generates approximately 7% of all global anthropogenic carbon dioxide emissions, particularly caused by incinerating of limestone and clay. Another aspect of concrete is the requirement of maintenance and retrofitting during its service life. The structural intervention and durability-related problems require a tremendously amount of repairing materials which otherwise generates additional impacts on natural resources consumption and increases carbon footprint The issues listed above are strongly emphasized that the cement industry has become a victim of its own achievement and thus, it is now confronting with multi-directional challenges. Particularly in the recent year, when sustainability issues are becoming more and more relevant to any human activities.

iii. Social aspects

Forbes [8] reported that "today workers avoid construction jobs, perceiving them as dangerous, difficult, and dirty. Millennials of all income backgrounds entering the workforce would prefer to go to a four-year college or take on jobs in retail or transportation. In the US alone, there are 434,000 vacant construction jobs as of April 2019, according to the US Labor Bureau." The master thesis of Chindasiriphan [9] stated that "construction industry across the world are struggling to find workers at all levels of experience, according to the National Association of Homebuilders. The association estimates that there are approximately 200,000 unfilled construction jobs just only in the U.S. - a jump of 81 percent in the last two years." Thereby construction and its related industries are facing ever-increasing difficulties in prioritizing skill labor resources, considering the labor requirements between the construction and maintenance section.

1.2 THEORETICAL BACKGROUND

Implementation of periodic inspection and maintenance could be challenging particularly in the circumstance of large-scale infrastructure where a significant amount of capital and time are required. Another issue such as the accessibility to the damage area in the targeted structure makes the maintenance even more challenging. Hence, the concept of self-healing resolves those issues with minimum labors and capital requirements. "Self-healing concrete" refers to a material that is capable of recovering its original properties or regaining in its functionality to match with the intended criterion after suffering degradations. The structural integrity comparison between normal structure versus self-healing structure are demonstrated in Fig. 1.2 whereas Fig. 1.3 shows life cycle cost comparison between normal structure versus self-healing structure. Wu et al. [10] reported that the first self-healing phenomena in cementitious materials was discovered by French Academy of Science in 1836. Then in 1926, the scientists had discriminated between self-healing and self-sealing. According to their definition, self-healing referred to an ability to recover

concrete strength while self-sealing defined as crack closure without strength recovery. In contrast, the modern studies of self-healing prefer to use the term autogenous healing and autonomous healing as explained in sections 1.2.1 and 1.2.2.

1.2.1 Autogenous healing

Autogenous crack-healing may be observed spontaneously when water infiltrates through small cracks (< 0.3mm wide) [11–17]. Crack-healing efficiency is influenced by many parameters, such as an initial crack width, healing duration, hydraulic pressure gradient, healing temperature, mix design, and exposure conditions. Extensive research has found that crack closure is dependent on several mechanisms, such as those incorporating autogenous self-healing by the continued hydration of unreacted cement, calcium carbonate crystallization, the deposition of impurities in water, and the swelling and expansion of C-S-H gel including C-S-H formation from pozzolanic reactions [13,17–19]. The series of autogenous crack healing mechanisms are summarized in Fig. 1.4. It is expected that the primary mechanism is attributed by the crystallization of calcium carbonate [10]. This evidence is confirmed by the presence of white residue at crack surface caused by the deposition of precipitated calcium carbonate. The calcium-based material is one of the dissolved products acquired through the cement hydration. Edvardsen [20] clarified that the mechanism is characterized by free calcium hydroxide leach outs along the cracking surfaces and reacts with the dissolved carbon dioxide, thus white crystals are developed, emerging from surfaces of the cracks and finally filled into the crack space. The crack-healing reactions could be described as follows.

$$H_2O + CO_2 \leftrightarrow H_2CO_3 \leftrightarrow H^+ \leftrightarrow HCO_3^- \leftrightarrow 2H^+ + CO_3^{2-} \quad (4)$$

$$Ca^{2+} + CO_3^{2-} \leftrightarrow CaCO_3 \quad (pH_{water} > 8) \quad (5)$$

$$Ca^{2+} + HCO_3^- \leftrightarrow CaCO_3 + H^+ \quad (7.5 < pH_{water} < 8) \quad (6)$$

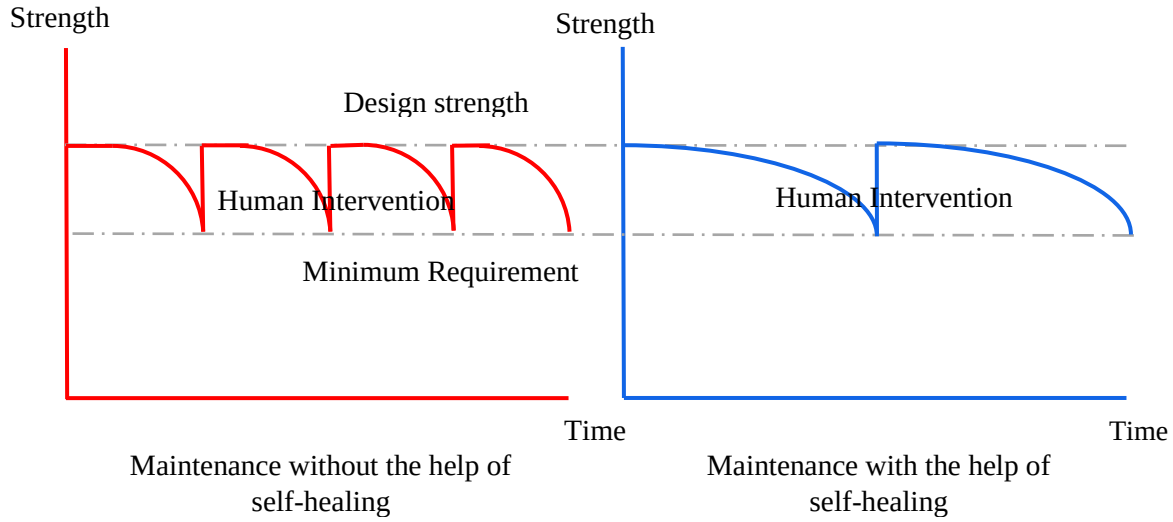

Fig. 1.2: Structural integrity comparison

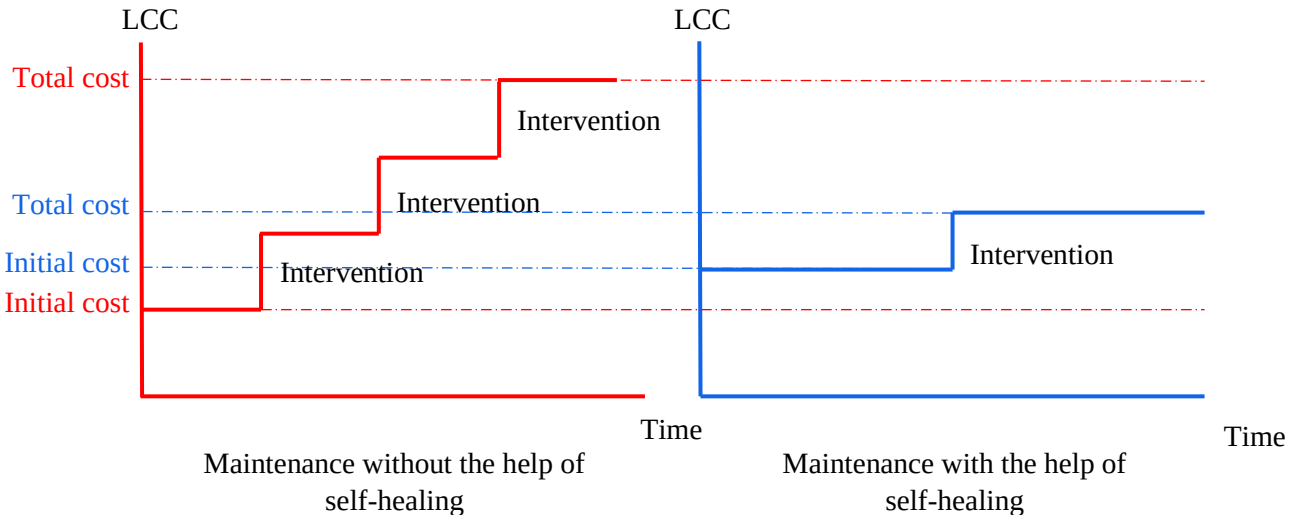

Fig. 1.3: Life cycle cost comparison

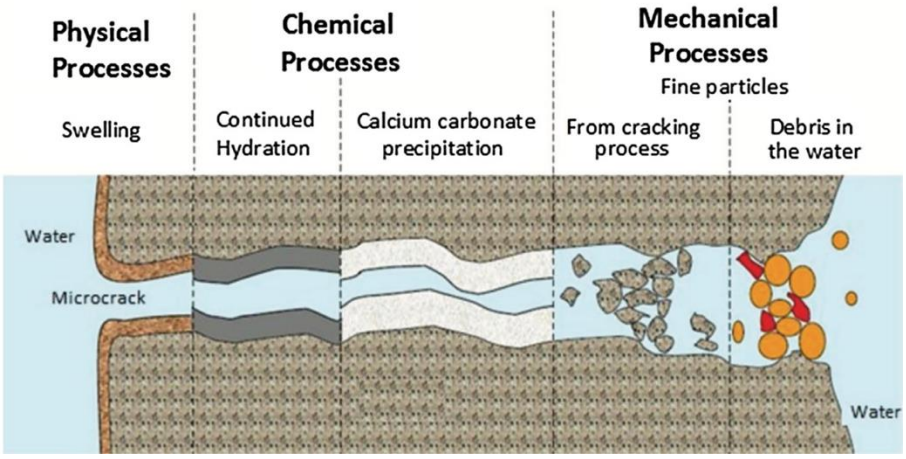

Fig. 1.4: A series of autogenous crack healing mechanisms [21]

i. Self-healing incorporated with supplementary cementitious materials

Pioneering research replaced cement with supplementary cementing materials (SCMs) to reduce the proportion of Portland cement, which has allowed cement manufacturers to optimize material costs and environmental friendliness [21, 22]. In addition, SCMs improve the hardening properties of concrete through pozzolanic reaction. Typical examples of SCMs are fly ashes, rice husk ashes, slag cements (ground, granulated blast-furnace slag), and silica fumes. Their benefits on self-healing ability of cracks such as permeability reduction and mechanical properties improvement have been well investigated by many studies. A fly ash-cement system was reported by Termkhajornkit et al. [24] that the progressive of pozzolanic reaction showed a positive impact on crack closure. Sahmaran et al. [25] observed that self-consolidated concretes incorporated with high volume fly ash shows a significant amount of unhydrated fly ash in their microstructure at early age. Thereby they heal the pre-existing cracks through the hydration of anhydrous fly ash particles at the damage areas. The extension work of Samaran et al. [26] compared self-healing performance between concrete replaced with either fly ash or blast furnace slag, the results showed that self-healed specimen containing blast furnace slag has lower chloride ion permeability compared to

that of fly ash. The microstructure analysis results confirmed that in fly ash ECC specimens, C-S-H and calcite were observed as the main hydrated products while the main hydrated product of blast furnace slag ECC system was calcite. They suggested that slag ECC develops greater amount of self-healing products because blast furnace slag contains CaO and has higher pH in cement pore solution which attributed to the formation of calcite. Huang et al. [27] investigated physico-chemical process of self-healing in blast furnace slag cement using thermodynamic modeling. His results showed that the crack bridging products consist of C-S-H, ettringite, hydrogarnet and OH–hydrotalcite. The significant amount of ettringite is found demonstrating the leaching of SO_4^{2-} ions from the bulk paste, consequently the recrystallization of ettringite in cracks is achieved. However, there is a limited study on the benefits of either RHA or silica fume on self-healing performance.

ii. Mineral admixture and expansive agents

Many studies have proposed that expansive agents and mineral admixtures contribute to self-healing ability in concrete system by leaching out of their hydration products which consequently recrystallize in water and accumulate to seal the cracks. Sherir et al. [28] investigated self-healing and expansion characteristics of cementitious composites with MgO-type expansive agent (MEA). The results showed that MEA effectively contributes to self-healing capability by its ability to enhance densification of microstructure through the development of Magnesium Silicate Hydrates (M-S-H) at early age. Then M-S-H further induces formation of C-S-H products which accounts for up to 16% increase in compressive strength of pre-cracked cube specimens under the accelerated autoclave curing compared to their water cured virgin counterparts. This evidence suggests a possibility of an autogenous healing on ECC-MgO system in the real structure. Sisomphon et al. [29] mentioned that cement-based materials incorporating calcium sulfoaluminate based expansive additive (CSA) and crystalline additive (CA) developed satisfactory results toward self-healing capability. In specimen with CSA and CA, a complete crack closure was found with an original crack width up to 400 μm which is approximately 2.6 times more effective compared to that of control specimen, considering the monitored over the course of 28 days. The crack closure was attributed by the development of calcium carbonate. A significant amount of calcium carbonate precipitation can be observed on crack surface of specimens with CSA/CA additions because specimens with CSA/CA additions were characterized by high pH in cementitious matrix and greater released of calcium ion than the control specimen. According to a review of Wu et al. [10], "a geo-material with a SiO_2 content of 71.3% and Al_2O_3 content of 15.4% was added with the expansive agent. It is reviewed that geo-polymers were formed by the polymerization of individual aluminate and silicate species, which were dissolved from their original sources at high pH in presence of alkali metals. Detailed studies showed that the geo-polymeric gel size was smaller than 2 μm and the crack interface phases of the original cracking zone formed several hydrogarnet phases. This indicated that hydrogarnet phases or AFt phases were formed from expansive agent. Therefore, played an important role as crack-bridging materials. EDS analysis also revealed that most of the modified geo-polymeric gel was structured by dense phases as compared to hydrogarnet phase."

1.2.2 Autonomous healing

The current trend of interdisciplinary approaches to the development of self-healing concrete shows attempts to seek for supplementary cementitious materials that afford higher efficiency and greater predictability. "Autonomous healing" refers to a healing mechanism that is engineered to enhance self-healing [30]. A decent self-healing system should employ ability to sense the damage and heal cracks in various environmental conditions. Many studies have been conducted and proposed many innovative strategies during the past few decades in order to maximize self-healing performance. The examples of their studies are summarized as below.

i. Encapsulation

Encapsulation methods are widely developed, involving brittle capsules filled with healing agents such as calcite-precipitating bacteria, other microorganisms, polymer fillers, or adhesives. The healing process is triggered by concrete cracking, when capsules containing the healing materials are broken. The healing agents are released into the cement matrix and damage areas through the capillary action which initiates polymerization and subsequently results in the closure of near-by cracks [31–33].

The work of Nishiwaki [34] used two types of microcapsules; either urea–formaldehyde formalin microcapsules filled with either epoxy resin or gelatin microcapsules filled with acrylic resin as a hardener. He reported many technical limitations such as the amount of healing additive stored in the microcapsules was insufficient as the capsules had relatively low bulk capacity. The low bond strength between the microcapsules and cement paste was observed which prevent the microcapsules from breaking. Therefore, it is concluded that this technique is still questionable without improvement of the its limitations. Self-healing by encapsulated polyurethane was investigated by Tittelboom et al. [35]. It was reported that the crack initiation using four-point bending triggered breakage of the capsules and caused releasing of the healing agent which subsequently resulted in crack repair. The leached out of polyurethane from the broken embedded capsules was confirmed by acoustic emission analysis. It was reported that a decrease of water ingress was found, but water leakage could not be perfectly prevented in this study. However, polyurethane encapsulate method is benefit over many self-healing approaches because it requires no water to initiate self-healing mechanisms. Therefore, this approach is applicable for multiple applications such as healing of bending cracks in beams of bridges, healing of thermal cracks in insulated concrete sandwich panels including those damaged interior structural components. While the study of Tittelboom et al. [31] on tubular capsules filled healing agent using MEYCO MP 355 1K from BASF, a commercially available healing agent which used to repair cracks water tightness and to cut off leakage. After capsule breakage, crack repair was observed through the filling of the cracks with healing agent which subsequently resulted in more than 50% recovery of its original strength and stiffness. While water permeability reduced which was attributed by autonomous crack healing.

ii. Hollow fibers or vascular technology

Self-healing using hollow fibers embedded within an engineering structure has a similar concept with encapsulate approach which self-healing can be activated by the breakage of the fibers. This concept was inspired by the blood vessel in biological organisms which has been investigated at different fiber lengths using various type of engineering materials such as polymeric composites.

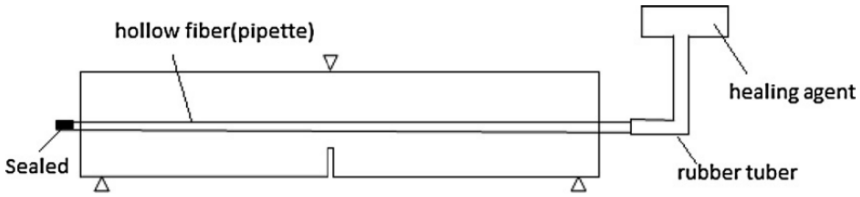

Fig. 1.5: Testing diagram of external healing agent supply system [10]

According to the review of Wu et al. [10], an experimental work of hollow fibers can be represented by testing diagram as shown in Fig. 1.5. Hollow fibers (pipettes) were embedded into a cementitious matrix, the open end was connected to healing agent source while the other end was sealed with epoxy. Glass pipes with outer diameter of 2 mm and inner diameter of 0.8 mm was introduced into concrete specimen. Diluted (27%), non-diluted alkali silica solution and two-component-blended-low-viscosity epoxy resin were used as the healing agent. The control cracks were generated by applying loaded till the Crack Mouth Opening

Displacement (CMOD) reach approximately 0.03–2 mm. The results showed that specimens with diluted and non-diluted alkali-silica solution obtained a notable strength recovery. However, it is worth noting that this recovery value was much lower compared to that of manually repair by injecting resin into the cracks.

iii. Bacteria

In 1995, environmentally friendly biological countermeasure in fixing cracks was first introduced by Gollapudi et al. [36] using mineral-producing bacteria to induce calcium carbonate precipitation. Jonkers et al. [7] mentioned that most of studies use ureolytic bacteria in the genus Bacillus as healing agent for the biological production of calcium carbonate-based minerals. Bacterial spores can be directly added to the mix. The biological activities of these bacteria are contributed by enzymatic hydrolysis of urea to ammonia and carbon dioxide. As a consequence, the formation of calcium carbonate results in the regained strength and the decrease of material permeability. Bacteria precipitation using B. sphaericus bacteria was further investigated by Tittelboom et al. [32] who mentioned that microbial precipitation of $CaCO_3$ was influenced by several parameters such as the concentration of dissolved inorganic carbon, the pH, the concentration of calcium ions and the presence of nucleation sites. The bacteria used in his research was characterized by a produced urease which catalyzes the hydrolysis of urea ($CO(NH_2)_2$) into ammonium (NH_4^+) and carbonate (CO_3^{2-}). The biological mechanism is simplified as below.

$$CO(NH_2)_2 + H_2O \rightarrow NH_2COOH + NH_3 \quad (1)$$

$$NH_2COOH + H_2O \rightarrow NH_3 + H_2CO_3 \quad (2)$$

$$H_2CO_3 \leftrightarrow HCO_3^- + H^+ \quad (3)$$

$$2NH_3 + 2H_2O \leftrightarrow 2NH_4^+ + 2OH^- \quad (4)$$

$$HCO_3^- + H^+ + 2NH_4^+ + 2OH^- \leftrightarrow CO_3^{2-} + 2NH_4^+ + 2H_2O \quad (5)$$

Due to negatively charged of bacteria cell wall, it induces cations from the environment, including $Ca^{2+}$to accumulate on their cell surface. The Ca^{2+}-ions subsequently react with the CO_3^{2-}-ions, leading to the precipitation of calcium carbonate at the cell surface which is described by Eq. 8 and Eq. 9.

$$Ca^{2+} + Cell \rightarrow Cell - Ca^{2+} \quad (8)$$

$$Cell - Ca^{2+} + CO_3^{2-} \rightarrow Cell - CaCO_3 \quad (9)$$

It worth mentioning that crack healing by microbial activities is considered as a pollution free process. Self-healing incorporated with B. sphaericus, protected in silica gel, improved ultrasonic pulse velocity, indicating that crack bridging was obtained. Visual inspection confirmed that microbial activities associated with epoxy treatment attributed to a complete filling of the cracks including permeability reduction attributed to crack filling into the sol–gel matrix.

iv. Shape Memory Materials

Advances in materials engineering have given rise to alternative materials, such as shape-memory polymers and shape-memory alloys integrated with cementitious matrix. The rehabilitation process is activated by heat, which allows a material of a predetermined shape to deform into a preset configuration and subsequently generates restraining force to close an open crack [10]. Zhang et al. proposed [37] that due to natural properties of shape memory polymer alloy (SMA), it can be converted from martensite phase (hardening form of steel crystalline structure) to austenite phase (contractible phase) when the material is subjected to heat. Therefore, this application allows the pre-strained SMA in concrete to recover it length

and diameter under the actuation of thermal energy (usually electrical currents). SMA has various composite systems, and the most regularly adopted system in concrete is NiTi SMA. The rapid change in phase transformation indicates a potential of SMA on an emergency repair of concrete matrix. Song et al. [38] reviewed that smart materials integrated structure can be characterized in multi-functionalities such as sensing, actuation and information processing which are essential to control the self-adapting and healing process of structures. By employing the actuation property of shape memory alloy (SMA) incorporates with the concept of Intelligent Reinforced Concrete (IRC). The IRC uses stranded martensite SMA wires for post-tensioning. The internal strain distribution in concrete is measured through electrical resistance changes of the shape memory alloy wires. Hence, the concept of intelligent concrete structure with an ability to sense and heal the existing crack can be developed using SMA. In the presence of cracks, heating the SMA wires using electricity can mitigate crack widening by generating contraction forces from wire strands. As a result, crack width can be reduced as demonstrate in Fig. 1.6. It is reported that this self-healing technique is able to mitigate structural damage up to macro-sized cracks.

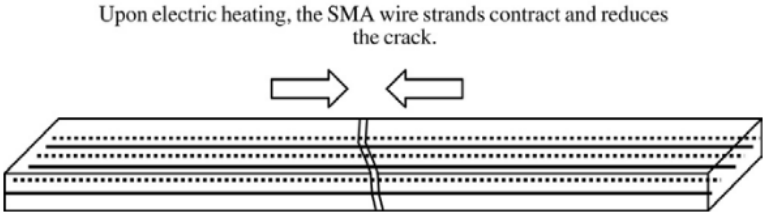

Fig. 1.6: Schematic of intelligent reinforced concrete specimen

The study of Li et al. [39,40] showed that the mid-span deflection of a concrete beam was improved by 74.3% with a minimum deflection of 1.27 mm after subjected to temperature at 110 ℃. It found that the contraction force exerted by the shape memory effect of SMA bundles in smart concrete beams can be modified considering influences of temperature variable applied to SMA bundles.

v. Electrodeposition technology

Electrodeposition is a phenomenal that observed through the deposition of material on the electrode through electrolysis [37]. In late 1980s, Japanese scientists investigated the potential of using an electric current to mitigate crack widening in reinforced concrete. Ryu and Otsuki [41] proposed that the electrodeposition technique could be developed for rehabilitation of cracked reinforced concrete, considering the electrochemical technique. Electrodeposition is the most useful for marine structures where sea water can be utilized as self-healing medium due to the presence of Ca^{2+} and Mg^{2+} from dissolved calcium carbonate and magnesium carbonate respectively. The formation of inorganic insoluble compounds layers act as a physical barrier and attribute to reduce the transportation property of concrete including filling of cracks. Electrodeposition is achieved by applying weak current when concrete surface acts as an anode (the electrode) and steel bar act as a cathode as shown in Fig. 1.7. Their results showed that during first 2 weeks of experiment, the rate of crack closure increased rapidly which accounted for approximately 0.5–2 mm thick of electrodeposit layer deposited on concrete surface. It is worth mentioning that their results showed approximately 70% decrease in chloride ion concentration after continuously applied current. The re-passivated in protection film was observed in most of the observations. Jiang et al. [42] evaluated the effects of electrodeposition method on the self-healing efficiency of cracks by simulating cracked concrete using porous concrete. Their observation at early age reviewed that the total void ratio of porous concrete had negligible effect on the healing performance associated with electrodeposition. While crack closure performance could be improved by considering greater current density, higher concentration of electrolyte

solution and higher solution temperature. In addition, the increase in w/c enhances self-healing efficiency of electrodeposition because the higher porosity in cementitious matrix allows higher current to pass through concrete.

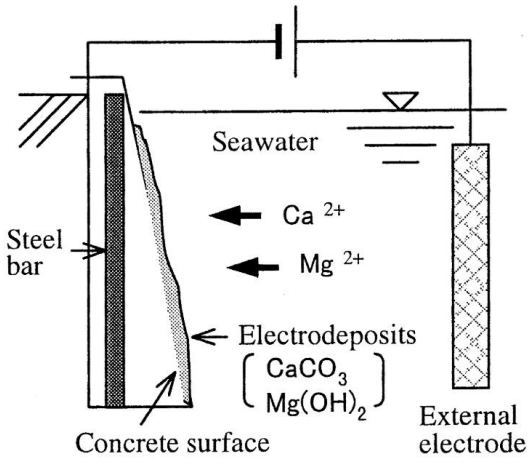

Fig. 1.7: Application of electrodeposition in marine structure [41]

vi. Superabsorbent polymers

SAPs or hydrogels are water-entrained admixtures that are able to absorb great volume of liquid, and subsequently swell forming watertight impermeable gels. Jensen and Hansen [43] suggested that SAP decreases the possibility of self-desiccation and shrinkage by providing extensive internal curing. Riyazi et al. [44] noted that SAP is able to mitigate freeze-thaw damage by achieving a satisfactory air void distribution. In the application of self-healing, Lee et al. [11] revealed that SAP swells after exposure to water. Its expansion enables SAP to fill into cracks and other cavities in concrete and subsequently restore the permeability of the concrete system. Fig. 1.8 illustrates the self-sealing mechanism incorporated with SAP. Snoeck et al. [45–47] stated that beside gel blocking effect, SAP has a significant contribution to autogenous processes such as carbonation of hydration products forming $CaCO_3$ precipitation, dissolution and re-precipitation of calcium hydroxide within the crack, including hydration of exposed unreacted cement particles which results in crack closure. This is because SAP serves as a water reservoir where releases a part of its absorbed water in low relative humidity. Lee et al. [11] concluded that SAP showed a notable performance in enhancement of instantaneous crack sealing after exposure to water. The peak flow rate and accumulative flow through a crack of samples containing cast-in SAP with a crack width up to 0.3 mm reduced by up to 85% and 98% respectively.

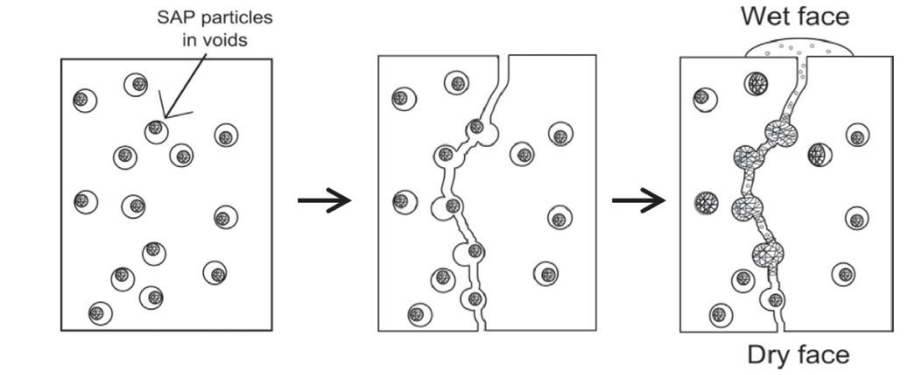

Fig. 1.8: Schematic of the crack self-sealing mechanism using SAP [11]

A comparison between advantages and disadvantages respected to the different self-healing technology are summarized in Table 1.1.

Table 1.1: A summarized comparison between different self-healing strategies [9]

Strategy	Advantage	Disadvantage
Encapsulation		
External supply system	1. Healing agent release on necessity 2. Adjustable large amount of healing agent 3. Effectiveness under multiple damage events	1. Difficulty in casting 2. Negative effect on the mechanical properties of the cement matrix if too many hollow fibers adopted
Internal encapsulation	1. Healing agent release on necessity 2. Medium amount of healing agent 3. Possible effectiveness under multiple damage events	1. Difficulty in casting 2. Negative effect on the mechanical properties of the cement matrix if too many hollow fibers adopted 3. Possible difficulty of healing agent release
Microcapsule	1. Healing agent release on necessity 2. Response to many damage locations at the same time 3. Possible effectiveness under multiple damage events	1. Difficulty in preparing capsules and in casting 2. Limited amount of healing agent 3. The bond between capsules and the matrix is a concern 4. Negative effect on the mechanical properties of the cement matrix if too many capsules adopted
Expansive agent and mineral admixtures	1. Good healing efficacy 2. Good compatibility of the generated healing products with the cement matrix	1. Undesirable expansion if not well treated 2. Healing products generated on necessity is not guaranteed 3. Effectiveness under multiple damage events could be a problem
Bacteria	Biological activities and a pollution free and natural way	1. Many prerequisites to be met 2. Measures should be taken to protect bacteria in concrete 3. Mechanical properties recovery and effectiveness under multiple damage events could be concerns
Shape memory materials	1. Macro-sized cracks can be handled 2. High ratio of mechanical properties recovery 3. Effectiveness under multiple damage events	1. Cost intensive 2. Heating to stimulate the healing process can lead to uncertainties

1.3 SCOPE OF THE RESEARCH

Despite the fact that fly ash and SAP are the common materials that have been long used in concrete work because of their versatility, availability, cost effective and sustainability. The coupling effects of fly ash and SAP on medium to long-term self-healing performance and the potential of using them in wet-dry exposure have not yet well been comprehended. In addition, sustainability awareness has pressurized on the operation of coal-fire powerplants, which makes the future of fly ash questionable. Therefore, fly ash substitution material requires to be investigated and RHAs have a great potential due to their advantages over physical and microstructure improvement of concrete.

In the first stage, this study investigates the effects of fly ash, RHAs and SAP on concrete self-healing ability, considering cement mortar under two different exposure conditions, such as continuous water immersion and exposure to wet-dry. Slump test and compressive strength test were carried out to investigate for the feasibility of mix design and to determine the behavior of concrete engineered with SCMs and SAP. Self-healing performance was evaluated by the improvement in physical properties which included the reduction in the volume of water discharge through a crack, visual crack closure observation and the recovery of ultrasonic pulse transmitting time. The results of physical properties analysis were used as a statistical reference for self-healing performance assessment by microstructure investigation done by stereomicroscopy and SEM. In addition, chemical analysis by thermogravimetric/differential thermal analysis (TG/DTA) was made to elucidate the effect of carbonation on self-healing, and energy dispersive X-ray spectroscopy (EDS) was used to identify newly formed self-healing materials.

In the second stage, superabsorbent polymer (SAP) and supplementary cementitious materials (SCMs) have been proposed as alternative self-healing materials. Despite of their benefits, SAP also has some negative effects on concrete properties. For example, the initial swelling of SAP generates SAP pores that would be a bypass allowing harmful agents to penetrate into concrete. Fly ash enhances self-healing capability of concrete, but it reduces concrete alkalinity because the pozzolanic reaction consumes calcium hydrate in the concrete. This stage of study is designed to investigate the risk of carbonation on self-healed concrete mixed with fly ash and SAP.

1.4 RESEARCH OBJECTIVES

The overall purpose of this research is to embrace sustainability development by developing self-healing technology that can be applied during casting of concrete which can automatically sense and heal cracks in various environmental conditions. The objectives of this study are listed below.

i. To investigate feasibility of crack healing by SCMs.

ii. To investigate feasibility of crack healing by using SAP.

iii. To investigate effectiveness of coupling effects of SCMs and SAP on self-healing performance.

iv. To evaluate risks and benefits of using SCMs and SAP on physical and microstructure properties of cement mortar.

1.5 SELF-HEALING ANALYTICAL APPROACHES

1.5.1 Water discharge through a crack

The flow measurement instrument was inhouse developed and specifically designed to apply sufficient hydrostatic pressure throughout the crack space of the specimens. The instrument consisted of PVC pipe of length 1 m called “the tower”. The first overflow outlet was located at 280 mm from the top of specimen surface and another 3 overflow outlets were located at every 250 mm from the first overflow outlet. The

hydrostatic pressure gradient can be calibrated through varying water head which can be done by selecting a suitable overflow outlet. The bottom face of selected specimen was mounted onto the upper section of the multi-joint while the upper face was connected to the joint. The joint was then connected to the tower as shown in Fig. 1.9. The specific dimensions of each components are listed in the Table 1.2. To perform the test, tap water was constantly supplied to the top of the instrument. The mass of water that flowed out though the crack was measured at measurement outlet. The reduction in flow through crack over time indicates the recovery of crack water tightness which is one of the indexes to evaluate on self-healing performance.

Table 1.2: Specific dimensions of the flow measurement instrument

Component	Outer diameter		Thickness		Approximate inner diameter
	Avg. Dimension (mm)	Avg. tolerance	Avg. Dimension (mm)	Avg. tolerance	
Tower	114	0.4	3.1	0.8	107
Joint	123	-	3.1	-	113
Multi-Joint	123	-	3.1	-	113

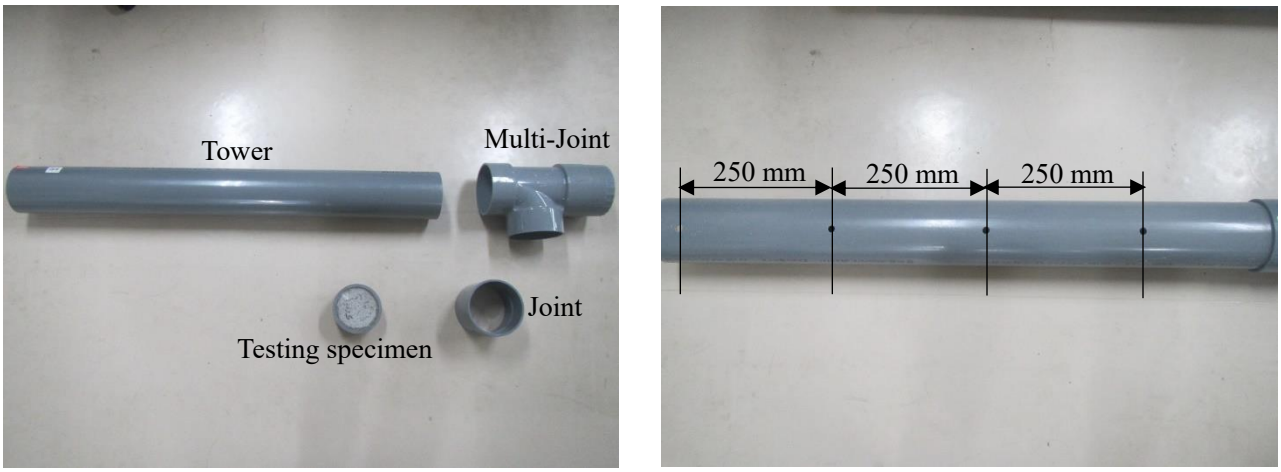

Fig. 1.9: Components of the flow measurement instrument

1.5.2 Visual crack closure observation

To evaluate crack closure, this study used stereomicroscope to observe the morphology of crack filling materials and measured crack widths. Crack closure performance was monitored considering:
(1) Crack healing defines as the complete or the partial crack closure observed visually.
(2) Crack width mitigation defines as a reduction of a crack width at the specific locations (marked points).
(3) Crack closure ratio defines as the percentage of the healed crack width reduction compared to the original crack width.

1.5.3 Ultrasonic pulse velocity test (UPV)

Ultrasonic pulse velocity test is a non-destructive test which has become more and more popular in civil engineering works. UPV test is applicable to evaluate the uniformity and relative quality of concrete which including the assessment of voids and cracks, and the evaluation of crack repairs quality. It is also used to indicate changes in the properties of concrete, and in the survey of structures to estimate the severity of

deterioration or cracking [48]. Abo-Qudais [49] stated that UPV is applicable to detect the internal defects of concrete such as cracks, delamination, and/or honeycombs including predicting concrete strength. Tittelboom et al. [30] used non-destructive acoustic techniques such as resonance frequency analysis and ultrasonic measurements to evaluate the self-healing efficiency. They observed that the autonomous crack healing influences the changes in transmission time of ultrasonic waves by allowing the waves to proceed through the healing agents. In healed specimens, the transmission time decreases as the wave follows the shortest pathway, considering that the pre-existing crack is filled with hydrated products. To evaluate self-healing performance, this study chose to monitor the self-healing activities using Indirect Surface method as shown in Fig. 1.10C. UPV test was carried out at 3 point fixed-testing locations along the crack and the tests were repeated at the same positions to monitor changes over time.

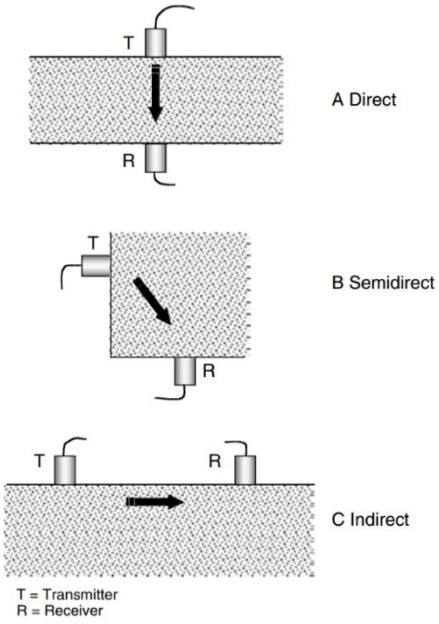

Fig. 1.10: Pulse velocity measurement configurations. (a) Direct method. (b) Semidirect method. (c) Indirect surface method [48]

1.5.4 Thermogravimetric/differential thermal analysis (TG/DTA)

Thermogravimetric and differential thermal analysis (TG/DTA) is a useful method for analyzing the characterization of cementitious materials in solid-state. According to Palermo [50] such characterization includes the investigations of loss on drying, phase transition temperatures, thermal stability, including bound water and physically bound water. In cement researches, TG/DTA is applicable for tentatively determining ettringite formation, chemically bound water and C-S-H content, while it is a useful technique to investigate portlandite content and calcite content in the hydrated sample. TG/DTA analysis simultaneously investigates the changes in mass of a sample as a function of temperature (TG) whereas DTA incorporates with heating or cooling a test sample and an inert reference under control environments [50].

1.5.5 Scanning electron microscope (SEM) with energy dispersive X-ray spectroscopy (EDS)

Scanning electron microscope (SEM) is general instrument for investigating the microstructure and morphology of the materials. SEM imaging is achieved through emitting of an electron beam at low energy to the material and scanning through the surface of the sample. According to Omidi et al. [51] “several

different interactions occur as the beam reaches and enters the material, which leads to the emission of photons and electrons from or near the sample surface. In order to form an image, the receiving signals produced from the electron–sample interactions are detected with different types of detectors depending on the mode of SEM being used. Different modes of SEM exist for characterization of materials (including biomaterials) such as the X-ray mapping, backscattered electrons imaging, secondary electrons imaging, electron channeling and Auger electron microscopy." The example of backscattered electrons imaging and secondary electrons imaging are shown in Fig. 1.11.a and 1.11b respectively.

Energy dispersive X-ray Spectroscopy (EDS or EDX) spectroscopy (EDS) is a chemical microanalysis technique for identifying and quantifying elemental compositions of material, is typically performed in incorporated with an SEM. During the operation of SEM, an electron beam is skimmed across the sample surface. The atoms on the surface are accelerated to the excited state due to the bombardment of electron beam, generating specific wavelengths of X-rays that are distinguished by the atomic structure of the elements. An energy dispersive detector analyzes these X-ray emissions by measuring the number of emitted X-rays versus their energy. In consideration of the emitted X-ray energy which is distinctive to each chemical element from which the X-ray was emitted, the composition and quantitative results of the elements presence in the specimen surface can be yield. In addition, the EDS analysis is applicable to investigate X-ray mapping showing variations of elements in the sample which can be analyzed through sweptwing over of the electron beam on surface of the sample [52,53]. The example of materials mapping and quantitative analysis results are shown in Fig. 1.12a and 1.12b respectively. As stated in section 3, this study used SEM-EDS to observe and identify newly formed self-healing materials including investigating effects of self-healing additives on microstructure level of cement mortar.

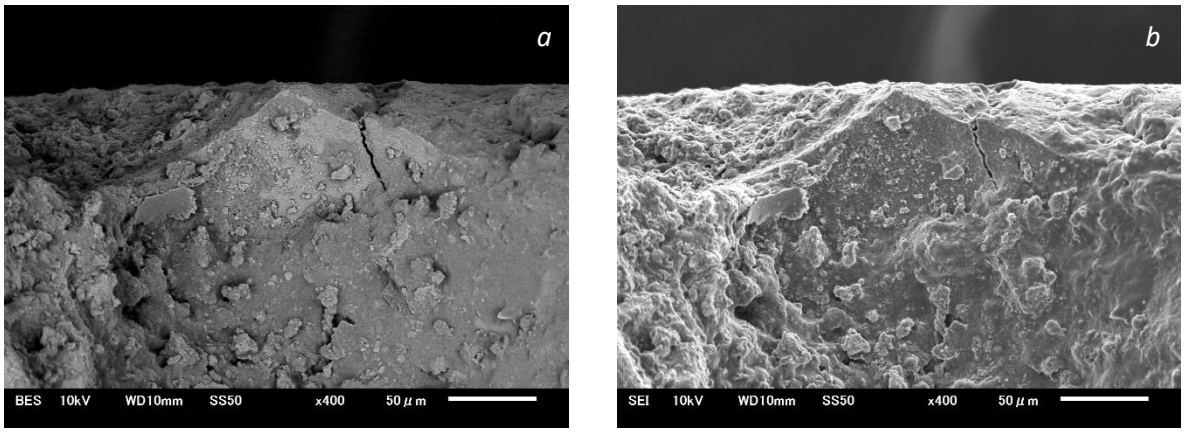

Fig 1.11: Example of backscattered electrons imaging (a) and secondary electrons imaging (b)

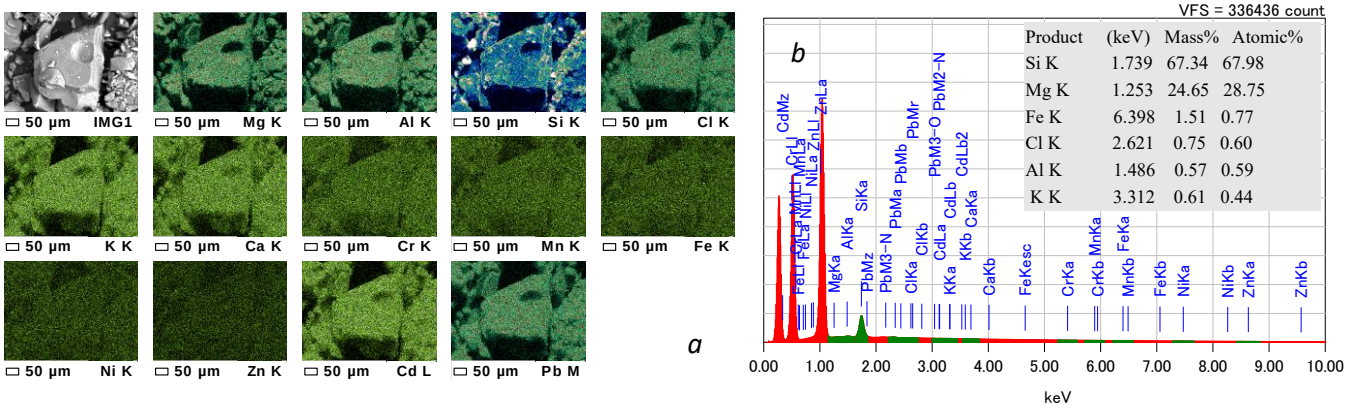

Fig. 1.12: Example of EDS results on materials mapping (a) and EDS quantitative analysis results (b)

1.6 THESIS STRUCTURE

This thesis is divided into five chapters as explained below:

Chapter 1: mentions problems on crack development and research inspirations toward sustainability development. The brief theoretical backgrounds and concepts of self-healing concrete associated with physical and microstructure properties development are provided, along with the research scope of the present study and thesis layout.

Chapter 2: presents experimental results on effect of fly ash and SAP on mortar self-healing capability. It discussed the effects of both materials on rheological behavior, compressive strength, crack closure performance, carbonation and the recovery of concrete permeability.

Chapter 3: discusses effects of fly ash and RHAs on mortar self-healing performance. It discussed and compared the effects of both materials on the recovery of compressive strength, crack closure performance, carbonation and the recovery of concrete permeability. Microstructure analysis by TG/DTA and SEM-EDS were performed to observe materials phases transformation and self-healing behavior of mortar incorporated with SCMs and SAP.

Chapter 4: investigates the effect fly ash and SAP on risk of carbonation of self-healed mortar. Carbonation was determined using phenolphthalein indicator, and thermal analysis technique was used to quantitatively investigate the progress of carbonation. The progress of carbonation within 20 years' service life was predicted and presented in terms of the carbonation depth.

Chapter 5: gives conclusions and some recommendations for future works.

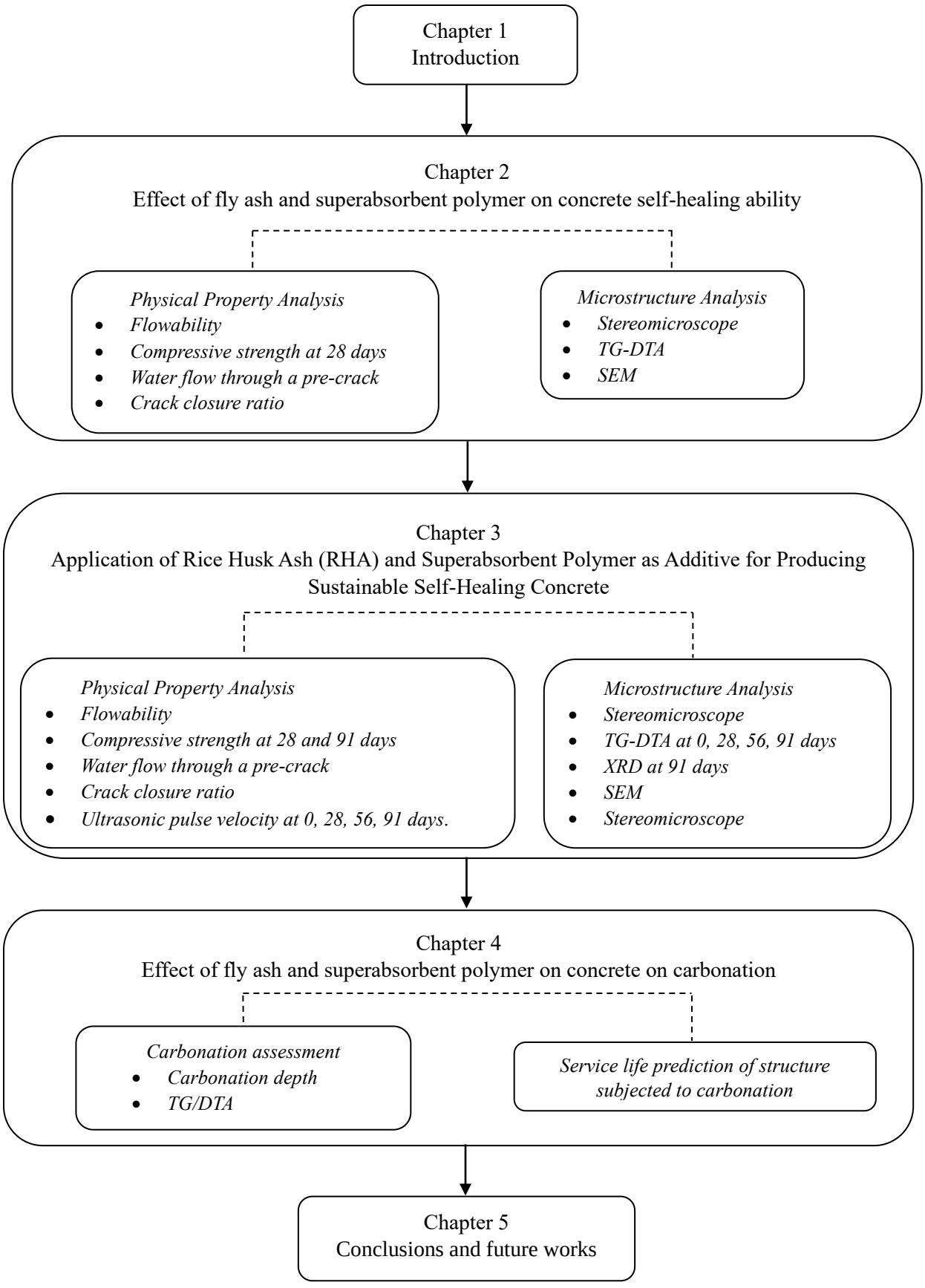
Chapter 1
Introduction
Chapter 2
Effect of fly ash and superabsorbent polymer on concrete self-healing ability
Physical Property Analysis
Flowability
Compressive strength at 28 days
Water flow through a pre-crack
Crack closure ratio
Microstructure Analysis
Stereomicroscope
TG-DTA
SEM
Chapter 3
Application of Rice Husk Ash (RHA) and Superabsorbent Polymer as Additive for Producing Sustainable Self-Healing Concrete
Physical Property Analysis
Flowability
Compressive strength at 28 and 91 days
Water flow through a pre-crack
Crack closure ratio
Ultrasonic pulse velocity at 0, 28, 56, 91 days.
Microstructure Analysis
Stereomicroscope
TG-DTA at 0, 28, 56, 91 days
XRD at 91 days
SEM
Stereomicroscope
Chapter 4
Effect of fly ash and superabsorbent polymer on concrete on carbonation
Carbonation assessment
Carbonation depth
TG/DTA
Service life prediction of structure subjected to carbonation
Chapter 5
Conclusions and future works

REFERENCES

[1] C. Meyer, The greening of the concrete industry, Cem. Concr. Compos. 31 (2009) 601–605. doi:10.1016/j.cemconcomp.2008.12.010.

[2] H. Naseri, H. Jahanbakhsh, P. Hosseini, F. Moghadas Nejad, Designing sustainable concrete mixture by developing a new machine learning technique, J. Clean. Prod. 258 (2020). doi:10.1016/j.jclepro.2020.120578.

[3] Self-healing concrete could save £40bn in maintenance costs, (2017). http://www.materialsforengineering.co.uk/engineering-materials-news/self-healing-concrete-could-save-40bn-in-maintenance-costs/109230/ (accessed October 8, 2018).

[4] D. Gardner, R. Lark, T. Jefferson, R. Davies, A survey on problems encountered in current concrete construction and the potential benefits of self-healing cementitious materials, Case Stud. Constr. Mater. 8 (2018) 238–247. doi:10.1016/j.cscm.2018.02.002.

[5] W. Zhang, N. Wang, Bridge network maintenance prioritization under budget constraint, Struct. Saf. 67 (2017) 96–104. doi:10.1016/j.strusafe.2017.05.001.

[6] Road infrastructure maintenance in Japan, Road Bur. - MLIT Minist. Land, Infrastructure, Transp. Tour. (2020) 1–6. https://www.mlit.go.jp/road/road_e/s3_maintenance.html.

[7] H.M. Jonkers, A. Thijssen, G. Muyzer, O. Copuroglu, E. Schlangen, Application of bacteria as self-healing agent for the development of sustainable concrete, Ecol. Eng. 36 (2010) 230–235. doi:10.1016/j.ecoleng.2008.12.036.

[8] The Construction Labor Shortage: Will Developers Deploy Robotics?, Forbes. (2019) 1–6. https://www.forbes.com/sites/columbiabusinessschool/2019/07/31/the-construction-labor-shortage-will-developers-deploy-robotics/#1d0df4e71988 (accessed August 8, 2020).

[9] P. Chindasiriphan, SELF-HEALING ABILITY OF CONCRETE MADE WITH FLY ASH AND SUPERABSORBENT POLYMER- Master thesis, Hokkaido University, 2017.

[10] M. Wu, B. Johannesson, M. Geiker, A review: Self-healing in cementitious materials and engineered cementitious composite as a self-healing material, Constr. Build. Mater. 28 (2012) 571–583. doi:10.1016/j.conbuildmat.2011.08.086.

[11] H.X.D. Lee, H.S. Wong, N.R. Buenfeld, Self-sealing of cracks in concrete using superabsorbent polymers, Cem. Concr. Res. 79 (2016) 194–208. doi:10.1016/j.cemconres.2015.09.008.

[12] N. Hearn, Self-sealing, autogenous healing and continued hydration: What is the difference?, Mater. Struct. 31 (1998) 563–567. doi:10.1007/BF02481539.

[13] H.W. Reinhardt, M. Jooss, Permeability and self-healing of cracked concrete as a function of temperature and crack width, Cem. Concr. Res. 33 (2003) 981–985. doi:10.1016/S0008-8846(02)01099-2.

[14] H. Liu, Q. Zhang, C. Gu, H. Su, V. Li, Self-healing of microcracks in Engineered Cementitious Composites under sulfate and chloride environment, Constr. Build. Mater. 153 (2017) 948–956. doi:10.1016/j.conbuildmat.2017.07.126.

[15] P. Escoffres, C. Desmettre, J.P. Charron, Effect of a crystalline admixture on the self-healing capability of high-performance fiber reinforced concretes in service conditions, Constr. Build. Mater. 173 (2018) 763–774. doi:10.1016/j.conbuildmat.2018.04.003.

[16] S. Igarashi, A. Hosoda, T. Hitomi, K. Imamoto, Technical Committee on Repairing Technology in Cement-based Materials, 2011.

[17] Y. Yang, M.D. Lepech, E. Yang, V.C. Li, Autogenous healing of engineered cementitious composites under wet–dry cycles, Cem. Concr. Res. 39 (2009) 382–390. doi:10.1016/j.cemconres.2009.01.013.

[18] P. Chindasiriphan, H. Yokota, SELF-HEALING ABILITY OF CONCRETE MADE WITH FLY ASH AND SUPERABSORBENT POLYMER, in: 2nd ACF Symp. 2017 Conf. Innov. Sustain. Concr. Infrastructures, 2017.

[19] P. Termkhajornkit, T. Nawa, K. Kurumisawa, Effect of water curing conditions on the hydration degree and compressive strengths of fly ash – cement paste, Cem. Concr. Compos. 28 (2006) 781–789. doi:10.1016/j.cemconcomp.2006.05.018.

[20] C. Edvardsen, Water Permeability and Autogenous Healing of Cracks in Concrete, ACI Mater. J. 96 (1999) 448–454. doi:10.14359/645.

[21] A. Danish, M.A. Mosaberpanah, M.U. Salim, Past and present techniques of self-healing in cementitious materials : A critical review on efficiency of implemented treatments, J. Mater. Res. Technol. (2020). doi:10.1016/j.jmrt.2020.04.053.

[22] M. Harilal, V.R. Rathish, B. Anandkumar, R.P. George, M.S.H.S. Mohammed, J. Philip, G. Amarendra, High performance green concrete (HPGC) with improved strength and chloride ion penetration resistance by synergistic action of fly ash, nanoparticles and corrosion inhibitor, Constr. Build. Mater. 198 (2019) 299–312. doi:10.1016/j.conbuildmat.2018.11.266.

[23] J. Yu, C. Lu, C.K.Y. Leung, G. Li, Mechanical properties of green structural concrete with ultrahigh-volume fly ash, Constr. Build. Mater. 147 (2017) 510–518. doi:10.1016/j.conbuildmat.2017.04.188.

[24] P. Termkhajornkit, T. Nawa, Y. Yamashiro, T. Saito, Self-healing ability of fly ash-cement systems, Cem. Concr. Compos. 31 (2009) 195–203. doi:10.1016/j.cemconcomp.2008.12.009.

[25] M. Şahmaran, S.B. Keskin, G. Ozerkan, I.O. Yaman, Self-healing of mechanically-loaded self consolidating concretes with high volumes of fly ash, Cem. Concr. Compos. 30 (2008) 872–879. doi:10.1016/j.cemconcomp.2008.07.001.

[26] M. Sahmaran, G. Yildirim, T.K. Erdem, Self-healing capability of cementitious composites incorporating different supplementary cementitious materials, Cem. Concr. Compos. 35 (2013) 89–101. doi:10.1016/j.cemconcomp.2012.08.013.

[27] H. Huang, G. Ye, D. Damidot, Effect of blast furnace slag on self-healing of microcracks in cementitious materials, Cem. Concr. Res. 60 (2014) 68–82. doi:10.1016/j.cemconres.2014.03.010.

[28] M.A.A. Sherir, K.M.A. Hossain, M. Lachemi, Self-healing and expansion characteristics of cementitious composites with high volume fly ash and MgO-type expansive agent, Constr. Build. Mater. 127 (2016) 80–92. doi:10.1016/j.conbuildmat.2016.09.125.

[29] K. Sisomphon, O. Copuroglu, E.A.B. Koenders, Self-healing of surface cracks in mortars with expansive additive and crystalline additive, Cem. Concr. Compos. 34 (2012) 566–574. doi:10.1016/j.cemconcomp.2012.01.005.

[30] K. Van Tittelboom, N. De Belie, F. Lehmann, C.U. Grosse, Acoustic emission analysis for the quantification of autonomous crack healing in concrete, Constr. Build. Mater. 28 (2012) 333–341. doi:10.1016/j.conbuildmat.2011.08.079.

[31] K. Van Tittelboom, N. De Belie, D. Van Loo, P. Jacobs, Self-healing efficiency of cementitious

materials containing tubular capsules filled with healing agent, Cem. Concr. Compos. 33 (2011) 497–505. doi:10.1016/j.cemconcomp.2011.01.004.

[32] K. Van Tittelboom, N. De Belie, W. De Muynck, W. Verstraete, Use of bacteria to repair cracks in concrete, Cem. Concr. Res. 40 (2010) 157–166. doi:10.1016/j.cemconres.2009.08.025.

[33] S.R. White, N.R. Sottos, P.H. Geubelle, J.S. Moore, M.R. Kessler, S.R. Sriram, E.N. Brown, S. Viswanathan, Autonomic healing of polymer composites, Nature. 409 (2001) 794–797. doi:10.1038/35057232.

[34] T. NISHIWAKI, Fundamental Study on Development of Intelligent Concrete with Self-healing capability, Tohoku University, 1997.

[35] K. Van Tittelboom, J. Wang, M. Araújo, D. Snoeck, E. Gruyaert, B. Debbaut, H. Derluyn, V. Cnudde, E. Tsangouri, D. Van Hemelrijck, N. De Belie, Comparison of different approaches for self-healing concrete in a large-scale lab test, Constr. Build. Mater. 107 (2016) 125–137. doi:10.1016/j.conbuildmat.2015.12.186.

[36] U.K. Gollapudi, C.L. Knutson, S.S. Bang, M.R. Islam, A new method for controlling leaching through permeable channels, Chemosphere. 30 (1995) 695–705.

[37] W. Zhang, Q. Zheng, A. Ashour, B. Han, Self-healing cement concrete composites for resilient infrastructures : A review, Compos. Part B. 189 (2020) 107892. doi:10.1016/j.compositesb.2020.107892.

[38] G. Song, N. Ma, H. Li, Applications of shape memory alloys in civil structures, Eng. Struct. 28 (2006) 1266–1274. doi:10.1016/j.engstruct.2005.12.010.

[39] H. Li, Z. Liu, J. Ou, Behavior of a simple concrete beam driven by shape memory alloy wires, Smart Mater. Struct. 15 (2006) 1039–1046. doi:10.1088/0964-1726/15/4/017.

[40] L. Li, Q. Li, F. Zhang, Behavior of Smart Concrete Beams with Embedded Shape Memory Alloy Bundles, J. Intell. Mater. Syst. Struct. 18 (2007) 1003–1014. doi:10.1177/1045389X06071974.

[41] J.S. Ryu, N. Otsuki, Crack closure of reinforced concrete by electrodeposition technique, Cem. Concr. Res. 32 (2002) 159–164. doi:10.1016/S0008-8846(01)00650-0.

[42] Z. Jiang, F. Xing, Z. Sun, P. Wang, Healing effectiveness of cracks rehabilitation in reinforced concrete using electrodeposition method, J. Wuhan Univ. Technol. Sci. Ed. 23 (2008) 917–922. doi:10.1007/s11595-007-6917-x.

[43] O.M. Jensen, P.F. Hansen, Water-entrained cement-based materials: II. Experimental observations, Cem. Concr. Res. 32 (2002) 973–978.

[44] S. Riyazi, J.T. Kevern, M. Mulheron, Super absorbent polymers (SAPs) as physical air entrainment in cement mortars, Constr. Build. Mater. 147 (2017) 669–676. doi:10.1016/j.conbuildmat.2017.05.001.

[45] D. Snoeck, S. Steuperaert, K. Van Tittelboom, P. Dubruel, N. De Belie, Visualization of water penetration in cementitious materials with superabsorbent polymers by means of neutron radiography, Cem. Concr. Res. 42 (2012) 1113–1121. doi:10.1016/j.cemconres.2012.05.005.

[46] D. Snoeck, P. Van Den Heede, T. Van Mullem, N. De Belie, Water penetration through cracks in self-healing cementitious materials with superabsorbent polymers studied by neutron radiography, Cem. Concr. Res. 113 (2018) 86–98. doi:10.1016/j.cemconres.2018.07.002.

[47] D. Snoeck, L.F. Velasco, A. Mignon, S. Van Vlierberghe, P. Dubruel, P. Lodewyckx, N. De Belie,

The effects of superabsorbent polymers on the microstructure of cementitious materials studied by means of sorption experiments, Cem. Concr. Res. 77 (2015) 26–35. doi:10.1016/j.cemconres.2015.06.013.

[48] V.M. Malhotra, Handbook on nondestructive testing of concrete, 2nd, illustr ed., CRC Press, 2003. doi:10.1159/000138316.

[49] S.A. Abo-Qudais, Effect of concrete mixing parameters on propagation of ultrasonic waves, Constr. Build. Mater. 19 (2005) 257–263. doi:10.1016/j.conbuildmat.2004.07.022.

[50] P.J. Palermo, 6 - Solid Dosage-Form Analysis, in: S. Ahuja, S.B.T.-S.S. and T. Scypinski (Eds.), Handb. Mod. Pharm. Anal., Academic Press, 2001: pp. 235–267. doi:https://doi.org/10.1016/S0149-6395(01)80008-8.

[51] M. Omidi, A. Fatehinya, M. Farahani, Z. Akbari, S. Shahmoradi, F. Yazdian, M. Tahriri, K. Moharamzadeh, L. Tayebi, D. Vashaee, 7 - Characterization of biomaterials, in: L. Tayebi, K.B.T.-B. for O. and D.T.E. Moharamzadeh (Eds.), Biomater. Oral Dent. Tissue Eng., Woodhead Publishing, 2017: pp. 97–115. doi:https://doi.org/10.1016/B978-0-08-100961-1.00007-4.

[52] J. Bergström, 2 - Experimental Characterization Techniques, in: J.B.T.-M. of S.P. Bergström (Ed.), Mech. Solid Polym., William Andrew Publishing, 2015: pp. 19–114. doi:https://doi.org/10.1016/B978-0-323-31150-2.00002-9.

[53] S. Ebnesajjad, Chapter 4 - Surface and Material Characterization Techniques, in: S.B.T.-S.T. of M. for A.B. (Second E. Ebnesajjad (Ed.), Surf. Treat. Mater. Adhes. Bond. Surf. Treat. Mater. Adhes. Bond. (Second Ed., William Andrew Publishing, Oxford, 2014: pp. 39–75. doi:https://doi.org/10.1016/B978-0-323-26435-8.00004-6.

CHAPTER 2

EFFECT OF FLY ASH AND SUPERABSORBENT POLYMERE ON CONCRETE SELF-HEALING ABILITY

- General background
- Coupling effects of fly ash and superabsorbent polymer on self-healing capability
- Physical properties and microstructure changes due to self-healing

2.1 INTRODUCTION

Concrete with self-healing capability supports sustainable development goal by decreases maintenance costs and extends service life of structures. Many self-healing techniques require prolong moisture supply to activate crack-sealing. This chapter investigates on the effect of fly ash and superabsorbent polymer (SAP) to promote self-healing. A portion of this work can be found elsewhere as a part of its data has been published in Construction and Building Materials Vol. 233 (2020). Eight series of mix proportions with varying fly ash and SAP replacement ratios were examined. Self-healing performance was evaluated by temporal decreases in water discharge through a crack, crack closure observation, stereomicroscopy, scanning electron microscopy (SEM), thermogravimetric/differential thermal analysis (TG/DTA), and energy-dispersive X-ray spectroscopy (EDS). The pre-cracked was generated with a control crack width of 0.2±0.1 mm and these pre-cracked specimens were healed in two exposure conditions; either continuous water immersion or exposure to wet-dry conditions. Crack closure was observed to be associated with the deposition of self-healing products while a significant reduction in crack width was found with increase in the fly ash replacement ratio. Higher volume of SAP effectively mitigated water discharge through the crack because SAP swell against the ingress liquid forming the insoluble gel. The coupling effect of SAP and fly ash in combination showed a maximum of 100% crack closure and permeability restoration by the 28th day of healing. It worth mentioning that the midterm self-healing ability of cement mortar is improved by the coupling effect of fly ash and SAP. Crack filling materials were found to be associated with the development of calcium carbonate and C-S-H.

2.2 EXPERIMENTAL PROGRAM

a. Material

Materials used in this chapter consisted of ordinary Portland cement (OPC), sand, SAP, and fly ash. Fly ash with high CaO content (44.07%) was selected because its ability to suppress the initial swelling of SAP during mortar mixing which occurs when the dissolved Ca^{2+} bind to carboxylic groups in acrylate chains of SAP [1,2]. The chemical compositions of cement and fly ash are given in Table 2.1. The SAP used in this experiment is characterized by the rough surface which has minimal absorbency when contacted with an ionized solution. Figure 2.1 demonstrates secondary electron image (SEI) of SAP particles. The particle sizes are approximately in between 10-500 μm and have non-uniform morphology. The properties of the SAP are presented in Table 2.2.

b. Mix proportions design

Eight series of mixes were produced by the absolute volume. The mass of water was kept constant at 237 kg/m^3 which generates w/c of approximately 0.45 for the control series whereas the effective w/c ratios were vary upon the SAP replacement ratio as SAP spontaneously withdrew free water from the fresh mix. The mass of binder was controlled at 524.7 kg/m^3. Cement was partially replaced by fly ash in mass proportion of 15%, 25%, 35% and 45%. Fly ash content of 45% was used to blend with SAP to enhance rheological properties and decrease the initial swelling of SAP during mixing. SAP replacement ratios were varied in a portion of 4%, 6% and 8% by mass of cement in accordance with the report of Chindasiriphan and Yokota [3] who proposed that the increasing in SAP replacement ratio attributes to higher self-healing performance as it increases the probability of SAP to expose to the crack. The mass of sand was fixed at 1458.8 kg/m^3 for all mix proportions. The details on mix proportions are presented in Table 2.3.

Table 2.1: Chemical composition of Portland cement and fly ash

Chemical composition (mass%)	Cement	Fly ash
Silicon dioxide (SiO_2)	21.2	26.6
Aluminum oxide (Al_2O_3)	5.2	10.96
Ferric oxide (Fe_2O_3)	2.8	9.05
Calcium oxide (CaO)	64.2	44.07
Magnesium oxide (MgO)	-	1.85
Sulfur trioxide (SO_3)	2.0	5.36
Alkalis (Na_2O)	0.65	-
Chlorine (Cl)	0.004	-
Sum (SiO_2+ Al_2O_3+ Fe_2O_3)	29.2	46.61

Table 2.2: Properties of SAP

Material	Apparent density (g/cm^3)	Water absorption (g/g)
SAP	0.7	417

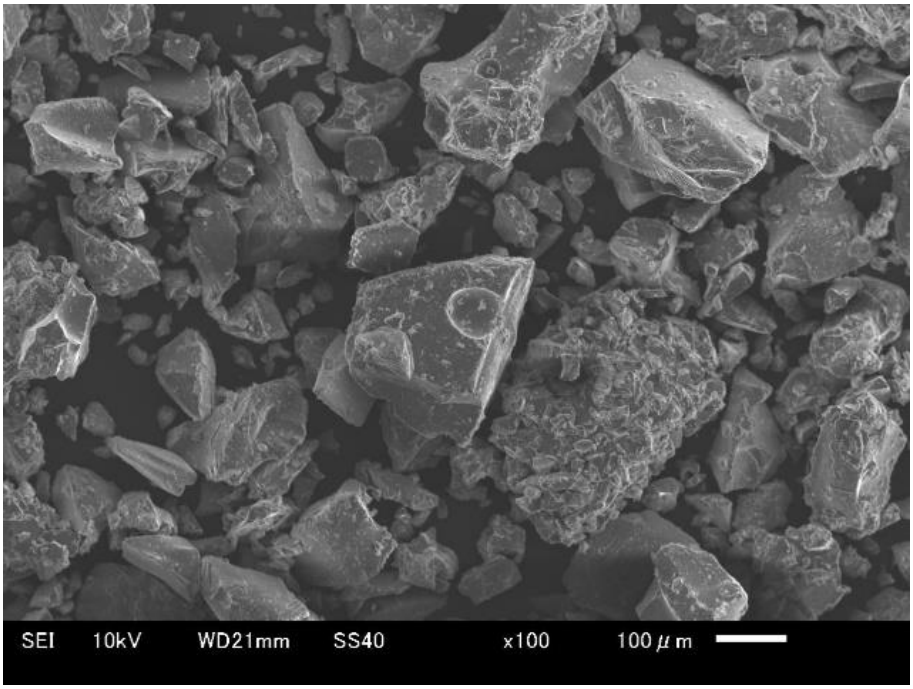

Fig. 2.1: SEM image of SAP particles

Table 2.3: Mix proportions of mortar

Specimen	Cement (kg/m^3)	Fly ash (kg/m^3)	Water (kg/m^3)	Sand (kg/m^3)	SAP (mass% cement)
F00	524.7	0	237	1458.8	0
F15	446.0	78.7	237	1458.8	0
F25	393.5	131.2	237	1458.8	0
F35	341.1	183.6	237	1458.8	0
F45	288.6	236.1	237	1458.8	0
F45S4	288.6	236.1	237	1458.8	4%
F45S6	288.6	236.1	237	1458.8	6%
F45S8	288.6	236.1	237	1458.8	8%

c. Mixing and specimen preparation

The premix was performed incorporated with cement, sand, fly ash and half of the SAP for 1 minute, then the remaining SAP was gradually added, and mixing continued for 2 more minutes to achieve most possible materials distribution. The premixed was required to mitigate adhesion effect from the swollen SAP which develops instantaneously after water exposure. Once the ingredients were well-mixed, water was added, and mixing was carried out for 3 more minutes. Cylindrical molds were used to cast eight series of cement mortars producing specimens with a diameter of 100 mm and a height of 200 mm. The demolding was carried out after 24 hours of setting time, then the specimens were water-cured for 28 days at room temperature. The cured specimens were allocated into two series: The first series was used to investigate the compressive strength test, while the second series was used to examine self-healing behavior associated mechanical properties development and microstructure changes.

In the second series, each cylinder specimen was cut into four discs (50×100ϕ mm). The topmost and the bottom most discs were discarded. Therefore, each cylinder produced two usable specimens “middle disk”. The discs were strengthening using PVC jacket to achieve a controllable crack width and prevent severe damage (Fig. 2.2). A single crack was generated using the universal testing machine (UTM). Specimen was stabilized on UTM using two steel pins retaining on each side. One point load was steadily applied through a steel plate at the top of the specimen (Fig. 2.3). At failure, the jacket lateral support achieved pre-cracking with the control crack width of 0.2±0.1 mm. The initial crack width was assessed by averaging the crack widths measured at 6 locations: 3 on the top surface and 3 on the bottom surface. The measuring points were 25 mm apart and 25 mm from the edge of the specimen.

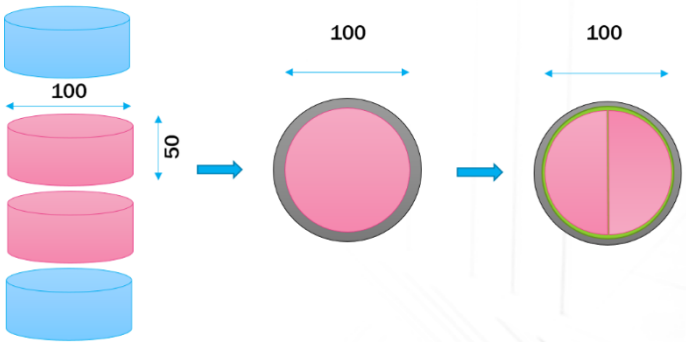

Fig. 2.2: The specimen (pink) was mounted in a PVC pipe (gray) with epoxy

Fig. 2.3: The specimen subjected to splitting load

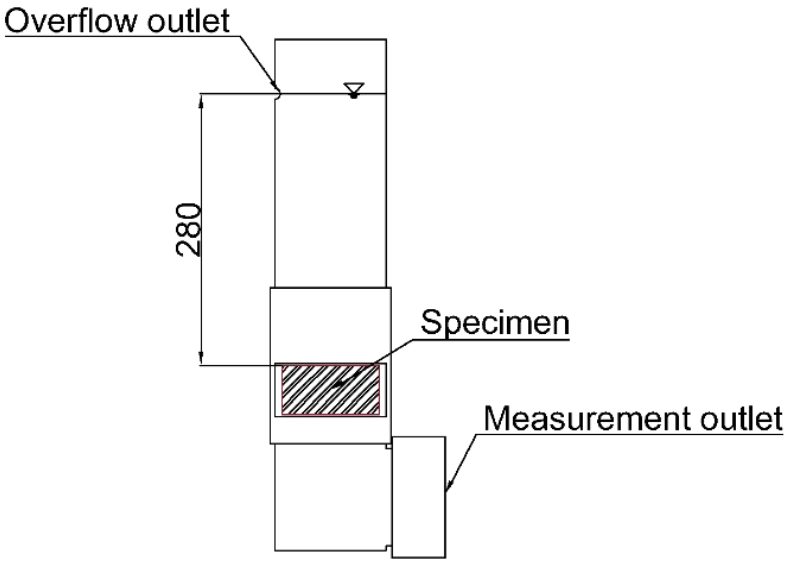

Fig. 2.4: The water discharge measurement apparatus

d. Exposure conditions

Two healing conditions were stimulated. Wet-dry repetition was performed to simulate concrete cracking in a splash zone of hydraulic structures. Water immersion was executed to simulate concrete damage in a submerged zone. The healing duration was set on the course of 28 days under the conditions below.

- FXX (specimen blended with fly ash): submerged in water at 40 °C.
- F45SX (specimen blended with fly ash and SAP): submerged in water at 40 °C.

- F45SX_WD (specimen blended with fly ash and SAP): submerged in water at 40 °C and air curing for 1 day each and repeated as loop.

The water temperature was kept constant at 40 °C to accelerate the hydration of cement and fly ash [4], meanwhile such a temperature range has no disadvantageous effect on long-term strength development.

2.3 TEST PROCEDURE

2.3.1 Mechanical properties investigation

The compressive strength was performed in accordance with ASTM C39 [5] to evaluate the effect of the fly ash and SAP on the strength development. The crack permeability recovery was assessed using a temporal decrease in water discharge through the crack executed periodically during the post-curing stage. The test was performed using the instrument shown in Fig. 2.4. which was developed to supply a constant water head adequate to achieve water penetration throughout the crack. The instrument components consist of an inlet which supplies water to the instrument, a runoff channel that is used to drain excessive flow and to control the water head at 280 mm above the surface of the specimen, and a measurement outlet located at the bottom for measuring the volume of water that flowed out through the crack.

At the 28 days of healing, crack width was measured at the original mark points (see Section 2.3). The widths of the crack were averaged among six different locations to obtain the final crack width. The crack closing ratio was calculated in accordance to Roige-Flores et al. [6] as denoted in Eq. (1).

$$\text{Crack closing ratio} = 1 - \frac{\text{Final crack width}}{\text{Initial crack width}} = 1 - \frac{w_{28}}{w_0} \prec 0 \quad (1)$$

w_0 = Average initial crack width measured at pre-cracking
w_{28} = Average final crack width measured at the 28th day of healing

2.3.2 Chemical and microstructural analyses

An optical stereomicroscope was used to confirm the results of crack closure associated to the deposition of crack filling materials. Image processing was adopted to improve the quality of the photo. The effects of fly ash and SAP on microstructure development were studied using scanning electron microscopy (SEM). The samples were collected from the crack interface and the inner cracking area of healed specimens. Each sample was trimmed to a 10 mm ×10 mm ×10 mm cube, oven-dried at 50 °C for 24 hours, and then stored in a desiccator to avoid carbonation until the time of the analysis. The samples were mounted onto the SEM sample stage and impregnated with gold. An accelerating voltage of 10-20 kV was set as the operation condition.

Thermogravimetric/differential thermal analysis (TG/DTA) was used to study physicochemical changes due to self-healing activities. The cement powder was collected from the crack area. Then the particle size that passed through 100 μm sieve was achieved using a planetary ball mill operated at 450 rpm for 10 min. The heating program was set at a constant heating rate of 10 °C/min until reaching 1000 °C. The mass loss on ignition occurred at the elevated temperature was monitored. The quantity of portlandite ($Ca(OH)_2$) was calculated considering the mass change at approximately 450-550 °C altered by dehydroxylation reaction [7,8], whereas the quantity of calcium carbonate or calcite ($CaCO_3$) was estimated considering mass change due to decarbonation that occurs between 650-900 °C [8,9]. Due to the relation between molecular mass of portlandite (MW_{CH}), the molecular mass of water (MW_{H20}), the mass of the reference sample (W_{ref}) and the mass measured at two inflection points on the TG curve (ΔW), the content of compounds was obtained as shown in Eq. (2), and a similar equation was used as Eq. (3) to determine the amount of calcite.

$$CH(\%) = \frac{\Delta W}{W_{ref}} \times \frac{MW_{CH}}{MW_{H_2O}} \quad (2)$$

$$CaCO_3(\%) = \frac{\Delta W}{W_{ref}} \times \frac{MW_{CaCO_3}}{MW_{CO_2}} \quad (3)$$

2.4 RESULTS AND DISCUSSION

2.4.1 Mortar flow

The mortar flow was determined in accordance with ASTM C1437, a standard test method for the flow of hydraulic cement [10]. The results are presented in Table 2.4. The increase in fly ash replacement ratio shows an increase in flowability. This is in a good agreement with a report from the American Coal Ash Association [11] mentioning that because smooth spherical surface of fly ash particles, it enhances the rheological property of fresh concrete by behaving like tiny ball bearings which subsequently increase the plasticity. Every 10% increase in fly ash content improves flow diameter by approximately 1.9%. In contrast, the slump was decreased in presence of SAP and that decrease was remarkable at high SAP replacement ratio. F45S4 and F45S6 were observed with 17% and 27% lower flow diameter than F45, and F45S8 was observed with the lowest flow diameter. These evidences show that SAP absorbed aqueous solution forming an insoluble gel from which an adhesive effect was found. It worth noting that the SAP was accountable for withdrawal of free water, which generated a lower w/c ratio for the concrete system.

Table 2.4: Flow diameters

Specimen	Flow diameter (mm)	Flow diameter difference compared to F00 (%)
F00	194	0
F15	195	0.5
F25	195	0.5
F35	199	2.6
F45	202	4
F45S4	167	-13.9
F45S6	148	-23.7
F45S8	101.6	*

(*The specimen has no slump.)

2.4.2 Compressive strength

The results of compressive strength at 28 days of curing are presented in Table 2.5. The compressive strength was the mean value among 3 specimens. From results, the presence with fly ash and SAP was characterized by a tendency for compressive strength reduction at SAP content of higher than 4%. The F45S4 had approximately 19% compressive strength decrease compared to that of F45, while those of F45S6 and F45S8 obtained approximately 28% and 25% decrease, respectively. The result is in line with the study of Lee et al. [12] and Hasholt et al. [13], who proposed that the initial swelling of SAP produces a significant amount of as macropores (≥ 50 nm in diameter). The voids produced by the pre-swelling of

SAP has been also known as SAP pore. Snoeck et al. [14] claimed that in fresh mix, macropores are occupied by SAP gel. In hardening stage, cement pore solution and ambient moisture are being consumed by the progress of hydration which also leads to the release of the entrapped water, causing the SAP to shrink. These mechanisms leave SAP pores unoccupied and remain hollow, resulting in the increase in the total porosity of the concrete system. Conversely, a few studies claimed that concrete in existence of SAP possibly characterizes by decrease or increase in strength depending on which side of the mechanism is outweighing [10, 37]. Strength loss is caused to the porosity increases while strength gain is found to be incorporated with a combination of a set of mechanisms. First, strength improvement alters by the decrease in w/c ratio. Second, strength gain occurs due to the densification of the pore structure and the improved hydration degree found to be associated with the effect of an internal curing of SAP. Third, SAP mitigates the risk of self-desiccation. The results showed that SAP content higher than 4% is dominant by of the porous matrix causing a reduction in compressive strengths. This phenomenal is becoming remarkable at high SAP content.

The compressive strength results at 28 day of curing showed that the specimens with partially substituted cement with fly ash had a slight reduction in compressive strength. The compressive strength of F15, F25 and F35 showed a slight decrease compared to F00. Meanwhile, a sharply decrease in compressive strength was found with increase in the fly ash proportion. F45 was found with approximately 20% of strength reduction compared to that of F00. However, the long-term strength is expected to be greater than that of the F00, as the pozzolanic reaction in fly ash is progressive with time which subsequently contributed to a gradual increase in strength [15]. Thus, the fully hydrated specimen with partial fly ash replacement is anticipated to yield greater final strength compared to the control specimen.

Table 2.5: Compressive strength at 28 days of curing

Type	**Compressive Strength**			
	Strength (MPa)	Standard deviation (MPa)	Coefficient of variation (%)	Strength reduction (%)
F00	55.4	0.35	0.63	0
F15	54.2	0.64	1.19	2.16
F25	54.8	1.52	2.78	1.03
F35	52.2	1.34	2.57	5.79
F45	49.1	1.23	2.50	21.28
F45S4	40.0	2.20	5.50	27.70
F45S6	35.3	2.62	7.42	36.31
F45S8	36.7	0.87	2.38	33.79

2.4.3 Effect of fly ash on SAP replacement ratio.

As mentioned in section 2.1, this study utilizes the benefit of fly ash with a significantly high CaO content (44.07%) to suppress SAP initial swelling. ASTM C618 specifies this type of fly ash to be in class C [16]. It possesses pozzolanic properties and some cementitious properties which attributes to a fast strength development and great in final strength. As the benefit of dissolve calcium ion has been well examined by Moon et al. [17], Huber [18], Lee et al. [2], and Mechtcherine et al. [1] The dissolve calcium ions in the cement pore solution increases the possibility of Ca^{2+} binding with the carboxylic groups in acrylate chains

of SAP—binding that consequently leads to a decrease osmotic pressure and suppresses the initial absorbent capacity of the SAP particles. The results suggested that at 45% fly ash replacement ratio, the highest achievable SAP replacement ratio up is limited to 8%. This optimum replacement ratio is approximately 2 times greater than that for mortar with 25% fly ash content [3]. The replacement ratio of higher than 8% was unachievable as it led to severe rheological properties loss due to SAP withdrew all available water in the mix.

The initial swelling is the main disadvantages in the technical point of view which generates negative effects toward rheological properties and compressive strength development due to the possession of an adhesive effect and the development of SAP voids generated from swollen SAP gel. It is worth to mention that the initial swelling of SAP can be restrained by the utilization of the suitable type of fly ash. This enables the mix proportion to increase SAP content which leads to better self-healing performance due to the increasing of a probability for SAP to exposed with an opening crack.

2.4.4 Effect of admixture content on crack closure performance

Table 2.6. shows crack widths of pre-cracked and healed specimens. The crack initiation procedure stated in Section 2.3 allowed the specimens to attain the pre-cracked widths of 0.18 to 0.32 mm. The crack closure ratio calculated from Eq. (1) is adopted to assess the crack closure performance. The results of cracking load demonstrate that fly ash caused a minor reduction in cracking load. In post-healing stage, the crack closure was found to be associated with the development carbonate-like material which primarily formed and filled into the crack cavity. Fig. 2.5 and Fig. 2.6 demonstrate the crack opening and crack closure at 28 days of healing and stereomicroscopic observation showing the morphology of hydrated products to be crystallized calcium carbonate. Ramm and Biscoping [19], Yang et al. [20] and Stuckrath et al. [21] claimed that crack-closure mechanism is attributed by the continuing hydration of unreacted materials, the swelling of C-S-H, and the deposition of calcium carbonate including the accumulation of solid impurities in water are the vital mechanism that promote self-healing. Calcium carbonate is observed notably consolidated at the open crack interface compares to the deeper depth of the crack. Edvardsen [22] and Wu et al. [23], proposed that calcium hydroxide was a product of cement hydration leaks out and greatly concentrates at the cracked surface where then reacts to atmospheric carbon dioxide. The dissolved calcium ions then bind to the carbon dioxide, resulting in the following crack-healing reactions.

$$H_2O + CO_2 \leftrightarrow H_2CO_3 \leftrightarrow H^+ \leftrightarrow HCO_3^- \leftrightarrow 2H^+ + CO_3^{2-} \quad (4)$$

$$Ca^{2+} + CO_3^{2-} \leftrightarrow CaCO_3 \quad (pH_{water} > 8) \quad (5)$$

$$Ca^{2+} + HCO_3^- \leftrightarrow CaCO_3 + H^+ \quad (7.5 < pH_{water} < 8) \quad (6)$$

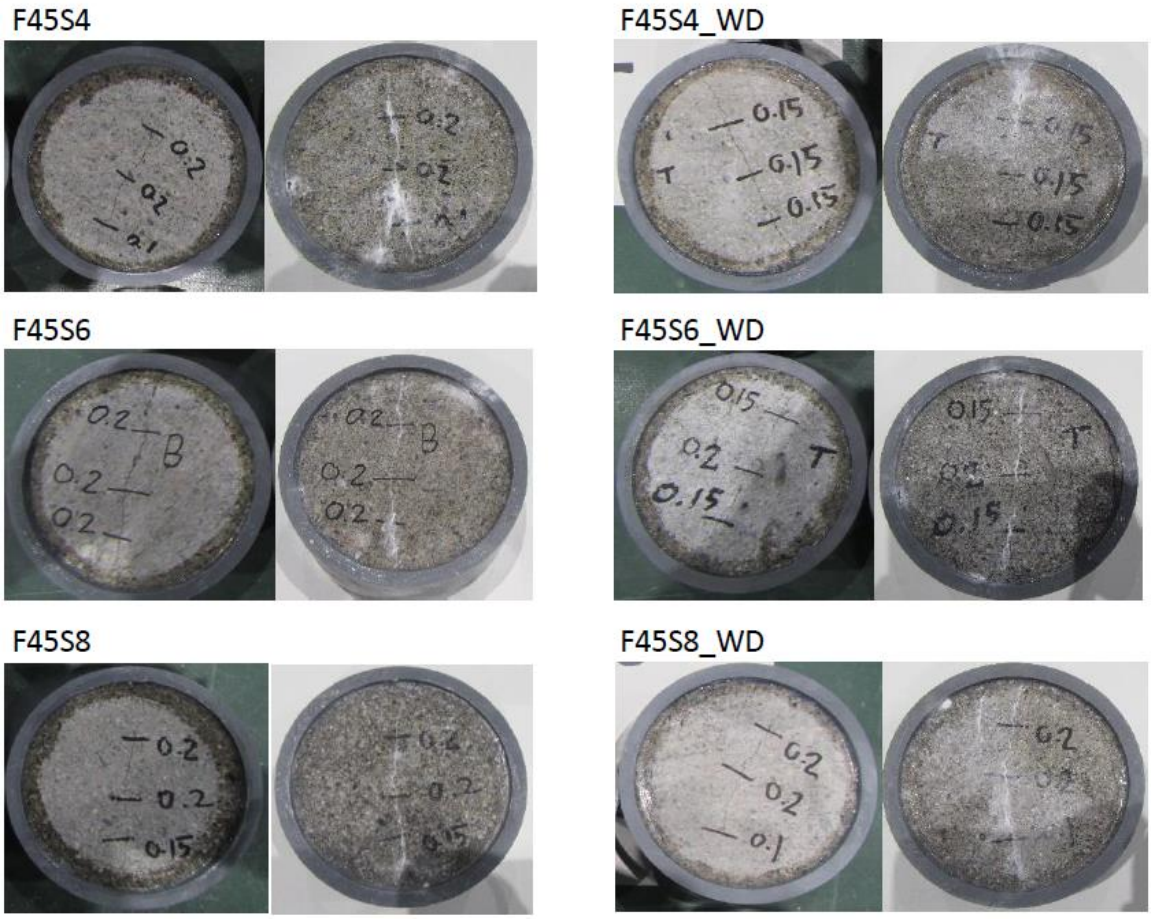

Fig. 2.5: Examples of crack opening (left) and crack closure at 28 days of healing (right)

Figure 2.7 demonstrates SAP morphology in pre-wetting stage. The stereomicroscopic images were adopted to investigate the crack-closure associated with the swelling of SAP gel. The process was triggered by the exposure of water at the damage areas, where SAP absorbed water and swelled against the ingress liquid forming an impermanent crack sealant. Fig. 2.8(a) confirmed that the crack is entirely sealed by the expansion of SAP gel, whereas the SAP particles embedded at the position disclosed in Fig. 2.8(b) show that crack cross section is partially mitigated by the expansive sealant, but it is incapable to completely seal the open cracks.

Specimens healed under wet-and-dry cycles (denoted as "WD") were observed with the lower crack closing ratio. The results confirm the importance of moisture in promoting the self-healing activities. In addition, the initial crack width has a significant effect on the crack-healing rate (the rate that indicates the rapidity of the rehabilitation process) and the healing performance, as smaller cracks have higher probability to be sealed completely disregarding of the exposure conditions. A narrower crack is dominated by concentrated Ca^{2+} ion accumulated at the open boundary, which leads to the increase potential of carbonation meanwhile it needs less volume of healing products to fill into the crack cavity. However, the crack closing ratios are observed in wide range, it is expected that because each crack has different degradation levels. Specimens with higher SAP content showed lower uncertainty for crack closure ratios compared to those shown by specimens with lower SAP content or no SAP. It is worth mentioning that increasing the SAP content notably enhances the crack closure performance through the ability to discharge their absorbed water by SAP.

Table 2.6: Cracking load and crack closure ratio at 28 days of curing

Specimen	Initial crack width (mm)	Final crack width (mm)	Cracking load (kN)	Crack closing ratio
F00	0.32	0.18	50.6	0.45
F15	0.26	0.07	50.9	0.73
F25	0.22	0.03	47.1	0.86
F35	0.20	0.04	48.8	0.80
F45	0.21	0.01	49.3	0.95
F45S4	0.20	0.03	37.1	0.84
F45S4_WD	0.18	0.06		0.67
F45S6	0.19	0.05	40.8	0.76
F45S6_WD	0.19	0.05		0.75
F45S8	0.18	0.00	40.3	1.00
F45S8_WD	0.19	0.00		0.98

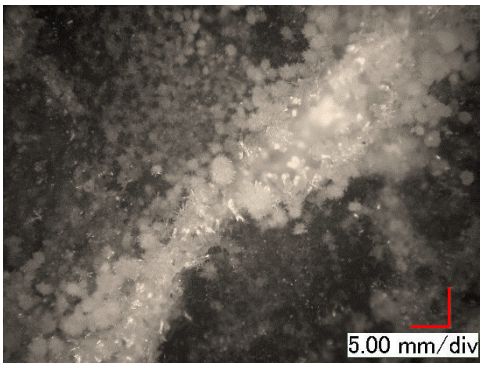

Fig. 2.6: Stereomicroscope image of self-healing products deposited along an open crack

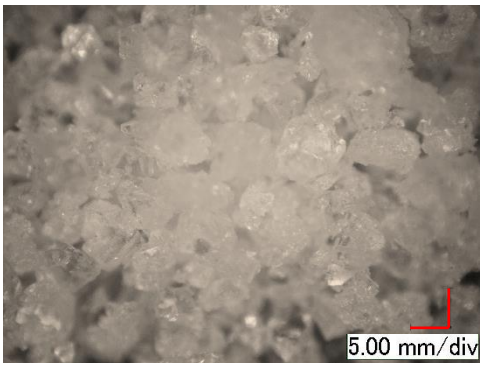

Fig. 2.7: Stereomicroscope image of dry SAP

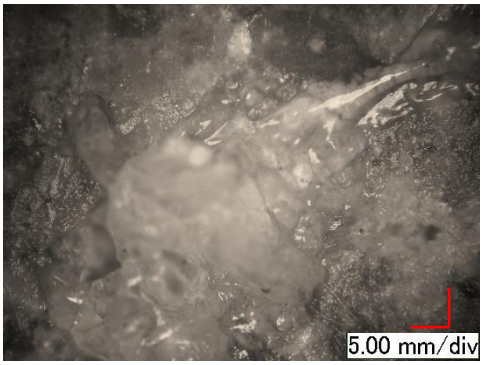

(a) Completely sealed crack by SAP

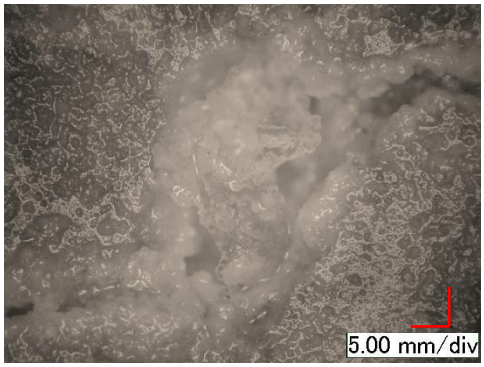

(b) Partially sealed crack by SAP

Fig. 2.8: Stereomicroscopy showing the crack sealing mechanism from SAP swelling

2.4.5 Effect of fly ash and SAP on water discharge through the crack

The rate of water discharge through the crack is plotted in Figs. 2.9-2.12. Crack closure is characterized by the development of self-healing products which also attribute to the reductions of water discharge. The SAP-containing specimens has a substantial reduction in water discharge after contact to water. The mean value of initial water discharge for the SAP-containing series was about half of that of F45. Considering specimens with SAP, F45S8 and F45S8_WD showed the lowest averaged initial water discharge of approximate of 72.1 mL/min, which is about one-quarter that of F45. The results confirmed the advantage of SAP and the benefit of increasing the SAP replacement ratio to enhance sudden crack sealing instantaneously after exposure to water. The sudden drop in water discharge was attributed by the sealing effect of the SAP gel which SAP swell against the ingress liquid. This finding is in line with the work of Lee et al. [12] and Snoeck et al. [24].

For SAP containing specimens healed under water immersion, a gentle decrease in the water discharge rate was observed after the first measurement because SAP is expected to reach its maximum swelling volume. Water discharge reduction at the second and the beyond measurement was restricted to hydration of cement paste and pozzolanic reaction. In the wet-dry exposure series (denoted as WD), the specimens showed a noticeable degree of uncertainty in the pattern of water discharge through the crack reduction. This caused by the decrease in SAP osmotic pressure which was found to be associated with insufficient water supply during air healing stage. In contrast, the fluctuation in the rate of water discharge for specimens in the WD series became stable at approximately 12 days of healing. It is expected that the crack permeability at that period was influenced by the crack closure, whereby permanent healing products developed to fill into the crack.

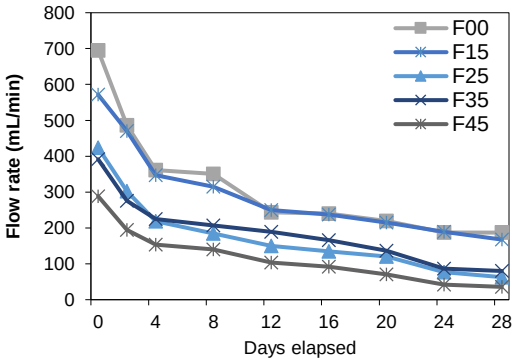

Fig. 2.9: Water discharge through cracks for F00-F45

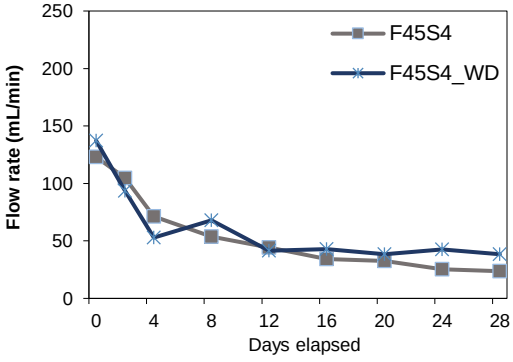

Fig. 2.10: Water discharge through cracks for F45S4 / F45S4_WD

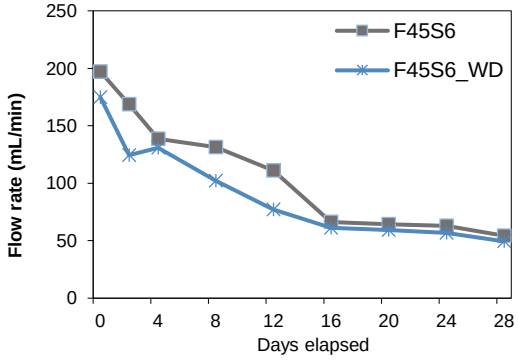

Fig. 2.11: Water discharge through cracks for F45S6 / F45S6_WD

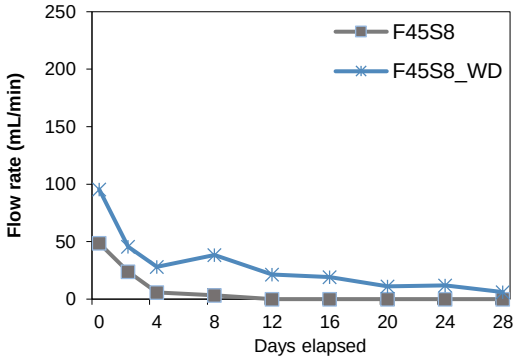

Fig. 2.12: Water discharge through cracks for F45S8 / F45S6_WD

Initial water discharge of the non-SAP specimens was considerable higher, and they were observed with lower water discharge reduction rate. At the end of the monitoring, none of the specimens in this series were able to fully recover crack watertightness. The crack permeability recovery was found to increase with increase in fly ash content, considering the tighter initial crack width of the pre-cracked specimens. The addition of fly ash showed no apparent effects on water discharge reduction. In contrast, F00 (the control specimen) showed a fast-self-healing rate for the first 4 days, then the rate declined and became similar to those of the other specimens. F00 had a final water discharge of approximately 250 mL/min. It is expected that due to F00 had the highest cement content, it is expected to contain highest non-hydrated cement particles which reacts rapidly with water at the early age of monitoring period. The rapid self-healing rate of cement paste is supported by Neville [25,26], who claimed that the further reaction of unhydrated cement paste is feasible only at young concrete age. Therefore, it is suggested that permeability recovery associated with self-healing ability of the non-SAP series is restricted to the autogenous crack healing.

At the end of healing period, F45 had a final water discharge of approximately 50 mL/min; the lowest water discharge in the non-SAP series. In contrast, in the SAP-containing series, F45S8 had a completely sealed crack at 12 days of healing. It is worth highlighting that the increase in SAP replacement ratio leads to the improved water discharge mitigation and the recovery of the specimen's crack permeability despite the exposure condition. The benefit of high fly ash content on water discharge mitigation is unclear. However, the benefit of higher fly ash content on the development of a tighter crack width under the uniform failure mode is clear. Therefore, the positive effects of fly ash toward self-healing efficiency are profound.

2.4.6 Relationship between flow rate and crack width

The relationships between initial crack widths and initial water discharge rates are shown in Fig. 2.13. The experimental results suggested that each crack has an identical characteristic although the crack width is well controlled, the different in the initial water-discharge rates can be found. It was assumed that because the fluid was discharged through a heterogeneous cementitious matrix. Although the pre-cracked specimens were achieved by a well-controlled procedure, the generated cracking patterns consisted of many forms, and these forms were influenced by multiple parameters, such as the internal aggregate configurations of the mortar structure and the damage degree of the specimens. The mentioned parameters accounted for the development of unique crack properties such geometries, patterns and crack surface roughnesses identical to each specimen. When water is assumed to be discharged as incompressible laminar flow through a porous channel, the permeability coefficient can be established using Darcy's law shown in Eq. (7) [24,27].

$$k = \frac{a \cdot L}{A \cdot t_f} \cdot \ln\left(\frac{h_0}{h_f}\right) \quad (7)$$

where a is the cross-sectional area of the testing tower (m^2), L is the thickness of the specimen (m), A is the specimen cross-sectional area (m^2), t_f is the monitoring time (s), h_0 is the initial head (m) and h_f is the measuring head (m). According to Tsukamoto and Woener [28], the relationship between permeability coefficient k and crack width w (m) can be obtained by the Eq. (8).

$$k = \frac{a_g \cdot l_s \cdot g}{12v} \cdot w^3 \cdot \frac{h}{d} \quad (8)$$

where a_g is a discharge rate coefficient specifying the crack surface roughness, l_s is the length of the crack at a right angle to the flow direction (m), g is the gravitational constant (m/s^2), v is the kinematic viscosity (m^2/s), w is the crack width on the inlet side (m), h is the height of the testing tower (m) and d is the crack depth (m) Eq. (8) suggests that the crack width on the inlet side has the greatest influence on the permeability of the cracked specimens. permeability of the cracked specimens.

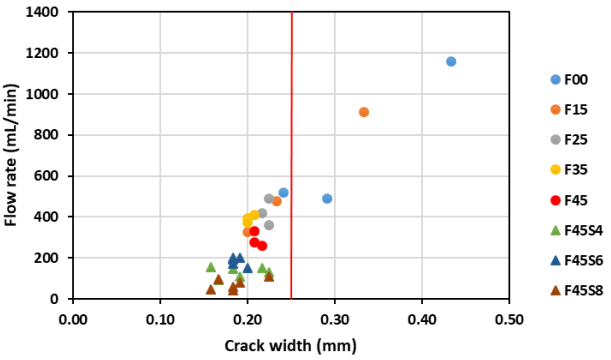

Fig. 2.13: Correlation between initial crack width and initial discharge rate

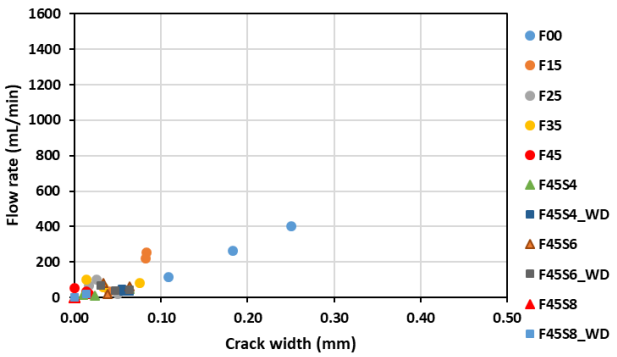

Fig. 2.14: Correlation between healed crack width and final discharge rate

For SAP-containing specimens, they showed lower average initial water discharge rates compared to those of the non-SAP containing specimens with a similar crack width. A highest initial water discharge rate of approximately 200 mL/min was observed for the SAP-containing series, while the highest initial flow rate for the non-SAP specimens was approximately 1400 mL/min. It is suggested that the effect of SAP which absorbs water and swells to form a watertight membrane is profound.

The correlation between healed crack width and final discharge rate is demonstrated in Fig. 2.14. The results review a linear relation between crack width and water discharge rate. The healed specimens are characterized by the reduced crack cross-sectional areas, which leads to a decrease in water discharge rate. These evidences indicate that evaluations of self-healing performance must address both water discharge through the crack and crack width.

The initial crack width has an important impact on self-healing efficiency. The initial crack width smaller than 0.25 mm had high potential to be closed completely. Yet, it is clearly seen that the self-healing activities can be observed for cracks wider than 0.25 mm while such activities continued beyond the observation period. Since, the concrete vulnerability is a great concern after a crack propagation, because the crack acts as a short cut where increases the possibility of hazardous agents entering the concrete and exacerbating steel corrosion. Angst et al. [29] and Wang and Lu [30] discussed that the corrosion rate of reinforced concrete is regulated by various parameters, incorporating a wide range of threshold chloride concentrations and environmental exposure conditions. Chlorine infiltration is naturally a permanent process, which may deteriorate concrete structures by accelerating reinforcement corrosion. A crack closure efficiency should be prioritized, therefore the time required for permeability recovery should be minimized. Beside self-healing performance, it is significantly important to emphasis more on the healing rate, and further research is required.

2.4.7 Thermogravimetric analysis of self-healing performance

The results of derivative thermogravimetric (DTG) curves are presented in Fig. 2.15. Self-healing activities is assessed through the increase in calcite content and C-S-H. Four distinct peaks were observed generating through mass loss due to decomposition of materials. The first noticeable peak at approximately 60 °C, denotes the evaporation of free water and the breakdown of ettringite. The second, at 120 °C, denotes that of monosulfoaluminate, followed by portlandite at 480 °C and calcite at approximately 680 °C. These peaks are in line with the work of Snoeck et al. [14].

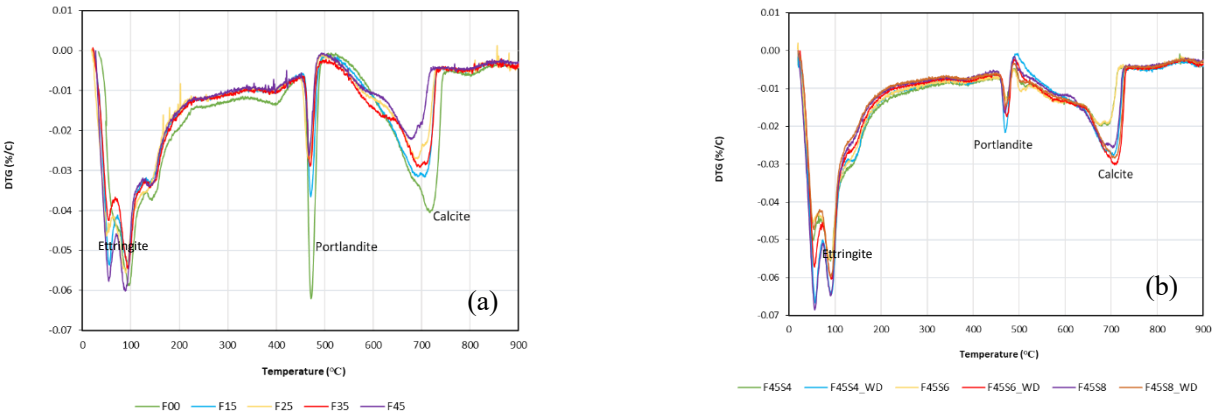

Fig. 2.15: DTG curves for ettringite, portlandite and calcite. (a) Specimens with fly ash. (b) Specimens with fly ash and SAP

The estimated amounts of portlandite and calcite are presented in Fig. 2.16. F00 shows a calcite content of 2.57%, versus 2.27% for F15, 1.91% for F25, 1.96% for F35 and 1.55% for F45, while F45S4 has a calcite content of 4.5%, versus, 5.8% for F45S4_WD, 5% for F45S6, 6.1% for F45S6_WD, 5.4% for F45S8 and 5.8% for F45S8_WD. SAP containing specimens have approximately three times the calcite formation of the non-SAP specimens. The increase in SAP replacement ratio slightly increases the calcite content. In addition, the specimens healed under wet-dry cycles show approximately 1% increase in calcite than that in the same type of specimens healed by water immersion.

Fig. 2.16: Thermogravimetric analysis results [mass%] for portlandite content and calcite content

A statistical data analysis by Hills et al. [31] proposed that there are a few environmental parameters governing carbonation rate. The key parameter is a moisture content, it has been reported that the concrete with complete saturated pores are characterized by a notable reduction in the diffusion rate as transportation property in air 10^4 times as fast as in water. In contrast, a suitable relative humidity is vital for the dissolution of calcium ions and carbon dioxide, as discussed in Eqs. (4), (5) and (6). An optimal condition for carbonation occurs at relative humidity of 50-70% [31,32]. F00 had the highest portlandite content (1.52%) while the lowest was observed in F45 (0.49%). In the existence of fly ash, specimens were altered with a reduction in portlandite content due to the progressive of pozzolanic reaction. All of cast-in SAP specimens had a portlandite content of approximately 1% regardless of the SAP replacement. Still, the evidence why the portlandite content of the cast-in SAP specimens deviated from that of F45 remains unclear, but it might be anticipated by the coupling reaction of fly ash and SAP. Further investigation on this reason is required. It is worth highlighting that the reduction in portlandite content is altered by the progressive of pozzolanic reaction in which fly ash compounds react with $Ca(OH)_2$ generated from cement hydration to form C-S-H that subsequently results in the gradual increase in compressive strength, the densification of the pore structure and the development of self-healing activities.

2.4.8 Microstructural analysis by SEM

Microstructure images were captured using SEM-EDS analyzer. This investigation is adopted to identify the morphology of hydration products developed through self-healing activities and their chemical compositions. The results suggested that the main elements of the hydrated products consisted of calcium and silicon compounds. It appears that hydrated products varied with regard to the position of the self-healing agent, the concrete depth and the confinement including exposure conditions.

Figure 2.17 imaging the external crack surface of F45S8. The newly formed self-healing products show the development of needle crystals emerging on rhombohedral crystals. Their morphology has the estimated lengths of 20-50 µm and the estimated diameters of 200-500 nm. They are observed developing in multi-directions over a layer of what seem to be calcite. From the results, the needle crystals can be analyzed as aragonite ($CaCO_3$ has three forms: aragonite, vaterite and calcite). The EDS results on chemical compositions are presented in Fig. 2.18. Multiple layers of self-healing materials have developed leading to a rough surface area, which has caused in refraction and absorption of the X-ray beams. EDS analysis is ineligible to accurately determine the chemical composition of the hydrated products.

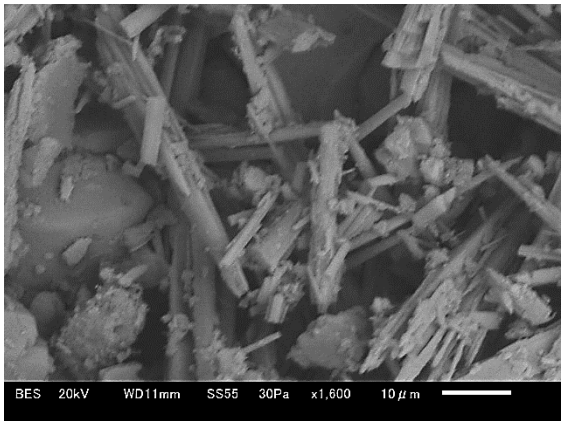

Fig. 2.17: SEM image of the healed crack surface

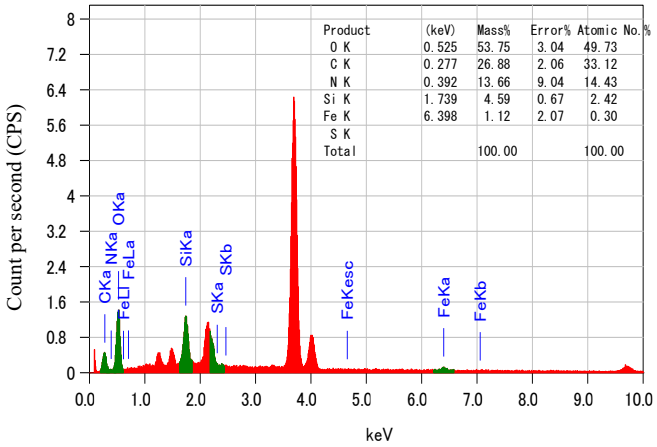

Fig. 2.18: EDS analysis results for the healed crack surface

Figure 2.19 demonstrates that the densification of the cement matrix is visible at the interfacial transition zone of F45S4. Figure 2.20 demonstrates the location of an SAP void (pore) on the crack surface of F45S8_WD. The small yellow rectangle indicates a crystal particle of approximate size of 80 µm that appears to be SAP. The efficacy of SAP as a water retaining agent, its ability to supply water to unhydrated materials and its benefits in self-healing are proven.

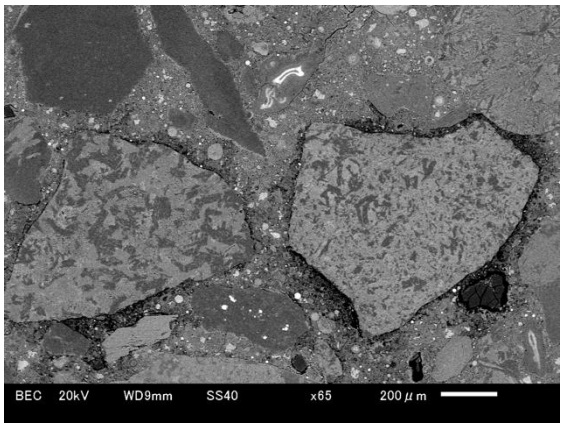

Fig. 2.19: SEM image of ITZ.

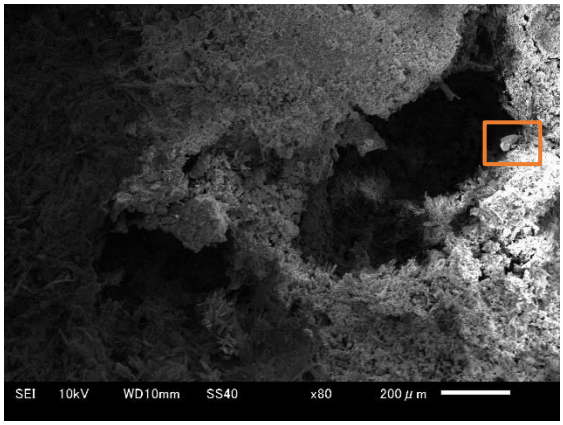

Fig. 2.20: SEM image of SAP void.

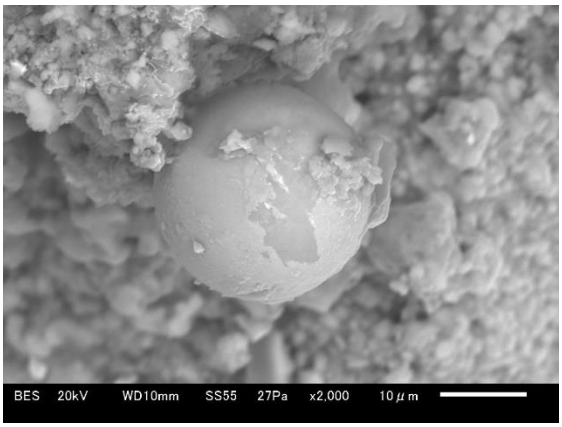

Fig. 2.21: SEM image of fly ash around the healed inner crack boundary

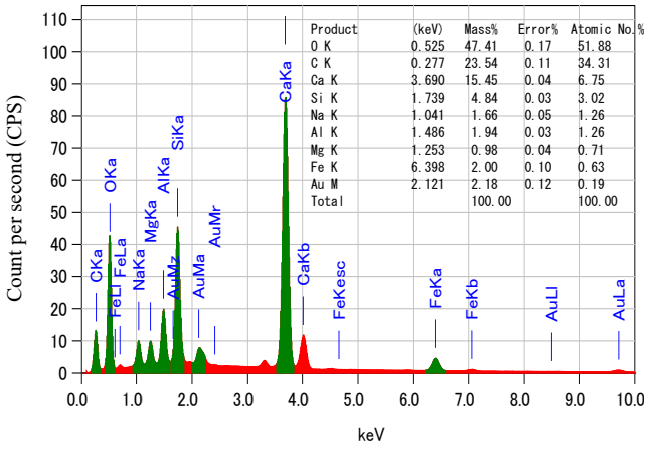

Fig. 2.22: EDS analysis results around the healed inner crack boundary

Fly ash was detected at the inner cracked depth of F45S8. In Fig. 2.21, newly formed products are observed to be the hydrated products of fly ash emerging from the particle surface, where they are developing to fill the crack cavity. The EDS results suggested that the main hydrated products include of high amounts of oxygen (O), carbon (C), calcium (Ca) and silicon (Si), and lower amounts of sodium (Na), aluminum (Al), magnesium (Mg) and iron (Fe) (Fig. 2.22). Regarding to the results of the Si and Ca contents, Fig. 2.23 (a) demonstrates that C-S-H is detected concentrated around and nearby the fly ash particles, while calcium carbonate is developed in significant amounts nearby the external region (Fig. 2.23 (b)). This is in good agreement with the results of Siad et al. [33], who proposed using the Ca/Si ratio to predict the tendency of material stiffness. Self-healing products is stiffer at lower Ca/Si ratios as it represents the development of C-S-H. It is worth noting that fly ash accounts for the formation of denser and more durable self-healing products. Figure 2.21 shows that at 28 days of healing, most of the fly ash particles remain unhydrated. This draws an attention to the potenitial of self-healing activities under pozzolanic reaction in the later age. The assumption is supported by the results of Hung and Su [34], who verified the reactivity of fly ash by comparing the silicon peak of a fly ash specimen healed underwater for 28 days to that of the same specimen healed underwater for 90 days. Their results show a significant increase in silicon peak at 90 days of healing which implies that the amount of new C-S-H increases with healing time.

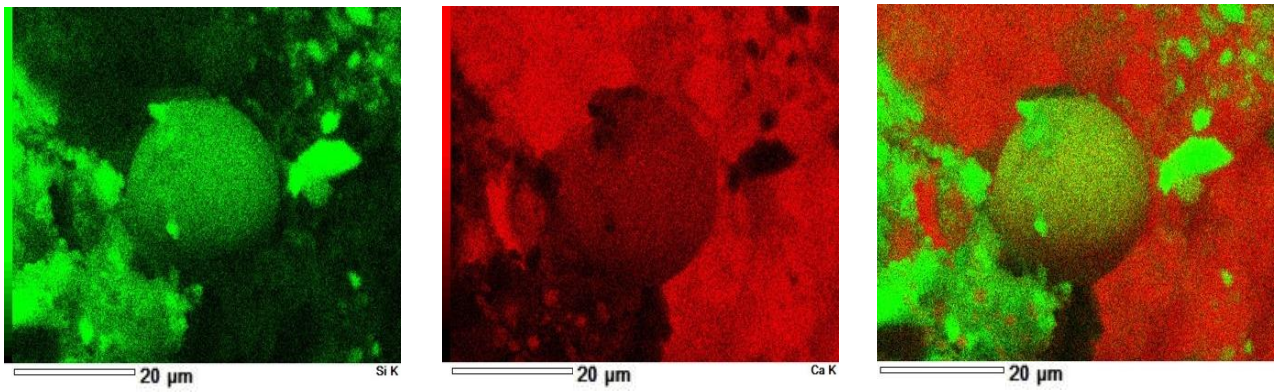

(a) C-S-H in green (b) $CaCO_3$ in red (c) C-S-H – $CaCO_3$

Fig. 2.23: SEM image around a fly ash particle.

2.5 CONCLUSIONS

The chapter investigated on how fly ash and SAP enhance the self-healing ability of concrete. It reviewed the effects of both materials on rheological behavior, compressive strength, crack closure performance, carbonation and the recovery of concrete permeability. The effect of fly ash and SAP on the water discharge through crack reduction obtained at 28 days of healing were focused. Specimens were healed in two different exposure conditions: with wet-dry cycles or with continuous water immersion. Conclusions are summarized as follows:

1. SAP accounts for slump decrease, which consequences from the development of adhesive effect from swollen SAP and the withdrawal of liquid in the mix proportion. The initial absorbency of SAP can be minimized by using dissolved Ca^{2+} to the concrete mixing solution, as it binds to the carboxylic groups in acrylate chains of SAP which alters the desorption of stored aqueous solution.
2. The utilization of fly ash mitigates excessive damage. Specimens containing fly ash achieve smaller cracks under controlled cracking loads than specimens without fly ash. In addition, the usage of fly ash with a high calcium content shows the potential to develop mix proportions with higher SAP replacement ratios. It is also worth mentioning that the self-healing performance is improved due to the development of newly formed C-S-H products from pozzolanic reaction in fly ash.
3. Specimens with increases in SAP dosage beyond 4 mass% are characterized by a tendency for decreasing in compressive strength. The strength development at 28 days is delayed associated with the presence of fly ash. F45 has approximately 20% lower compressive strength than cement mortar without fly ash.
4. Specimens that were healed in water immersion show greater self-healing performance than those exposed to wet-dry cycles, because the presence of water is essential to promote the hydration of fly ash and unhydrated cementitious materials, which subsequently increases self-healing activities.
5. SAP absorbs water and transforms to an impermeable gel that expands to seal an opening crack. The sealing mechanism occurs instantaneously after the SAP is exposed to water which evidenced by approximately 55% lower in the initial water discharge for the SAP-containing specimens than for the non-SAP specimens.
6. Increasing the SAP replacement ratio enhances the crack sealing performance, considering greater crack-widening mitigation and the development of hydration products attributed by internal curing effects from the SAP. Meanwhile, the SAP greatly induces carbonation activities which improve self-healing efficiency by promoting a higher degree of calcium carbonate deposition along the open crack compared to non-SAP containing specimens, which complies well with the results of water discharge through the crack.
7. The initial crack width possesses a substantial effect on the self-healing rate and self-healing threshold. The specimens with initial crack widths below 0.25 mm obtain satisfactory crack closure at 28 days of self-healing. The healed specimens are characterized by the development of hydrated substances deposited at the damage area.
8. The SEM-EDS analysis results of healed specimens confirm that calcium carbonate emerges in significant quantities over the crack interface and outer region of the healed specimens while the C-S-H highly develops nearby fly ash particles at the inner depth.
9. Midterm self-healing ability of cement mortar is improved by the coupling effect of fly ash and SAP. The crack closure is incorporated with the expansion of self-healing products such as the development of calcium carbonate and C-S-H.

REFERENCES

[1] V. Mechtcherine, E. Secrieru, C. Schröfl, Effect of superabsorbent polymers (SAPs) on rheological properties of fresh cement-based mortars — Development of yield stress and plastic viscosity over time, Cem. Concr. Res. 67 (2015) 52–65. doi:10.1016/j.cemconres.2014.07.003.

[2] H.X.D. Lee, H.S. Wong, N.R. Buenfeld, Effect of alkalinity and calcium concentration of pore solution on the swelling and ionic exchange of superabsorbent polymers in cement paste, Cem. Concr. Compos. 88 (2018) 150–164. doi:10.1016/j.cemconcomp.2018.02.005.

[3] P. Chindasiriphan, H. Yokota, SELF-HEALING ABILITY OF CONCRETE MADE WITH FLY ASH AND SUPERABSORBENT POLYMER, in: 2nd ACF Symp. 2017 Conf. Innov. Sustain. Concr. Infrastructures, 2017.

[4] Y. Maltais, J. Marchand, INFLUENCE OF CURING TEMPERATURE ON CEMENT HYDRATION AND MECHANICAL STRENGTH DEVELOPMENT OF FLY ASH MORTARS, Cem. Concr. Res. 27 (1997) 1009–1020. doi:10.1016/S0008-8846(97)00098-7.

[5] Standard Test Method for Compressive Strength of Cylindrical Concrete Specimens, 2009.

[6] M. Roig-Flores, F. Pirritano, P. Serna, L. Ferrara, Effect of crystalline admixtures on the self-healing capability of early-age concrete studied by means of permeability and crack closing tests, Constr. Build. Mater. 114 (2016) 447–457. doi:10.1016/j.conbuildmat.2016.03.196.

[7] M. Henry, I.S. , Darma, T. Sugiyama, Cracking and chemical composition of cement paste subjected to heating and water re-curing, J. Adv. Concr. Technol. 14 (2016) 134–143. doi:10.3151/jact.14.134.

[8] L. Alarcon-Ruiz, G. Platret, E. Massieu, A. Ehrlacher, The use of thermal analysis in assessing the effect of temperature on a cement paste, Cem. Concr. Res. 35 (2005) 609–613. doi:10.1016/j.cemconres.2004.06.015.

[9] E. Oniyama, P.G. Wahlbeck, Application of transpiration theory to TGA data : calcium carbonate and zinc chloride, Thermochim. Acta. 250 (1995) 41–53.

[10] ASTM C 1437:2007 Standard Test Method for Flow of Hydraulic Cement Mortar, 2007. doi:10.1520/C1437-07.2.

[11] American Coal Ash Association, Fly Ash Facts for Highway Engineers, n.d.

[12] H.X.D. Lee, H.S. Wong, N.R. Buenfeld, Self-sealing of cracks in concrete using superabsorbent polymers, Cem. Concr. Res. 79 (2016) 194–208. doi:10.1016/j.cemconres.2015.09.008.

[13] M.T. Hasholt, M.H.S. Jespersen, O.M. Jensen, Mechanical Properties of Concrete with SAP Part I: Development of Compressive Strength, in: Int. RILEM Conf. Use Superabsorbent Polym. Other New Addit. Concr., 2010. http://demo.webdefy.com/rilem-new/wp-content/uploads/2016/10/pro074-012.pdf.

[14] D. Snoeck, L.F. Velasco, A. Mignon, S. Van Vlierberghe, P. Dubruel, P. Lodewyckx, N. De Belie, The effects of superabsorbent polymers on the microstructure of cementitious materials studied by means of sorption experiments, Cem. Concr. Res. 77 (2015) 26–35. doi:10.1016/j.cemconres.2015.06.013.

[15] M.D.A. Thomas, Optimizing the Use of Fly Ash in Concrete, in: Portl. Cem. Assoc., 2007: p. 24. doi:10.15680/IJIRSET.2015.0409047.

[16] Standard Specification for Coal Fly Ash and Raw or Calcined Natural Pozzolan for Use in Concrete: ASTM C618, 2012. http://aip.scitation.org/doi/abs/10.1063/1.4756275.

[17] J. Moon, S. Kang, S. Hong, IONIC DEPENDENCE OF BEHAVIOR OF WATER-ENTRAINING ADMIXTURE IN EARLY AGE CONCRETE, in: 2nd ACF Symp. 2017, 2017.

[18] K. Huber, Calcium-induced shrinking of polyacrylate chains in aqueous solution, J. Phys. Chem. 97 (1993) 9825–9830. doi:10.1021/j100140a046.

[19] W. Ramm, M. Biscoping, Autogenous healing and reinforcement corrosion of water-penetrated separation cracks in reinforced concrete, Nucl. Eng. Des. 179 (1998) 191–200. doi:10.1016/S0029-5493(97)00266-5.

[20] Y. Yang, E.H. Yang, V.C. Li, Autogenous healing of engineered cementitious composites at early age, Cem. Concr. Res. 41 (2011) 176–183. doi:10.1016/j.cemconres.2010.11.002.

[21] C. Stuckrath, R. Serpell, L.M. Valenzuela, M. Lopez, Quantification of chemical and biological calcium carbonate precipitation: Performance of self-healing in reinforced mortar containing chemical admixtures, Cem. Concr. Compos. 50 (2014) 10–15. doi:10.1016/j.cemconcomp.2014.02.005.

[22] C. Edvardsen, Water Permeability and Autogenous Healing of Cracks in Concrete, ACI Mater. J. 96 (1999) 448–454. doi:10.14359/645.

[23] M. Wu, B. Johannesson, M. Geiker, A review: Self-healing in cementitious materials and engineered cementitious composite as a self-healing material, Constr. Build. Mater. 28 (2012) 571–583. doi:10.1016/j.conbuildmat.2011.08.086.

[24] D. Snoeck, K. Van Tittelboom, S. Steuperaert, P. Dubruel, N. De Belie, Self-healing cementitious materials by the combination of microfibres and superabsorbent polymers, J. Intell. Mater. Syst. Struct. 25 (2014) 13–24. doi:10.1177/1045389X12438623.

[25] A.M. Neville, Properties of concrete, 5th ed., Pearson, London, 2011.

[26] A. Neville, Autogenous healing - A concrete miracle?, 2002.

[27] H. Song, S. Kwon, Permeability characteristics of carbonated concrete considering capillary pore structure, Cem. Concr. Res. 37 (2007) 909–915. doi:10.1016/j.cemconres.2007.03.011.

[28] Permeability of cracked fibre-reinforced concrete, Darmstadt Concr. 6 (1991).

[29] U. Angst, B. Elsener, C.K. Larsen, Ø. Vennesland, Critical chloride content in reinforced concrete — A review, Cem. Concr. Res. 39 (2009) 1122–1138. doi:10.1016/j.cemconres.2009.08.006.

[30] W. Wang, C. Lu, Time-varying law of rebar corrosion rate in fly ash concrete, J. Hazard. Mater. 360 (2018) 520–528. doi:10.1016/j.jhazmat.2018.08.007.

[31] T.P. Hills, F. Gordon, N.H. Florin, P.S. Fennell, Statistical analysis of the carbonation rate of concrete, Cem. Concr. Res. 72 (2015) 98–107. doi:10.1016/j.cemconres.2015.02.007.

[32] S.K. Roy, D. Northwoodts, K. Poh, Effect of plastering on the carbonation of a 19-year-old reinforced concrete building, Constr. Build. Mater. 10 (1996) 267–272.

[33] H. Siad, M. Lachemi, M. Sahmaran, H.A. Mesbah, K.A. Hossain, Advanced engineered cementitious composites with combined self-sensing and self-healing functionalities, Constr. Build. Mater. 176 (2018) 313–322. doi:10.1016/j.conbuildmat.2018.05.026.

[34] C.C. Hung, Y.F. Su, Medium-term self-healing evaluation of Engineered Cementitious Composites with varying amounts of fly ash and exposure durations, Constr. Build. Mater. 118 (2016) 194–203. doi:10.1016/j.conbuildmat.2016.05.021.

CHAPTER 3

APPLICATION OF RICE HUSK ASH AND SUPERABSORBENT POLYMER AS ADDITIVE FOR PRODUCING SUSTAINABLE SELF-HEALING CONCRETE

- General background
- Self-healing performance comparison: fly ash vs. RHAs
- Results discussion

3.1 INTRODUCTION

Rice husk ash (RHAs) and fly ash are primary used as supplementary cementitious materials to improve hardening properties of concrete. They are characterized by long-term strength enhancement due to pozzolanic reaction. A significantly high silica content in RHAs is expected to improve the degree of hydration compared to that of fly ash and contribute to a remarkable self-healing efficiency. Superabsorbent polymer (SAP) is utilized as water-entraining admixture which acts as a water reservoir providing moisture to damage areas. This chapter investigates potential of using RHAs and SAP as self-healing additives. Compressive strength at 28 and 91 days were determined. A single crack with a control crack of 0.2 ± 0.1 mm wide specimens were healed either by continuous water immersion or wet-dry exposure. Self-healing performance was assessed by means of crack permeability reduction considering temporal decreases in water flow through a crack, crack closure and reduction of ultrasonic pulse transmitting time. Microstructure changes over times was observed using stereomicroscopy, scanning electron microscopy (SEM), thermogravimetric/differential thermal analysis (TG/DTA), and energy-dispersive X-ray spectroscopy (EDS). At healing duration of 28 days, cast-in RHA specimens presented a maximum flow reduction of 85%. Chemical and microstructure analysis confirmed that crack closure and permeability reduction was achieved through the development of C-S-H and calcium carbonate crystallization.

3.2 MATERIALS

The materials used in this study were ordinary Portland cement (OPC), sand, SAP, superplasticizer, supplementary cementitious materials.

RHA

Rice husk ash is a residue from igniting paddy rice which is considered as an agricultural by-product. The chemical composition of RHA varies depending on the combustion conditions such as the burning temperature. In construction material field, rice husk is burned at temperature below 700 °C giving the most suitable properties to be used as supplementary cementitious materials (SCMs) because the possession of high amorphous silica content [1]. RHA shows highly reactive pozzolanic activities which has been increasingly use as supplementary cementitious materials to partially replace with ordinary Portland cement or silica fume (SF) in concrete [1,2]. The work of Ferraro and Nanni [3] showed that the compressive strength and corrosion resistance of the concrete increases associate with the increase in RHA replacement ratio, while the porosity is found to decrease. As state in chapter 1, RHAs have a potential to be used as self-healing additives.

The experimental program nominated 2 classes of RHA; RHA type A (RA) and RHA type B (RB) which has SiO_2 content of 93.5% and 99.66% respectively. RHAs with high SiO_2 content was selected due to their possession of high pozzolanic properties. Therefore, it is expected that self-healing performance of cast-in RHA specimens should be remarkable because the existence of amorphous silica. The secondary electron images (SEI) demonstrate the morphology of RA and RB as shown in Fig. 3.1 and Fig. 3.2 respectively. Fig. 3.1 reveals that RA particles have quite porous structure with various forms of morphology and wide range of particle sizes. Fig. 3.2 shows that RB composes of finer particles, their partial sizes can be approximated in between 1-10 μm.

Fly ash

Fly ash used in chapter 2 was selected because its high CaO content (44.07%). As stated in chapter 2, the dissolved Ca^{2+} could bind with SAP and restrain the initial swelling effect of SAP during mortar mixing [4–6]. In addition, Papadakis [7] mentioned that high calcium fly ash is characterized by a rapid strength

development. Fig. 3.3 shows SEI image of fly ash, showing a perfectly spherical morphology. The chemical compositions and specific properties of cement, fly ash, RA and RB are stated in Table 3.1.

SAP

SAP used in this experiment was sponsored by Nippon Shukubai co. ltd. The specific information of SAP is presented in Table 3.2. It was selected base on the results of preliminary test which was carried out by a simplified teabag method [8]. Teabag is method to quantify amount of absorbent ratio of SAP under different solutions. This study defines suitable SAP for self-healing application using three criteria; (1) has low absorbency in cement pore solution, (2) poses of reswelling capability after expose to water and (3) is capable of releasing and absorbing water in repetition pattern. The water absorption was measured at 10 and 60 minutes after mixing with various solutions. The absorption ratio of SAP in different solution are listed in Table 3.3. According to Fig. 3.4, SAP particles have irregular shapes, and the particle sizes range from approximately 10-500 μm.

Superplasticizer (SP)

Polycarboxylate ether-based superplasticizer was selected among four types of superplasticizer listed in Table 3.3 because its advantage over workability enhancement and capability to restrain initial absorbency of SAP. It has relative density of 1.10±0.03 g/mL and approximate pH 6-8.

Table 3.1: Chemical composition of Portland cement, RHAs and fly ash

Chemical composition (mass%)	Cement	RA	RB	Fly ash
Silicon dioxide (SiO_2)	21.2	93.5	99.66	26.6
Aluminum oxide (Al_2O_3)	5.2	0.09	0.14	10.96
Ferric oxide (Fe_2O_3)	2.8	0.15	0.02	9.05
Calcium oxide (CaO)	64.2	0.74	0	44.07
Magnesium oxide (MgO)	-	0.52	0.01	1.85
Sulfur trioxide (SO_3)	2.0	0.52	0.06	5.36
Alkalis (Na_2O)	0.65	0.16	0.07	-
Chlorine (Cl)	0.004	0.16	0	-
Sum (SiO_2+ Al_2O_3+ Fe_2O_3)	29.2	93.74	99.82	46.61
Density (g/cm^3)		2.14	2	

Table 3.2: Properties of SAP

Material	Apparent density (g/cm^3)	Water absorption (g/g)
SAP	0.7	417

Table 3.3: SAP swelling capacity in solution.

Type	Water absorption (g/g)	
	At 10 min	At 60 min
Distilled water	414	414
RA20 pore solution	21	-
Polycarboxylic ether SP	3.6	3.6
Polycarboxylic acid SP	9.3	9.3
Lignin sulfonate and oxycarboxylate SP	3.9	3.9
Polycarboxylic acid SP	7.7	7.7

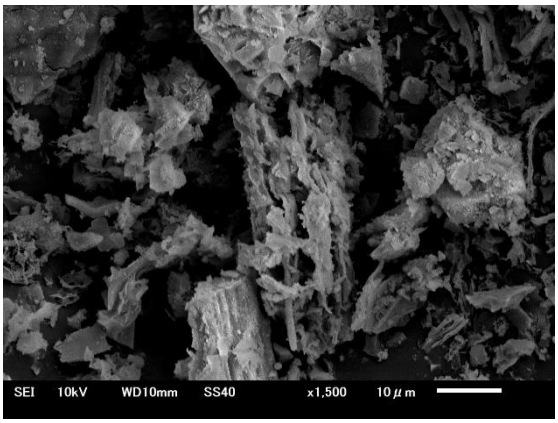

Fig. 3.1: SEM image of RA particles

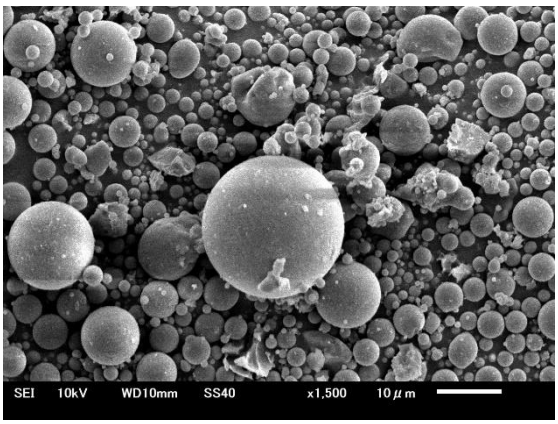

Fig. 3.3: SEM image of fly ash particles

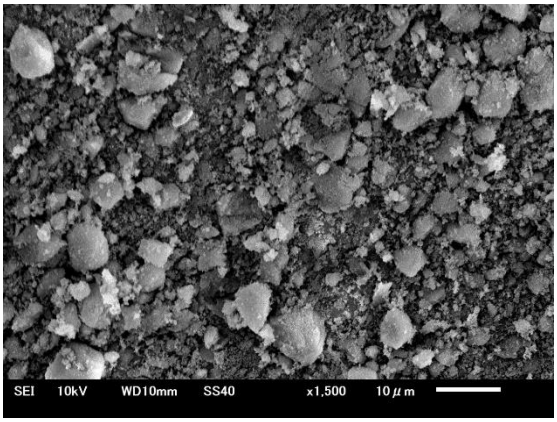

Fig. 3.2: SEM image of RB particles

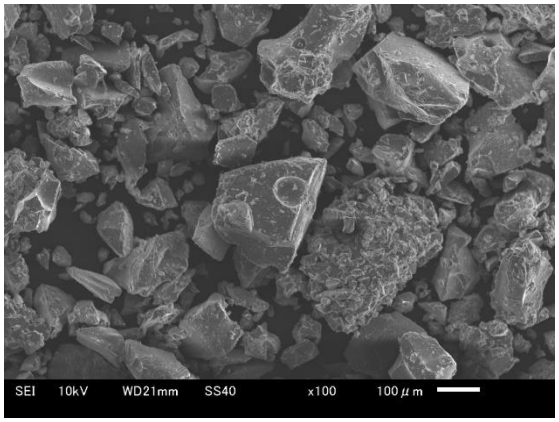

Fig. 3.4: SEM image of SAP particles

3.3 EXPERIMENTAL PROGRAM

Six series of mix proportions of cement mortar were developed by absolute volume. In present of both RHA and SAP, flowability loss is significant. Water-to-binder ratio (w/b) were varied to acquire an adequate flowability of mortar to be casted in cylinder mold. In addition, the amounts of superplasticizer were added to control flow diameter between 162-200 mm measured in accordance with to ASTM C1437, a standard test method for the flow of hydraulic cement [9]. The quantity of water and superplasticizer were determined by conducting many tried mixes. The amount of extra water was added for SAP containing series based on SAP absorbability and workability results from tried mix. The amount of binder and fine aggregate were kept constant at 524.7 kg/m^3 and 1458.8 kg/m^3 respectively. Cement was replaced with either RHA or fly ash at ratio of 20% in mass. High SAP replacement ratio is decent for promoting self-healing and crack sealing [6,10]. Thus, SAP replacement ratio of 3% and 4% by mass of cement were used. The mix design is presented in Table 3.4 where specimens are named after type of replaced binder followed by binder content and SAP replacement ratio respectively. For instance, RA20S4 indicates that 20% of cement is replaced by RHA type A and SAP replacement ratio is 4% by mass of cement.

Table 3.4: Mix proportion of mortar

Specimen	Cement (kg/m^3)	Cement replacement (kg/m^3)	Water (kg/m^3)	Superplasticizer (mass% cement)	Sand (kg/m^3)	SAP (mass% binder)
F00	524.7	0	237	0	1458.8	-
RA20	419.8	104.9	237 + 53.1	2%	1458.8	-
RB20	419.8	104.9	237 + 106.2	3%	1458.8	-
RA20S3	419.8	104.9	237 + 148.6	4%	1458.8	3%
RA20S4	419.8	104.9	237 + 148.6	5%	1458.8	4%
F20S4	419.8	104.9	237 + 77.4	3%	1458.8	4%

a. Specimen preparation

Specimens were prepared using the method mentioned in chapter 2. The preparation process is summarized as shown in Fig. 3.5. Superplasticizer retards the cement hydration which was influenced by a decrease in Ca^{2+}concentration. As Ca^{2+}ions react to carboxyl and hydroxyl group of superplasticizer and subsequently slow down the rate of hydration of alite due to the insufficient of Ca^{2+}[11,12]. To avoid the effects of high dosage of superplasticizer on setting time, the demolding was carried out at 24 hours for non-SAP series and 48 hours for cast-in SAP series. Then the demolded specimens were cured by water immersion for 28 days.

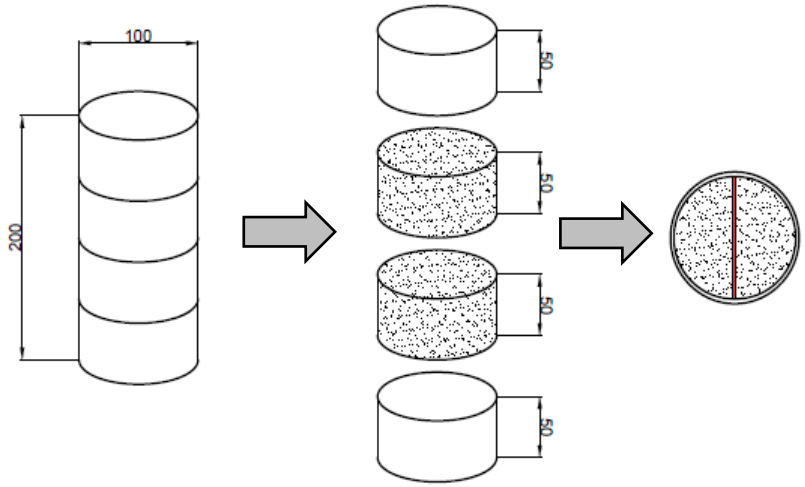

Fig. 3.5: The specimen (labeled) was mounted in a PVC pipe (gray)

b. Exposure environments

Two exposure conditions were used to simulate real environmental exposures condition, considering an availability of water.

- Immersed in water at 40 °C.
- Wet-dry exposure: water was spray onto one side of specimen using water pump with water flow of 3400 liter/hour. Another side of specimen was kept above water level. The spray was continued for 1 day 40 °C and air curing for 1 day each and repeated as loop.

The experimental program divided pre-crack specimens into 4 groups; healing at 0 day (unhealed), 28 days, 56 days and 91 days to investigate self-healing performance at different age. The healing temperature was constantly set at 40 °C to accelerate the hydration of cement and fly ash simulating self-healing performance of concrete in mid to long-term [13,14].

3.3.1 Mechanical properties assessment

a. Compressive strength

The compressive strength test is used to examine effects of SCMs, SAP and superplasticizer on strength development of cement mortar. The compressive strength test was conducted in accordance with ASTM C 39, standard test method for compressive strength of cylindrical specimens [15]. The compressive strength at 28 and 91 were determined by averaging compressive strength values among three specimens.

b. Flow discharge through the crack

Water discharge through the crack is used as an indicator to evaluate crack permeability recovery associated with self-healing activities. The test was carried out periodically during the post-curing stage using the measurement instrument shown in Fig. 3.6. The flow measurement instrument was inhouse developed to supply a constant hydrostatic pressure sufficient to achieve water infiltration throughout the crack. In this chapter, the water head was maintained at 280 mm.

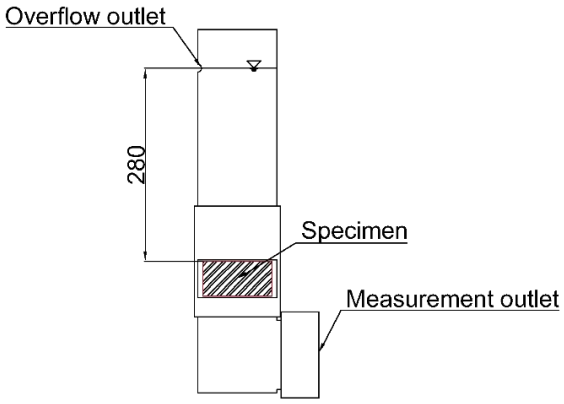

Fig. 3.6: The water discharge measurement instrument

c. Crack closure efficiency

As stated in chapter 2, crack closure efficiency is evaluated in term of crack width reduction compared to its original crack width, and simplified using crack closure ratio. The averaged initial crack widths of pre-cracked specimens were measured by a stereomicroscope, considering 6 measuring points; 3 on the top surface and 3 on the bottom surface. The measuring points were 25 mm apart and 25 mm from the edge of the specimen. At 28 days of healing, the measurement was repeated at the same position. Roig-Flores et al. [16] proposed that the crack closure efficiency can be found according to the relation shown in Eq. (1) .

$$\text{Crack closing ratio} = 1 - \frac{\text{Final crack width}}{\text{Initial crack width}} = 1 - \frac{w_{28}}{w_0} \prec 0 \quad (1)$$

w_0 = Average initial crack width measured at pre-cracking
w_{28} = Average final crack width measured at the 28th day of healing

d. Ultrasonic pulse velocity (UPV)

Ultrasonic pulse velocity test is used to evaluate the uniformity and relative quality of concrete which including the assessment of voids and cracks, and to investigate the quality of crack repairs. In self-healing application, autonomous crack healing influences the transmission time of ultrasonic waves by allowing the waves to proceed through the healing agents in the crack specimen. Therefore, the transmission time decreases as the wave follows the shortest pathway. In this study, the UPV test was conducted on cement

mortar using indirect method at undamaged stage, and at healing time of 0 day (pre-cracked stage), 28 days, 56 days and 91 days. Therefore, the internal changes in concrete can be identified. The measuring spots were marked at 20 mm on both side from crack measuring location, and the distance between transmitting node and receiver node was kept constant at 40 mm. Three measuring points were picked and the velocity of ultrasonic pulse traveling through mortar were averaged. The relation between ultrasonic pulse transmission time and velocity is established as shown in Eq. (2).

$$V_p = \frac{L}{\Delta t} \quad (2)$$

V_p = Ultrasonic pulse velocity (km/s)

L = Distance between receiving and transmission transducer

Δt = Transmission time (s)

3.3.2 Microstructure and physicochemical analyses

a. Scanning electron microscopy (SEM)

SEM was used to image the morphology and EDS (Energy-dispersive X-ray Spectroscopy) was used to analyze element compositions of the hydrated products of healed specimens. The samples were collected at the cracked zone of the specimen and trim into a 5 mm ×5 mm ×5 mm cube. Then treated in oven at approximately 50 °C for 24 hours. To minimize effect of carbonation, the treated samples were kept in a desiccator until the time of the analysis. The samples were divided into 2 series while the additional treatments were applied to increase the image quality. In the first series, samples were polished and epoxy-impregnated to investigate properties of ITZ and enhance the precision of EDS results. Mostly, polished samples were investigated by backscattered electron composition (BEI) while the beam energy between 10-15 kV was set as the operating condition. In the second series, samples were gold impregnated, these samples were used to observe and identify materials morphology. The accelerating voltage of 10 kV for EDS analysis and 20 kV for SEI (Secondary electron image) were set the operating condition while working distance was fixed at 10 mm for all analysis.

b. Thermogravimetric/differential thermal analysis (TG/DTA)

Thermogravimetric/differential thermal analysis (TG/DTA) was used to analyze newly hydrated materials found at the sealed crack. The mortar around the crack was collected to prepare cement powder. The cement powder with particle size of passing 100 μm sieve was obtained using a planetary ball mill set at 450 rpm. The temperature program was applied using a constant heating rate of 10 °C/min rising to 1000 °C; aluminum oxide was used as a reference material. The mass loss due to the decomposition of materials that occurred with increasing temperature was recorded at the below temperature range.

- The evaporation of free water and partially breaking down of bound water occur around 30 - 120 °C [17,18].
- The decomposition of carboaluminate hydrates occur around 110 – 170 °C; consist of decomposition of gypsum, ettringite and chemically bound water [17,18].
- The decomposition of C-S-H and carboaluminate hydrates occur around 180 - 300 °C [17,18].
- The amount of portlandite ($Ca(OH)_2$) was determined by the mass change at approximately 450-550 °C, as portlandite transforms into CaO and H_2O [18,19].

- The amount of calcium carbonate or calcite ($CaCO_3$) was obtained through mass change during decarbonation that occurs around 650-900 °C [18,20].

Based on the molecular mass of portlandite (MW_{CH}), the molecular mass of water (MW_{H_2O}) and the mass loss in percentage which occurs from dehydration of CH ($\%\Delta W$). The amounts of compounds were obtained as shown in Eq. (3).

$$CH(\%) = \%\Delta W \times \frac{MW_{CH}}{MW_{H_2O}} \quad (3)$$

Likewise, by considering decarbonation reaction shown in Eq. (4), the amount of calcite is calculated by the relation shown in Eq. (5); where $\%\Delta W$ is to the mass loss in percentage which occurs from decarbonation, MW_{CaCO_3} is molecular mass of calcite and MW_{CO_2} is the molecular mass of carbon dioxide.

$$CaCO_3 \rightarrow CaO + CO_2 \quad (4)$$

$$CaCO_3(\%) = \%\Delta W \times \frac{MW_{CaCO_3}}{MW_{CO_2}} \quad (5)$$

In addition, by considering the mass loss at approximately 50 ℃ - 550 ℃, chemically bound water can be estimated using Eq. (6) [21]; where M_{50} is mass of sample at 50 ℃ and M_{550} mass of sample at 550 ℃.

$$BW(\mathrm{g}/100\mathrm{g}) = \frac{(M_{50} - M_{550})}{M_{550}} * 100\mathrm{g} \quad (6)$$

3.4 RESULTS AND DISCUSSION

3.4.1 Rheological behavior

The results suggested that a significant reduction in flowability was found either in presence of RHAs or SAPs. RHAs absorb water through its porous structure whereas SAP is capable to store up 400 g of water per gram. This evidence suggested that both additives responsible for a withdrawal of free water from the mix. Therefore, it directly affects to the rheological properties of the fresh mix. The results of flow diameter are presented in Table 3.5.

To overcome this limitation, the experimental program was designed to compensate the workability loss by adding extra water and superplasticizer (SP) to achieve a control flow diameter at approximately at between 162-200 mm. The designed flow diameter was controlled to obtain an adequate flowability sufficient to fill into the casting mold with the minimal air void. According to the preliminary results, the technique of adding extra water and SP needs to be implemented with a great care as it could cause negative effects toward mortar properties such as bleeding and segregation. Mechtcherine et al. [4] suggested that SAP absorbability is not a constant value. In concrete, SAP absorbability is influenced by various factors, generally found to increase linearly until SAP reach its maximum swell capacity before SAP releases some of its absorbed water later. It is expected the effective w/b ratio of cast-in SAP specimens can be changes overtime. In most cases, it affects rheological behavior of fresh mortar. As stated in section 3.2, Polycarboxylate ether-based superplasticizer was selected because its advantage on workability enhancement and capability to restrain the initial absorbency of SAP. Therefore, in SAP-containing specimens, high quantity of superplasticizer was applied to minimize the initial swelling of SAP.

Table 3.5: Flow diameters

Specimen	Flow diameter (mm)	Flow diameter difference compared to F00 (%)	Extra water added (kg/m^3)	Superplasticizer (%mass binder)
F00	181	0	-	-
RA20	200	+10.5	53.1	2%
RB20	163	-9.9	106.2	3%
RA20S3	188	+3.9	148.6	4%
RA20S4	173	-4.4	148.6	5%
F20S4	158	-12.7	77.4	4%

According to SEM images, RB showed a significant higher surface areas and material finesse compared to that of RA. Since that RB20 needs higher dosage and of extra water and superplasticizer to attain the control flow diameter compared to that of RA20. In contrast, fly ash showed a positive effect on rheological properties enhancement as F20S4 needed 1% of superplasticizer and 71.2 kg/m^3 of water less than that of RA20S4. It is worth mentioning that because fly ash has smooth and spherical surface which help to improve workability. The advantage of fly ash on workability improvement is in a good agreement with many studies.

3.4.2 Strength development

Compressive strength at 28 days and 91 days are presented in Fig. 3.7. At 28 days, F00 had compressive strength of approximately 55 MPa which is the highest compared to other specimens. It is expected that because F00 was the only series without the partial replacement of supplementary cementitious materials. Younes et al. [22] stated that C_3S (alite) from cement particle spontaneously reacts with water and produces calcium silicate hydrate (C-S-H) gel contributing to strength development.

Among specimens that partially replaced with SCMs; RA20 had 28^{th} days compressive strength of 30.9 MPa followed by 26 MPa and 20.9 MPa in RB20 and F20S4 respectively indicating that RHAs greatly contribute to strength development compared to fly ash despite they are used in specimens with higher w/b ratio. Meanwhile, the strengths of cast-in SAP specimens were found to be lower than those of non-SAP series. This is because two reasons; First, the extra water is added to mitigate workability reduction which also increases w/b ratio. Second, the presence of SAP in fresh mixing produces SAP pore which is produced by the initial swelling of SAP.

At 91 days, all specimens showed a notable increase in compressive strength compared to each of that series at 28 days. F00 presented the greatest compressive strength of approximately 59.5 MPa, the gaining strength is account for about 6.9 % respected to F00 at 28 days. Fig. 3.8 discloses the compressive strength increase respect to the compressive strength of the same specimen at 28 days. In term of gaining strength, RA20S4 attained the most significant increase which is about 20.6% increase followed about 12% increase in F20S4 whereas RB20 gained the least strength increase after 28 days of hydration. Still, RB20 was influenced by a quick initial strength development which is clearly noticeable at early age.

The benefits of RHAs on compressive strength development is explained by two reasons [1,23–25]. First, a significant amount of reactive amorphous silica is found in RHAs which improves the mortar compressive strength through the progressive of pozzolanic reaction. Second, RHAs enhance internal curing as their porous structures act as water entraining material. In addition, it is worth mentioning that the increase in compressive strength was observed in specimens stored in the air and the increase was notable when SAP replacement ratio was increased. For example, RA20S4 developed lower compressive strength at 28 days respected to RA20S3 but it showed a greater improvement in final strength at 91 days. The evidence emphasis that the strength improvement at later age occurred because the effect of comprehensive curing from SAP and the presence of SCMs.

The use of RHAs as cement replacement material contributed to higher strength development compared to fly ash at all curing stages. In contrast, it is proposed that the hydration duration of 91 days was insufficient for observing specimen with supplementary cementitious materials to develop higher compressive strength than the ordinary cement mortar. The lower in final strength is potentially affected by either an inadequate hydration time or an insufficient amount of portlandite. There is a possibility that RHA may contain excessive amounts of reactive silica causing all available portlandite to be reacted. Therefore, unhydrate silica leftovers because lacking of its coupling substrates [26]. The amount of the portlandite content in each specimen will be discussed in TG/DTA section. Moreover, the reactivity of pozzolanic reaction in each SCMs and efficiency of mix proportion design should be considered in detail and more investigation is necessary.

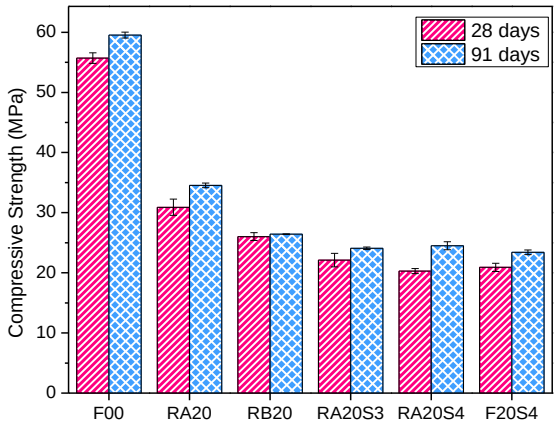

Fig. 3.7: Strength development of mortar specimens at 28 days and 91 days.

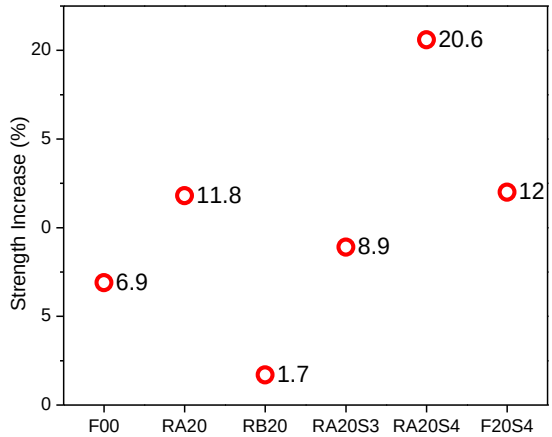

Fig. 3.8: The compressive strength at 91 days respected to the compressive strength of the same specimen at 28 days.

3.4.3 Crack permeability

The volume of water discharge through a crack was demonstrated in Fig. 3.9-3.14. SAP-containing series exhibited about 50% lower of water flow compared to non-SAP series. The lowest averaged initial flow of approximately 150 mL/min was found in F20S4, whereas RA20S4 had the second lowest averaged initial flow value of approximately 230 mL/min. The noteworthy reduction of water flow in the first measurement was contributed by the crack sealant effect of the swollen SAP which was achieved instantaneously after water exposure. Chindasiriphan et al. [6] suggested that after SAP reaches its maximum swelling volume, the self-healing progress is governed by hydration of cement paste and pozzolanic reaction. In contrast, RA20S3 had quite high initial flow rate which could be presumed that the SAP swelling effect on permeability recovery was inefficient.

In non-SAP series, the higher initial flow through cracks were observed. F00 had initial flow rate of about 375 mL/min meanwhile RA20 and RB20 had initial flow of 330.6 mL/min and 272.9 mL/min respectively. In contrast, F00 showed a notable reduction of water discharge reduction during first eight days. After eight days of monitoring, F00 had almost the least water discharge decreasing rate compared to other specimens. This is because the self-healing due to the reaction of unhydrate cement particles can react very rapidly however it is only feasible at early age. This is in good agreement with other researches who mentioned that a rapid self-healing activities at early age is applicable by the hydration of non-hydrated cement paste [6,27,28]. In contrast, specimens that were partially replaced cement with supplementary cementitious materials showed a slower water discharge reduction at the beginning of monitoring period, but the rate of water flow reduction was gradually increase and greater at later age compared to the ordinary cement mortar. This is because they have quite low cement proportion meanwhile the pozzolanic reaction is progressive with time.

An inconsistence pattern of water flow through a crack was observed in specimens exposed to wet-dry cycled. Particularly for F00_WD which had a much lower flow reduction rate compared to that of F00. The flow through crack of F00_WD increased when the measurement was performed after the dry exposure. The similar results can be observed in cast-in SAP specimens. The evidences suggested that the oscillation in water flow occurred from shrinkage of SAP and shrinkage of other hydrated products due to an inadequate moisture supply.

However, the oscillation in water flow through crack was mitigated in case of RA20_WD and RB20_WD which suggested that RHAs potentially act as water entraining agent. The theory on effect of water-entrain admixture on self-healing performance is established and confirmed by the testing results from SAP containing specimen, as the vibration of water discharge curves were insignificant. Although SAP may be subjected to the decrease in osmotic pressure in dry healing stage, but the results suggested the vibration in water flow through a crack were mitigated ever further because the coupling effects of RHAs and SAP. In dry healing stage, water-entrained admixtures facilitate hydration by discharging theirs absorbed moisture and liquid providing for unhydrate-particles. Thus, self-healing activities can be continued in low relative humidity and subsequently promotes permeability reduction by the development of a permanent self-healing products emerging to seal the crack. The function of SAP to discharge its absorbed solution incorporated with an increasing self-healing degree is found elsewhere [4–6,8,10,29]. Moreover, Tuan et al. claimed that the discharged solution from RHA has a potential to enhance pozzolanic reaction due to ion induction between the free Ca^{2+} and silica ions from RHA particles [23].

The final flow is defined as the water flow through a crack measured at 28 day of healing. F00 presented a final flow of 95.4 mL/min which is about 2 times lower compared the same specimen healed under wet-dry

cycle. A significant higher final flow in specimens healed under wet-dry exposure than that of specimens healed under water immersion were also observed in case of RA20 and RB20.

In contrast, RA20S3, RA20S4 and F20S4 showed similar value of the final flow in all of exposure conditions. RA20S4 and F20S4 show a substantial low final flow value. It is explained that SCMs improve crack permeability recovery due to development of pozzolanic reaction [30]. From the results, it is suggested that fly ash is the most suitable self-healing additive compared to RHAs. Papadakis [7] suggested that high calcium fly ash reacts rapidly with water to produce a significant amount of portlandite. The rich in portlandite subsequently enhance hydration progress of the tricalcium aluminate which exist in high calcium fly ash. Moreover, the existence of other compounds, excluding silica, leads to additional gain of bound water content and reduction of porosity with time. The presence of water-rich and pore- filling ettringite at early age is then converted to other hydrate products generate significant impact on enhancing hydration and reduction of porosity. Therefore, self-healing performance at early age is attributed by high calcium fly ash. It is concluded that self-healing by mean of permeability recovery can be maximized through the coupling effect of fly ash and SAP. In consideration of other SCMs, RB contributes to a greater self-healing performance compared to RA.

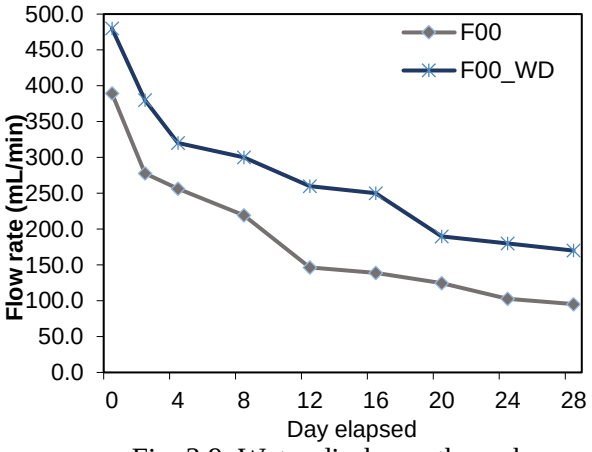

Fig. 3.9: Water discharge through cracks for F00 and F00_WD

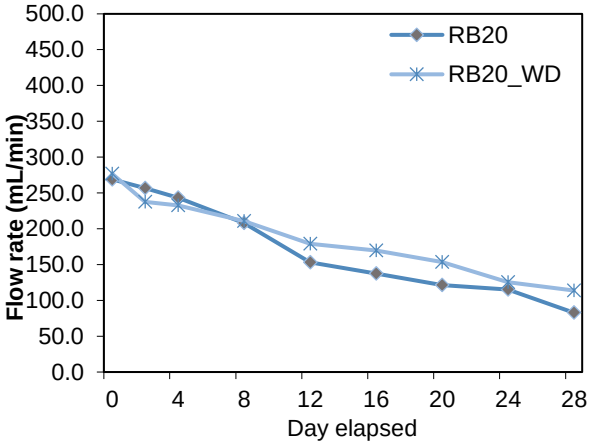

Fig. 3.11: Water discharge through cracks for RB20 and RB20_WD

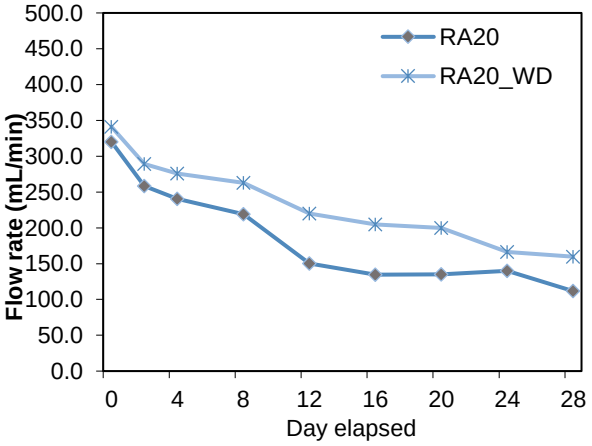

Fig. 3.10: Water discharge through cracks for RA20 and RA20_WD

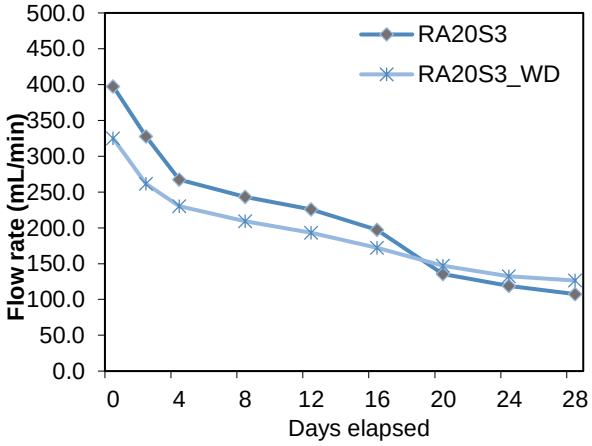

Fig. 3.12: Water discharge through cracks for RA20S3 and RA20S3_WD

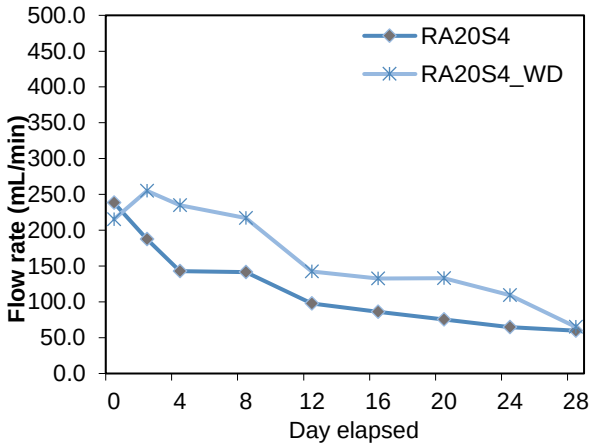

Fig. 3.13: Water discharge through cracks for RA20S4 and RA20S4_WD

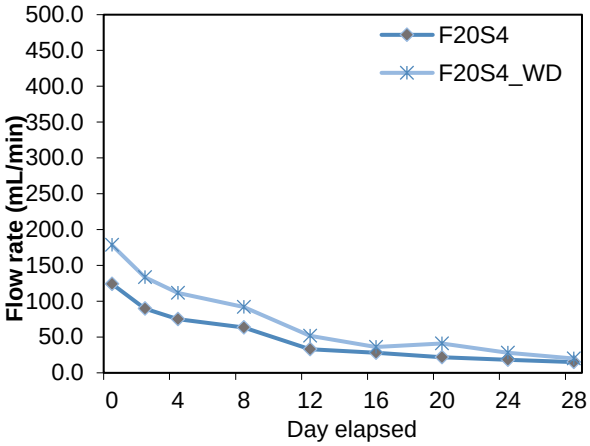

Fig. 3.14: Water discharge through cracks for F20S4 and F20S4_WD

3.4.4 Evaluation of autogenous crack repair

3.4.4.a Crack closure by mean of visual inspection

Crack widths of healed specimens at 28 days of healing were examined. One of self-healing indicators is crack closure defined as a temporal crack width reduction compared to the crack width before healing. The measurement was performed using a stereomicroscope. The results are demonstrated using crack closing ratio as derived from Eq. (1). The cracking load of 22-42.4 KN were used to produce the control crack. The control crack widths were targeted in between the range of 0.19-0.27 mm. The experimental results on an initial crack width, final crack width and crack closure ratio are summarized in table 3.6. According to the results, cracking loads have a direct variation to the compressive strength. However, in case of F20S4 and F20S4_WD; specimens needed a remarkable higher superimpose cracking load respected to compressive strength of those specimens. Crack closure was generally seen in all specimens regardless of healing conditions. It is observed that the crack closure occurs from the accumulation of white precipitated materials filling into the crack space. The examples of healed crack at 28 days are presented in Fig. 3.15-3.18. The white precipitation is appeared to be calcium carbonate which develops by the reaction between dissolved $Ca(HCO_3)_2$ and calcium hydroxide from the cement mortar or progress of carbonation [31].

Among specimens that healed in water, F20S4 has the smallest averaged final crack closure of 0.01 mm and crack closing ratio of 0.95. The higher value in crack closure ratio represents better crack closing efficiency. The crack closure ratio is range from 0.95 in F20S4, while the second highest is RA20S3 showing a ratio of 0.67 whereas RB20, RA20S4, F00 and RA20 has a crack closure ratio of 0.65, 0.63, 0.50 and 0.46 respectively. The crack closure results suggested that SAP has insignificant effects on crack closure performance for specimens healed under water, considering the saturation of water in cementitious matrix. However, SAP-containing series had a slightly higher degree of crack closure respected to non-SAP series. It is expected that the presence of SAP may enhance self-healing performance in term of chemically reactive material. In addition, most of specimens that partially replaced with SCMs had superior crack closing ratio compared to control specimen. Meanwhile a notable rise in crack closing ratio was influenced by the existence of fly ash. In particular F20S4 had a significant increase in crack closure ratio because the deposition of calcium carbonate at crack in a remarkable amount. This evidence highlighting the advantage of fly ash on crack closure efficiency. While it remains unclear for benefit of RA and RB over closure performance as their crack closure efficiency was found slightly higher compared to that of control cement

mortar. This may occur either due to materials have low self-healing efficiency or an insufficient healing time.

Table 3.6: Cracking load and crack closure ratio at 28 days of curing

Type	Cracking load (KN)	Initial crack (mm)	Final crack (mm)	Crack Closing Ratio
F00	42.4	0.22	0.11	0.50
F00_WD		0.23	0.2	0.13
RA20	24.8	0.24	0.13	0.46
RA20_WD		0.21	0.19	0.10
RB20	22.0	0.20	0.07	0.65
RB20_WD		0.20	0.17	0.15
RA20S3	26.2	0.24	0.08	0.67
RA20S3_WD		0.26	0.19	0.27
RA20S4	24.6	0.19	0.07	0.63
RA20S4_WD		0.27	0.19	0.30
F20S4	37.6	0.21	0.01	0.95
F20S4_WD		0.23	0.10	0.57

The specimens healed under wet-dry condition showed a much lower crack closing performance compared to same specimen healed under water. This evidence confirmed a necessary of water to provoke self-healing activities. In wet-dry exposure series, the self-healing products are densely deposited at the outlet side of the crack. The results are confirmed by of Snoeck et al. [29], Wu et al. and [32] Yang et al. [33] who mentioned that deposition of hydrated products at outlet side was caused by leaching and the deposition of washing out materials such as calcium carbonate, spalling-off debris particles in cement matrix including the wash out of hydration products. In some specimens, although a completed crack closure was found at water outlet side of crack, but the inlet side of crack showed a significant lower crack closure. Therefore, the obtained crack closure ratio was significant lower respected to that of the same specimen healed under water submersion. In wet-dry exposure, F20S4_WD has the highest crack closure ratio which draw an attention to benefit of fly ash on self-healing enhancement whereas the benefit of SAP on crack closure associated with a comprehensive curing was well discussed in section 3.4.3.

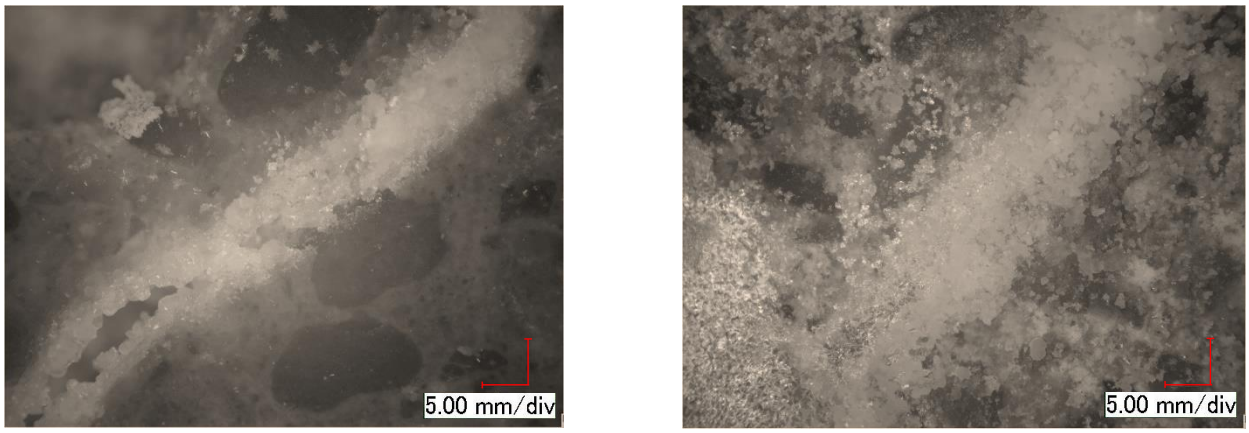

Fig. 3.15: Healed crack of F00 (left) and F00_WD (right)

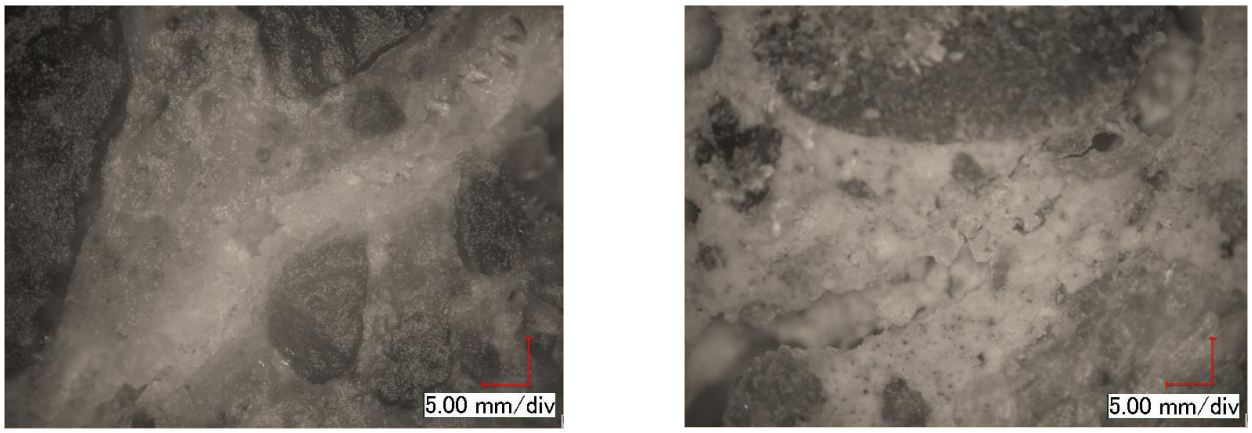

Fig. 3.16: Healed crack of RB20 (left) and RB20_WD (right)

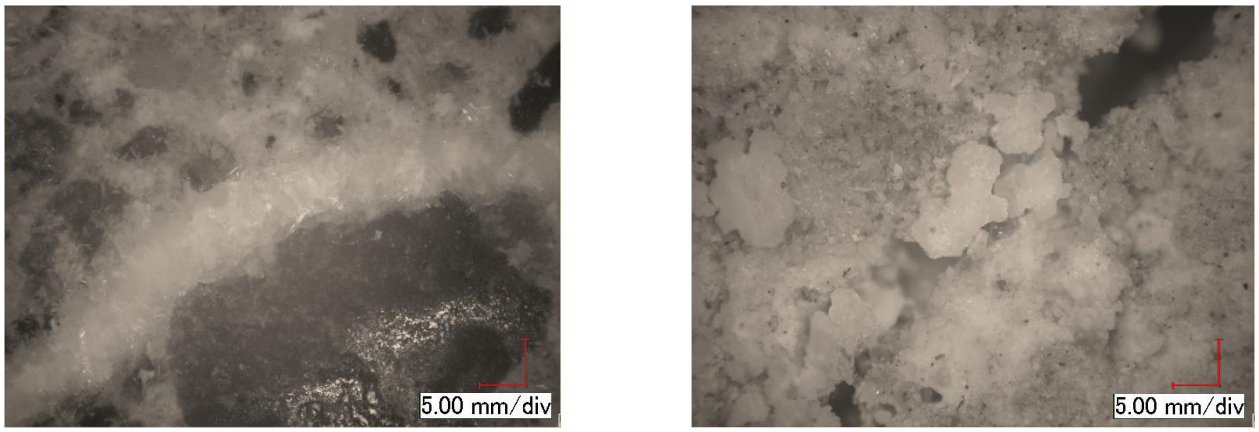

Fig. 3.17: Healed crack of RA20S4 (left) and RA20S4_WD (right)

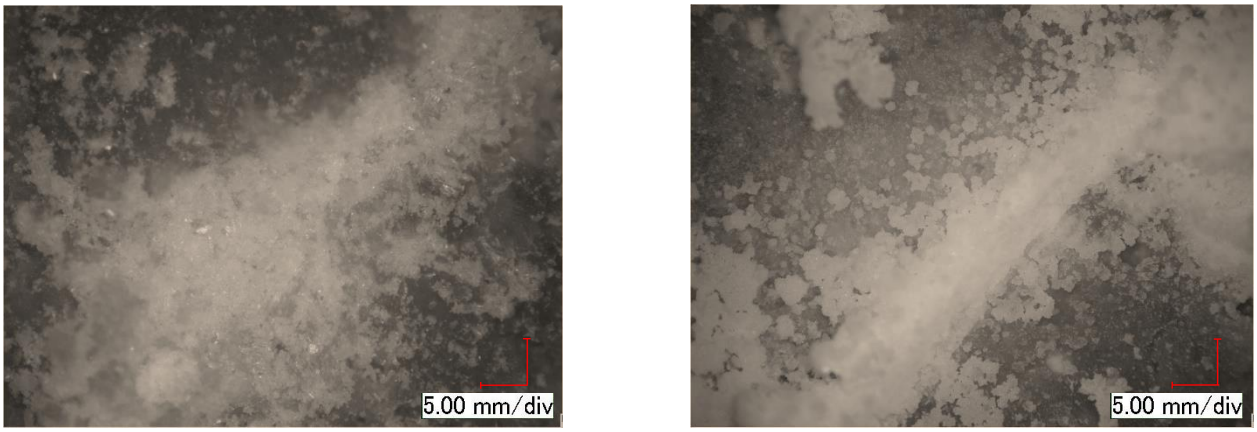

Fig. 3.18: Healed crack of F20S4 (left) and F20S4_WD (right)

3.4.4.b Crack closure and internal changes by mean of ultrasonic pulse velocity

Ultrasonic pulse velocity (UPV) is a non-destructive testing method used to investigate the internal defects of concrete such as cracks, delamination, and/or honeycombs including its application to predicting concrete strength. UPV test also capable of determining self-healing efficiency through assessment of the quality of crack repairs, considering the reduction of ultrasonic waves transmission time. In general, crack formation was characterized by an increasing in ultrasonic pulse transmission time as the wave cannot travel through the crack. Crack closure reduces the transmission time by allowing the waves to transmit through the healing agents. Thereby, a reduction in transmitting time can be used to indicate self-healing performance.

The results of ultrasonic pulse transmission time measured in cement mortar at different healing ages are presented in Fig. 3.19-3.20. The UPV test performed on undamaged specimens showed that the wave transmitting time is an inverse function of the compressive strength of specimen. The results show that undamaged specimens had transmitting times between 7.5 – 13 μs. After a single crack was generated (0 day), transmitting times were significantly increased to 29.5 - 44.2 μs. The increase in transmitting time caused by the prolonged traveling distance as ultrasonic pulse makes a detour to avoid the crack.

A notable reduction in UPV transmitting times were found in all specimens at healing duration of 28 days. The results suggested that a progress of self-healing occurred at a significant rate at the beginning of healing course. Particularly, specimens that fully submerged in water had healed transmitting times ranged between approximately 16.3 - 27.6 μs whereas healed transmitting times of specimens exposed to wet-dry cycle were measured in between 21.4 - 31.2 μs. Tittelboom et al. claimed that the healed crack is characterized by the decreasing of transmitting time as ultrasonic wave travels through a shortest path including through crack filling materials [34]. The relation of between ultrasonic pulse velocity transmitting duration and transit length are established in Eq. (2). In F00 and F00_WD, specimens showed almost no decrease in transmitting time after 56 of healing. The results confirmed that self-healing due to unhydrate cement paste was limited to young concrete. In contrast, a notable decrease in transmitting times after 56 days were observed in all specimens that contain SCMs. Since the direct relation between compressive strength and transmitting time is confirmed [35], it is expected that the progressive of self-healing activities potentially contributes to the recovery of mortar compressive strength. At 91 days, the minimum transmitting time is approximately 11.3 μs in RA20S3 which is almost equal to that of undamaged RA20S3. It is highlighted that RHAs containing specimens showed slightly better transmitting time reduction compared to that of fly ash containing specimens. It suggests that pozzolanic reaction in RHAs is greater than fly ash at later age which also indicates higher capability of compressive strength recovery.

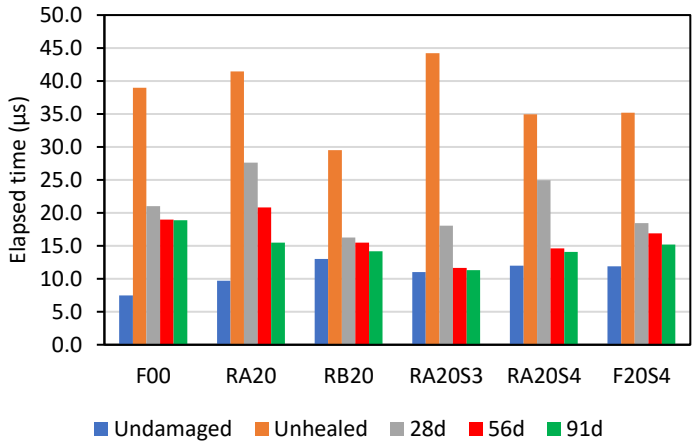

Fig. 3.19: Travel time of ultrasonic pulse of specimens healed under water

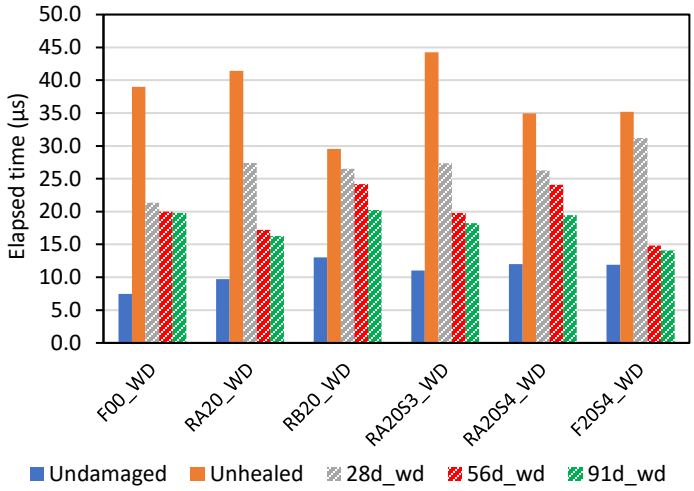

Fig. 3.20: Travel time of ultrasonic pulse of specimens healed under wet and dry exposure.

3.4.4.c. The relationship of ultrasonic pulse and crack closure

The relationships between crack width and ultrasonic transmitting time are presented in Fig. 3.21. The results showed that pre-cracked specimens (0 day) has UPV transmitting times about 30-45 µs. The transmitting times showed a wide range of variation which may cause by either uniform pattern of crack or external factors such as the variation in porosity in each cement mortar. However, the UPV results are reliable enough to assess the internal damage level and the changes influenced by autogenous healing.

Fig. 3.21b demonstrated relationship between wave traveling time and healed crack width at 28 days of healing. The transmitting time at 28 days of all specimens were found to decrease. The mean value of transmitting time at 28 days of healing was about 20.8 µs which accounted for 50% decrease compared to the mean value of transmitting time measured at 0 day. The results suggested that there is a direct variation between a decreasing in crack width and transmitting time which was affected by crack closure as mentioned in section 3.4.4.b. Cast-in RA specimens presented the most notable reduction in traveling time. However, at healing duration of 28 days, there were no specimens which had lower ultrasonic traveling time compared to undamaged specimen.

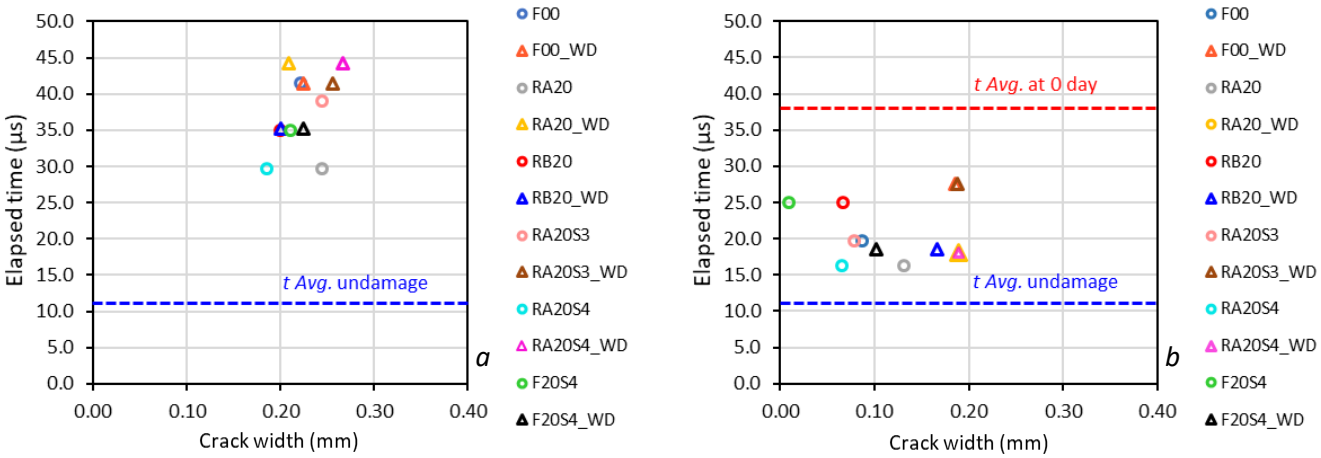

Fig. 3.21: The correlation between wave traveling time and crack width at 0 day of healing (a) and at 28 days of healing (b)

In contrast, healing under wet and dry condition showed that lower water supply has no significant effects on the recovery of traveling time. However, it should be noted that the wave transmitting time was ineligible to accurately confirm the crack closure. For example, F20S4 showed nearly 100% crack closure, but the time that ultrasonic travel through F20S4 was slightly higher than the averaged elapsed time of RA20S4 and RA20. It is presumed that alongside crack closure effect; the wave traveling time is influenced by development of mortar pore structure as well as the density of hydrated products. Therefore, it is suggested that the healing products of RA is denser than that of fly ash. However, more details investigation is required in the future experiment.

3.4.5 Thermogravimetric analysis of self-healing performance

Thermodynamic analysis was used to investigate the chemical phases presence in cement mortar at different healing ages. The TG and DTG curves of specimens at hydration time of 0, 28, 56 and 91 days are exposed in Fig. 3.22-3.28. A shift in DTG peaks demonstrated a transformation of the phase composition. At different healing stages, differences among chemical system are noticeable. In general, DTG profile shows a significant mass loss below 100 °C except in case of F00, indicating that there is a significant amount of free water evaporated from testing samples. Out of all samples, RB20 presented the most significant loss in free water. Therefore, it can be clarified that RB had a notable high absorptivity although all samples were oven-dried at 50 °C for 24 hours before the time of analysis. The results also showed that samples are strongly influenced by leaching. This is evident from the content of portlandite. Therefore, it seems reasonable that the contents of bound water and portlandite do not increase with increasing time. Also, the unhydrated cement tends to react during healing, these contents will be compensated by leaching. The effect of leaching is confirmed by a reduction of chemical bound water as the significant decrease was observed with time. The effect of leaching can be clearly observed in F00 at 91 days of healing as the peaks of AFt/AFm phases are disappeared. However, in SCMs containing series, the reduction of portlandite can be altered by the progressive pozzolanic reaction, producing C-S-H. A shift in DTG peaks are observed at approximately at approximately 450 °C which represents the decomposition of portlandite follows by a shift at approximately 500 °C observed in all SAP containing specimen. It is presumed that the mass loss at the second shift occurred due to the decomposition of SAP particles. This is in good agreement with Lee et al. [5] who suggested that at such a temperature range, SAP is converted to a liquid substance, and disperses into the cement paste. Then the third distinctive peak is observed at approximately 700 °C, representing the mass loss due to decarbonation reaction. The specific content of bound water, portlandite and calcite are estimated as shown in table 3.7.

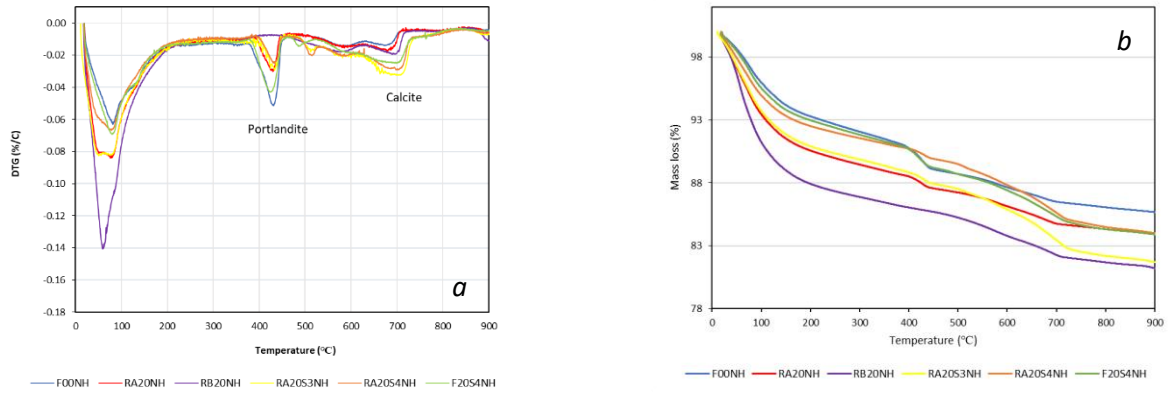

Fig. 3.22: Results of specimens healed for 0 day (a) DTG curves for portlandite and calcite (b) TGA curves for powder fired to various temperature regimes.

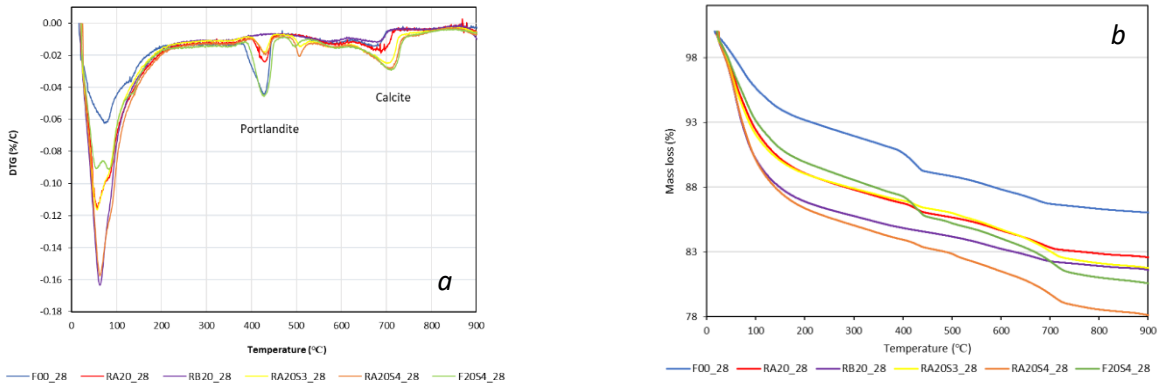

Fig. 3.23: Results of specimens healed for 28 day in water (a) DTG curves for portlandite and calcite (b) TGA curves for powder fired to various temperature regimes.

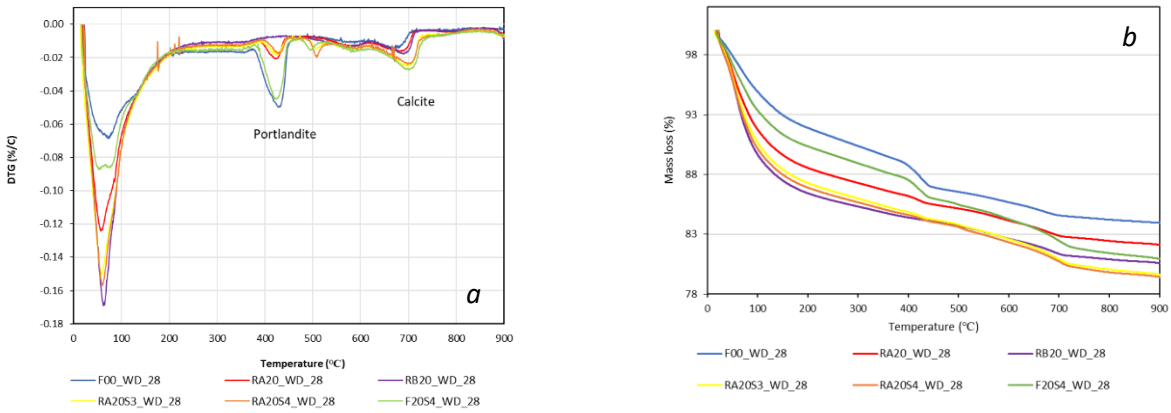

Fig. 3.24: Results of specimens healed for 28 day in wet-dry conditions (a) DTG curves for portlandite and calcite (b) TGA curves for powder fired to various temperature regimes.

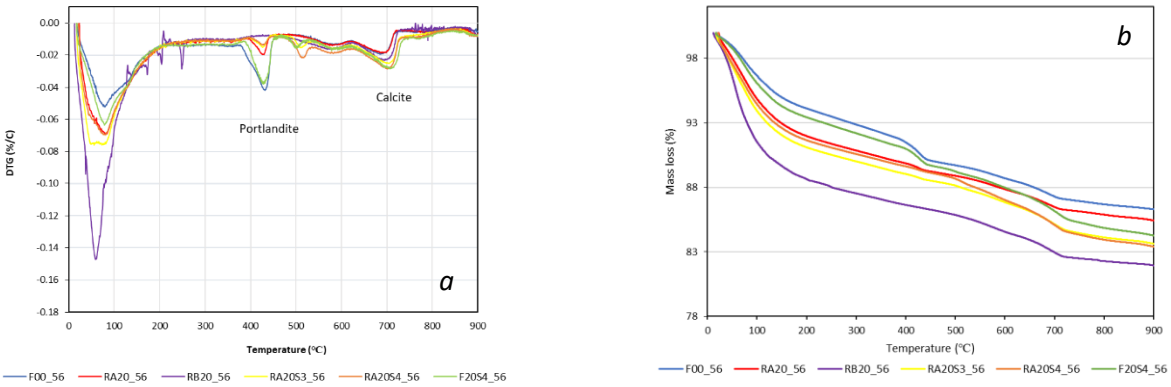

Fig. 3.25: Results of specimens healed for 56 day in water (a) DTG curves for portlandite and calcite (b) TGA curves for powder fired to various temperature regimes.

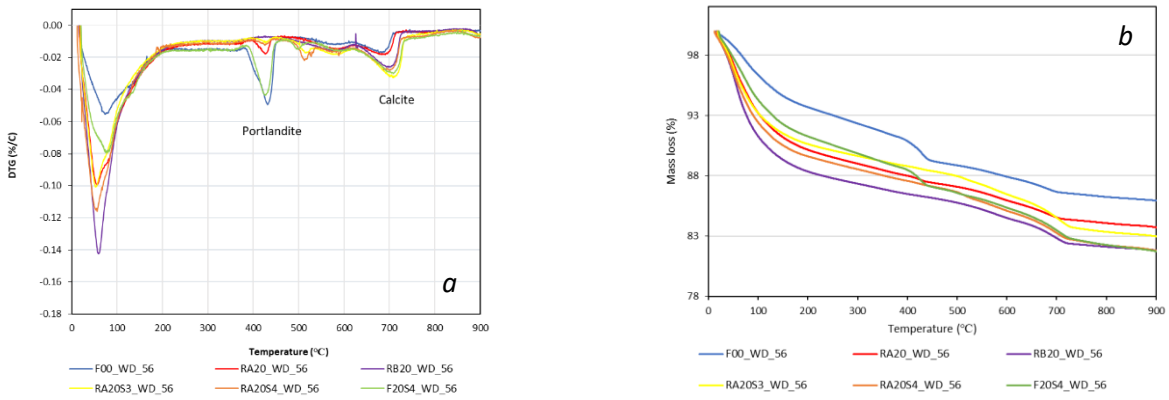

Fig. 3.26: Results of specimens healed for 56 day in wet-dry conditions (a) DTG curves for portlandite and calcite (b) TGA curves for powder fired to various temperature regimes.

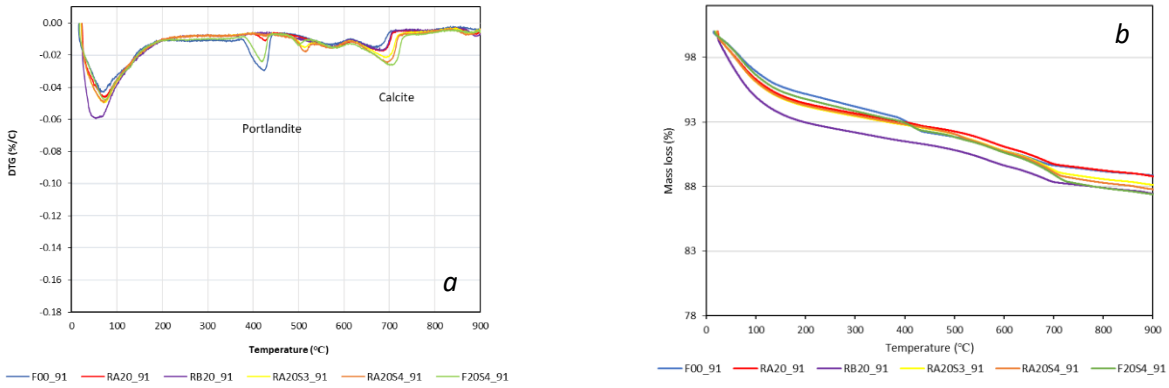

Fig. 3.27: Results of specimens healed for 91 day in water (a) DTG curves for portlandite and calcite (b) TGA curves for powder fired to various temperature regimes

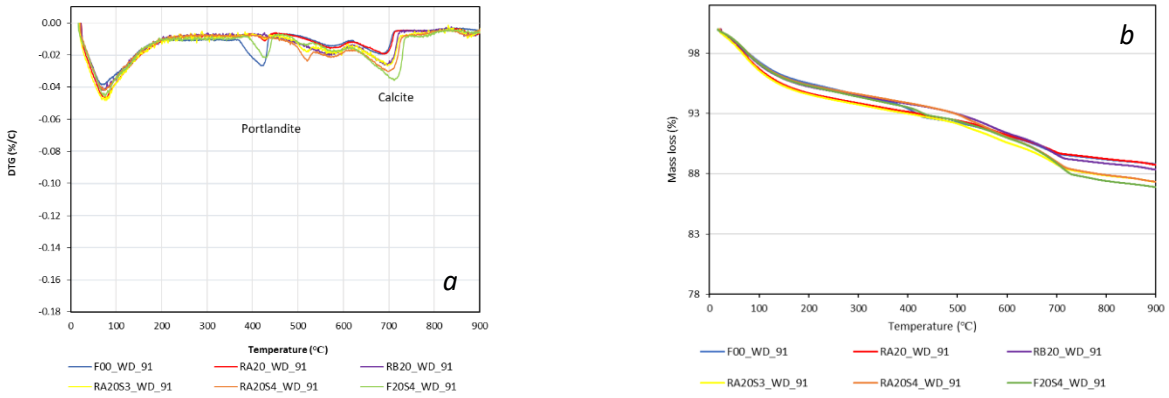

Fig. 3.28: Results of specimens healed for 91 day in wet-dry conditions (a) DTG curves for portlandite and calcite (b) TGA curves for powder fired to various temperature regimes

TG results exposed that the mass loss of samples was significantly higher when specimens were healed in short healing period. At 0-56 days, F00 showed the lowest mass loss when sample subjected to the increasing temperature. Kang et al. [1] suggested that the loss in mass is influenced by the combustion of

unburn organic materials. Although the greater mass losses are observed in SCMs containing specimens, the rate of loss in mass decreased particularly after specimens were healed for 91 days. However, the further investigation is required to fully understand the ignition loss incorporated with healing time variables.

Table 3.7: Content of BW, CH and calcite.

Specimen	Phase	Time elapsed (days)						
		0	28	56	91	28wd	56wd	91wd
F00	BW (g/100g)	11.75	11.24	10.8	8.14	13.7	11.65	7.95
	Portlandite (%)	7.26	6.41	7.12	4.70	8.40	7.41	9.12
	Calcite (%)	3.55	3.40	4.58	3.63	3.32	3.79	4.42
RA20	BW (g/100g)	12.02	13.96	10.81	7.23	14.0	12.31	7.51
	Portlandite (%)	3.13	2.56	1.57	1.14	1.71	1.42	1.14
	Calcite (%)	4.03	4.03	4.50	4.19	3.87	4.26	4.58
RB20	BW (g/100g)	14.27	15.08	13.29	8.02	15.2	13.09	7.3
	Portlandite (%)	0.00	0.00	0.00	0.00	0.00	0.00	0.00
	Calcite (%)	4.82	3.00	5.13	3.95	3.95	5.37	5.76
RA20S3	BW (g/100g)	12.14	13.29	11.28	7.57	15.6	11.17	8.01
	Portlandite (%)	2.56	1.57	1.14	0.00	1.14	0.85	0.00
	Calcite (%)	8.37	5.92	6.16	4.97	5.76	7.11	6.16
RA20S4	BW (g/100g)	10.39	17.41	11.1	7.64	15.7	12.55	7.7
	Portlandite (%)	2.42	1.85	1.14	0.00	1.71	1.14	0.00
	Calcite (%)	7.58	6.63	6.95	5.61	5.61	6.48	7.26
F20S4	BW (g/100g)	11.68	14.91	11.4	8.16	14.5	13.64	7.99
	Portlandite (%)	5.98	5.98	5.27	2.99	6.69	5.56	2.99
	Calcite (%)	7.03	6.79	7.11	6.40	6.40	7.03	8.21

a. Portlandite content

It has been reported that the SCMs consumed portlandite through progressive of pozzolanic reaction. For this reason, a notable decrease of portlandite with time was found in SCMs containing specimens. Although it was discussed earlier that the reduction of portlandite may be affected by leaching, but the progressive of pozzolanic reaction in SCMs containing specimens is observed from a significant decrease in portlandite content compared to an ordinary cement mortar which can be observed at all healing age. Table 3.7 exposed that RB containing specimen was characterized by the lowest portlandite content, followed by RA and fly ash containing specimen. The mentioned phenomenal can be observed at all healing age. The outpacing in reduction is clearly noticeable when healing time increases. This evidence initially suggested that RB has the highest pozzolanic reactivity followed by RA and fly ash. At 91 days, RA20 and F20S4 healed either by water immersion or exposed to wet-dry conditions possess portlandite content of approximately 1% and 3% respectively which suggested that there still is a possibility for further pozzolanic reaction to take place. In contrast, almost 100% of portlandite was consumed in case of RB20, RA20S3 and RA20S4.

b. Calcite content

The results in Table 3.7 discloses that SAP containing specimens have roughly 2-3 times calcite content compared to that of non-SAP containing specimens at 0 day of healing. It is worth noting that the exposure

condition has effects on calcite formation behavior, considering the strong influences of leaching and hydrated productions wash out. The observed results are described below.

- Water immersion
  Most of specimens healed under water immersion showed an inconsistence trend of calcite formation pattern as a majority of non-SAP containing series demonstrated the highest calcite content at 56 days of healing which is slightly higher compared to that of 0 day while a decrease in calcite content was observed at 28 and 91 days. In contrast, SAP containing specimens have highest calcite content at 0 day before their calcite content gradually with time.

- Wet and dry exposure
  Specimens exposed to wet and dry exposure presented a decrease in calcite content after 0 day of healing before the calcite content gradually increase to reach the maximum value at 91 days of healing. It is observed that all specimens healed in wet-day expose have approximately 1-2% increase in calcite formation at 91 days of healing compared to the same type of specimens healed under water immersion at 91 days. This evidence is explained by Hills et al. and Chindasiriphan et al. [6,36] who proposed that carbonation can occurs faster in unsaturated pore environment which has relative humidity of 50-70%.

3.4.6 Microstructure analysis using SEM-EDS

The important microstructural changes were found in existence of SAP as the cement matrix is influenced by an initial swelling and the internal curing effect. Fig. 3.29-3.30 are examples of SAP images observed from cement matrix. The densification of cement matrix is observed meanwhile it can be seen that macro pores are isolated and presented through the initial swelling of SAP. SAP pores can be seen through dark black color, their sizes are approximately between 100-200 μm, depending on the size of swollen SAP. Lee et al. [10] suggested that the shape of SAP void is influenced by the original shape of SAP particles and the way in which it is confined by the cement matrix. This is in good agreement with the work of Snoeck et al. [37] who claimed that the collapsed SAP particles do not contribute to the load transfer, considering insufficient bonding between the particles and cement matrix. Therefore, they act like an ordinary air void. Although an increasing SAP replacement ratio enhances self-healing performance, but the total volume of macro pores also increases. This is in line with the study of Hasholt et al. [38] who mentioned that mechanical properties of cast-in SAP specimens are the offset between the improved microstructure and the increased porosity. Therefore, it should be emphasis that the usage of SAP as self-healing additive in cement mortar should be handle with great care.

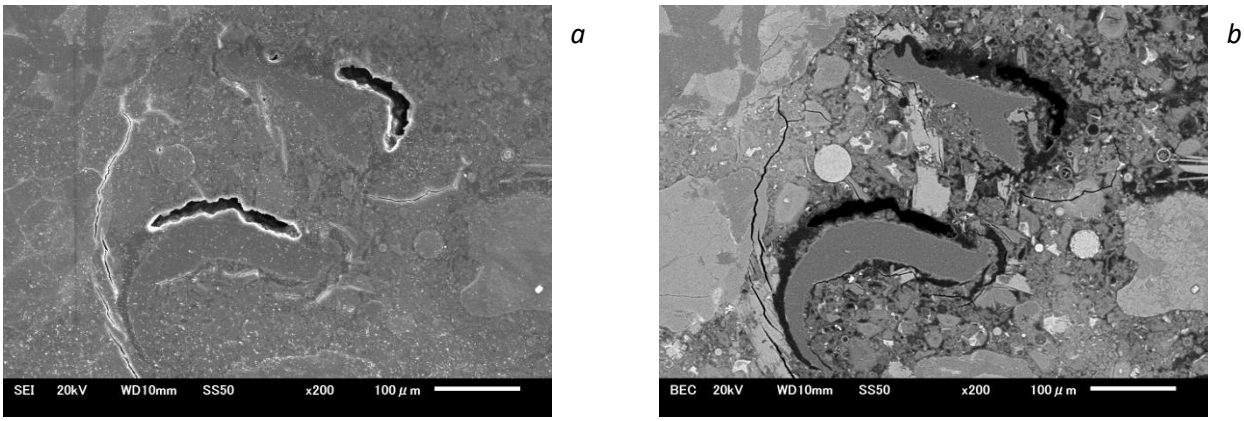

Fig. 3.29: Examples of (a) SEI and (b) BEC image demonstrate the location of SAPs and SAP pores.

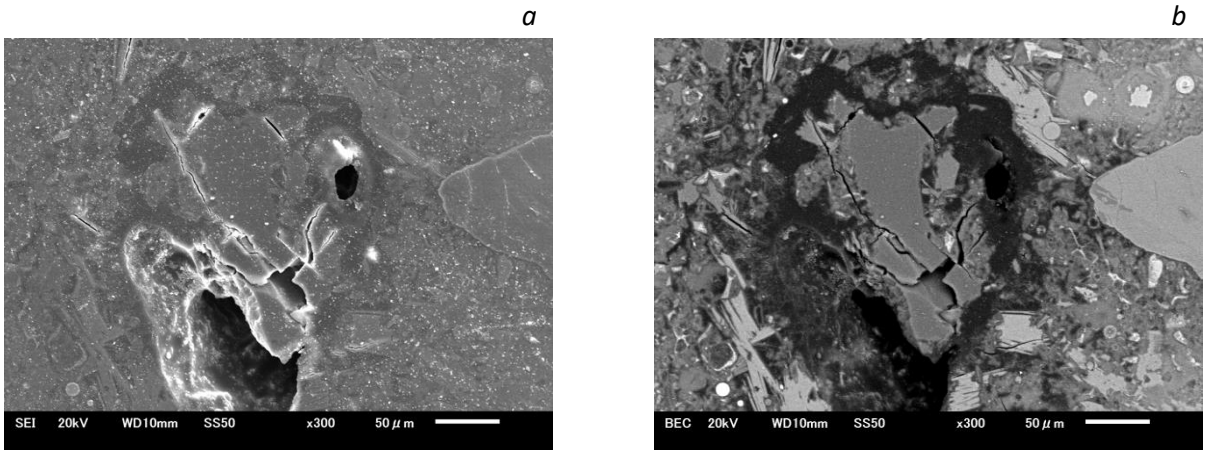

Fig. 3.30: Examples of (a) SEI and (b) BEC image demonstrate the location of SAPs and SAP pores.

SEM observations with EDS analyzer were used to identify the morphology and chemical compositions of the crack filling materials. Samples were collected from the healed crack boundary. Fig. 3.31 displays microstructure changes of F20S4 which was observed through the development of long needle shaped crystals, appeared to be ettringite. Therefore, it seems reasonable that specimen containing high calcium fly ash showed a significant value of flow discharged through a crack reduction which attributed by expansions of some materials such as ettringite. It is supported by Hosoda et al. [39] claiming that ettringite precipitated inside the healed crack and it is generally observed at interface between the cement matrix and the crack boundary. The formation of ettringite is found to be associated with the formation of calcite as it acted as a nucleus for the deposition of calcite. Ettringite has a large bulk volume, which makes the development of ettringite effectively seals the crack and subsequently enhances the crack water tightness. The SEM results are in good agreement with the study of He et al. [40] who suggested that pozzolanic reaction of high calcium fly ash is remarkable through a significant amount of ettringite formation. High calcium fly ash system is characterized by three patterns associated with CH content; considering: (1) the fast increase due to hydration of free CaO, (2) the increase from the hydration of cement and (3) the consumption from the pozzolanic reaction.

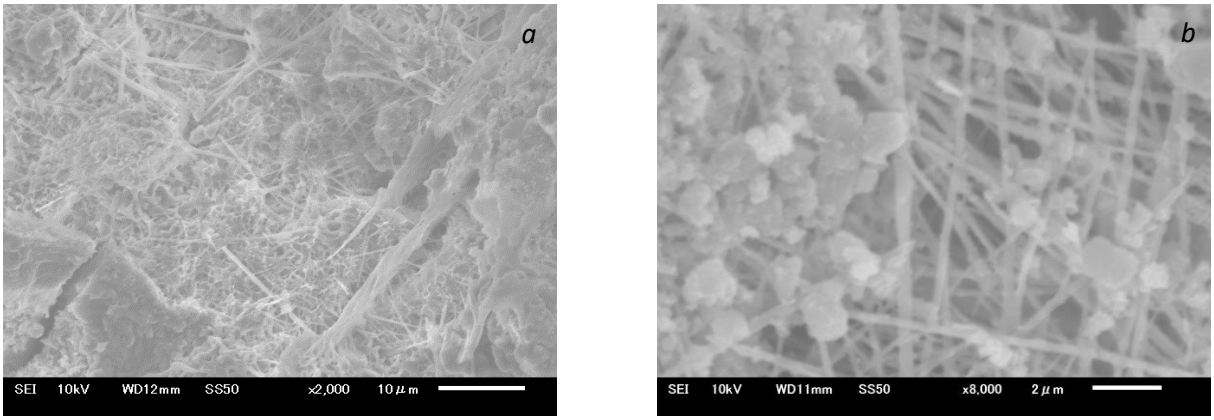

Fig. 3.31: SEM images demonstrate morphology of ettringite (a) magnification x2000 (b), magnification x8000

Fig. 3.32a demonstrates the fly ash particle after 91 days of healing. The new hydrated products emerging from the surface of fly ash particle was observed. Fig. 3.32b shows EDS results of the hydrated products, showing high amount of Ca, Si, Al, Mg and Fe. To identify hydrated products, the ratios of the main chemical elements such as Ca/Si, and Al/Si were estimated through polished specimens. This is because performing EDS directly onto rough surface materials yields a significant degree of uncertainties due to the refection and the absorbent effects of X-ray beam through dimensions in-depth. The Ca/Si ratio reviews a tendency of material stiffness as the lower value represents stiffer hydrated product. Fig. 3.33 shows that Ca/Si ratio of fly ash is estimated approximately 0.24. This value is significantly lower when compared to the averaged Ca/Si ratio of bulk area (1.9) obtained whereas Al/Si ratio is estimated approximately 0.64. This implied that self-healing products consist of C-S-H and other calcium-based materials. Papadakis [7] explained that high calcium fly ash is characterized by simultaneous pozzolanic and series of complex cementitious reactions. C-S-H is developed from the progressive of pozzolanic activities of the reactive silica that exists in high calcium fly ash. The early products include ettringite and tricalcium aluminate hydrate, and as time proceeds, converted into the most stable Ca-monosulfoaluminate and tetracalcium aluminate hydrates.

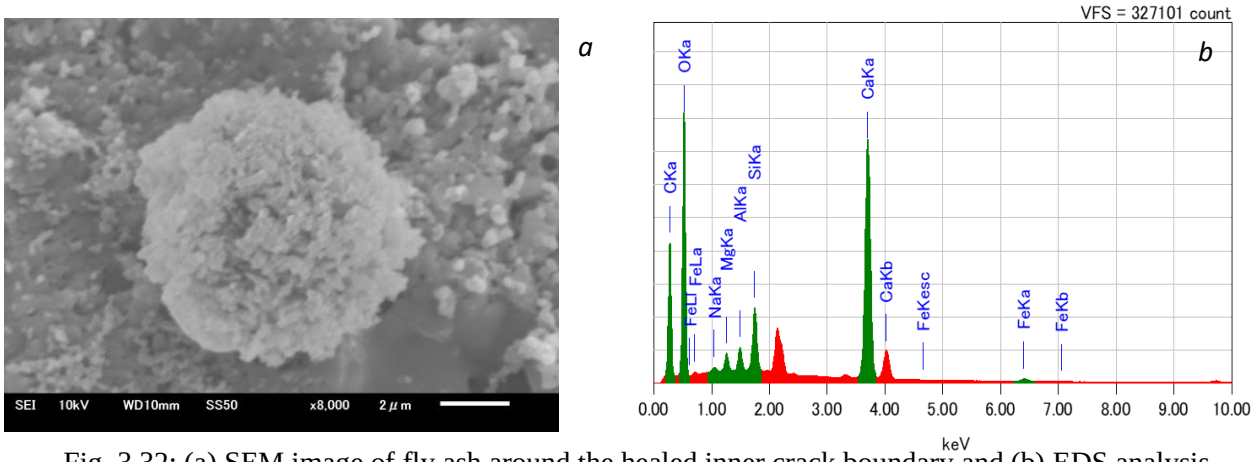

Fig. 3.32: (a) SEM image of fly ash around the healed inner crack boundary and (b) EDS analysis results around the healed inner crack boundary

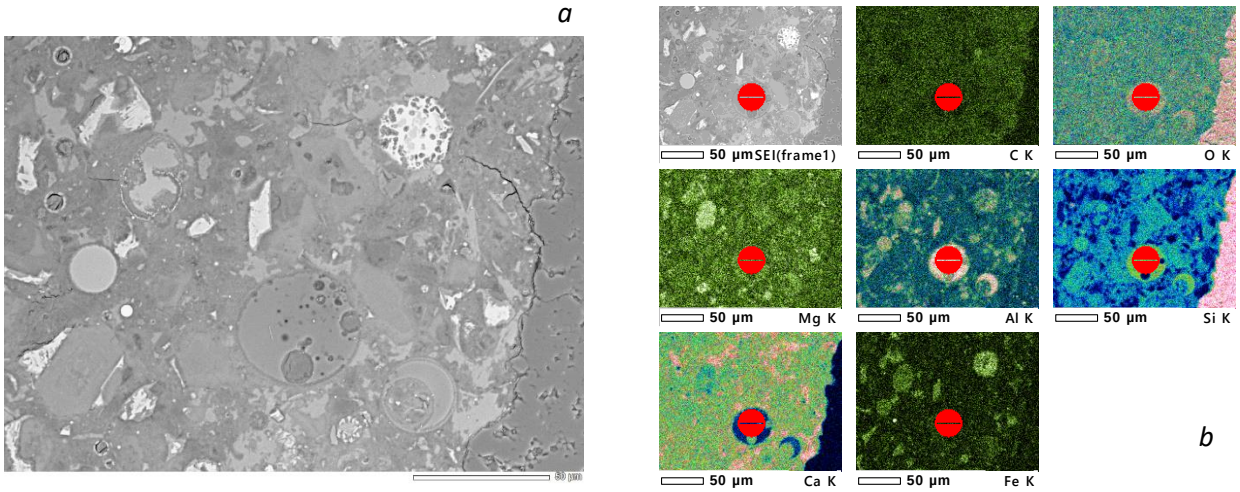

Analyzed element: C, K, Mg, Al, Si, Ca, Fe (reflection electron pattern)

Fig. 3.33: (a) BSE image and (b) elemental mapping images of the interface between the fly ash, aggregate and cement mortar

Fig. 3.34(a) shows an image of interface between the RB particles, aggregates and cement mortar of RB20 at 91 days of healing. It shows good bonding at the interfacial transition zone (ITZ) between cement paste and RB particles. By judging from textures and Ca/Si ratios as shown in Fig. 3.34(b), it appears that the typical RB particles can be identified as morphologies shown in Fig. 3.34(c). Fig. 3.34(b) demonstrates that silica is highly concentrated at RB boundary where is expected to be hydration products. The estimated Ca/Si ratio at RB boundary is estimated approximately 0.22 which is about 4 time lower compared to that of the averaged bulk area. In addition, hydration products of RB are approximately 7% richer in Si content compared to that of fly ash indicating the significant amounts of C-S-H formation is found in presence of RHA. These evidences supported by the results of ultrasonic pulse velocity recovery mentioned in section 3.4.4.b that pozzolanic reaction in RHAs is greater than fly ash because the hydration products possess significant amounts of C-S-H. The results are well supported by Van et al. [41] and Tuan et al. [23] who proposed that the absorbability of RHA induces Ca^{2+} from pore solution into RHA cellular space resulting in the enhancement of the pozzolanic reactivity. Van et al. [41] also suggested that the densification of ITZ between cement matrix at RHA boundary is achieved through the improvement of mesopores as they were filled with calcium and the products from pozzolanic reaction. The evidences show a great potential of RHAs to be used as self-healing additives in term of compressive strength recovery.

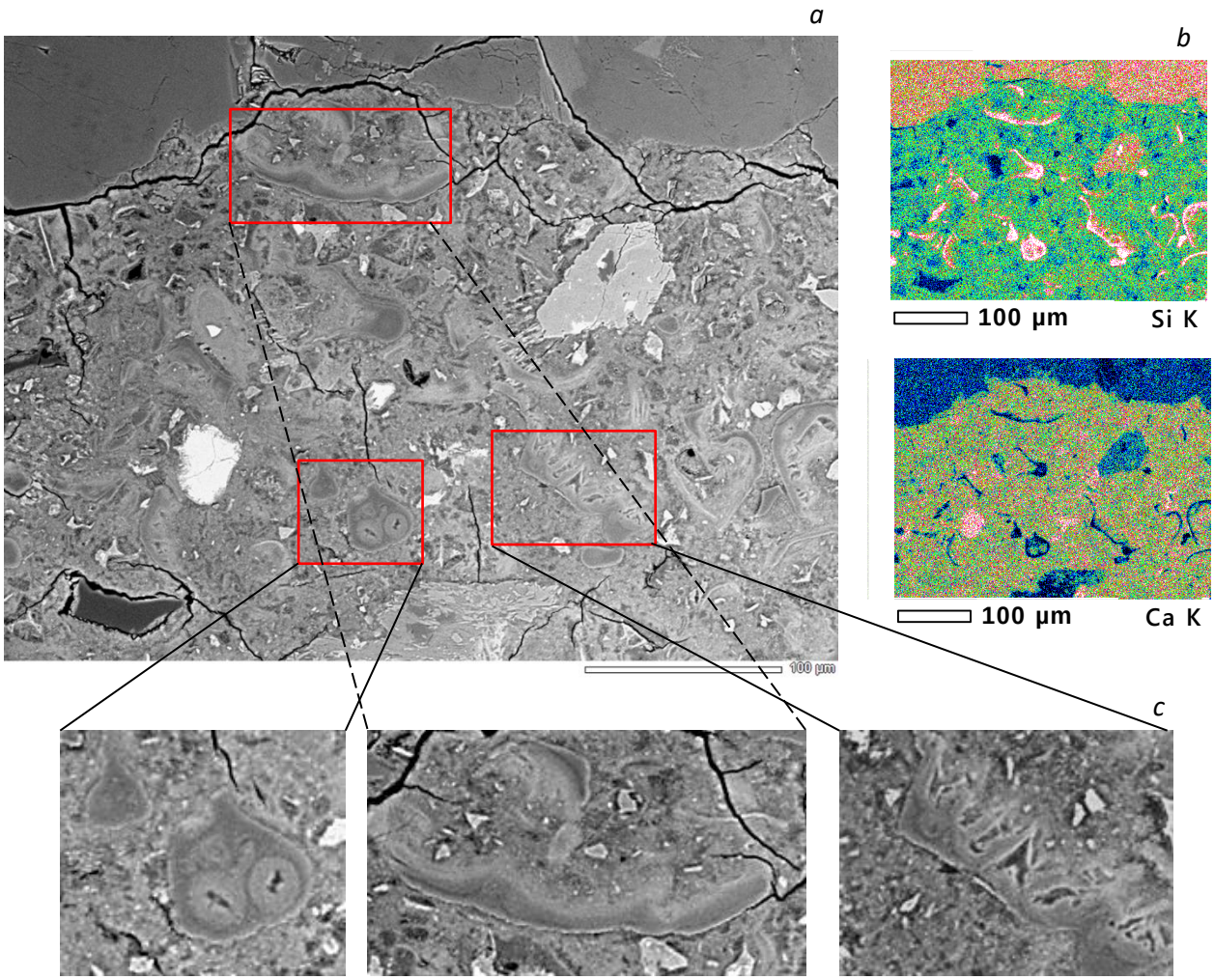

Fig. 3.34: (a) BSE image of interface between the RB particles, aggregate and cement mortar (b) EDS analyzed element: Si and Ca (reflection electron pattern) and (c) Typical images of RB particles

In term of water entraining effects, RHAs show better performance compared to SAP. Because the disadvantage of SAP is found to be associated with the effect of initial swelling which generates a reasonable volume of SAP pores and leads to the increase in the total porosity. As a result, it strongly exacerbates mechanical properties of cement mortar. Also, RHAs are more prominent considering the distribution of particles in cement matrix [41]. Thus, the comprehensive presence water reservoir minimizes uncertainty of self-healing system through comprehensive curing effect. However, the application of SAP to instantaneous mitigate crack permeability remains the most effective.

Fig. 3.35 shows an image of interface between aggregate and cement paste of F00 healed by water immersion at 91 days. Unhydrated cement was observed, indicating that self-healing due to hydration of cement paste remains possible if crack develops toward the unhydate location. However, due to small amount of the remaining, it is expected that the self-healing is limited up to the damage with sizes of microcracks.

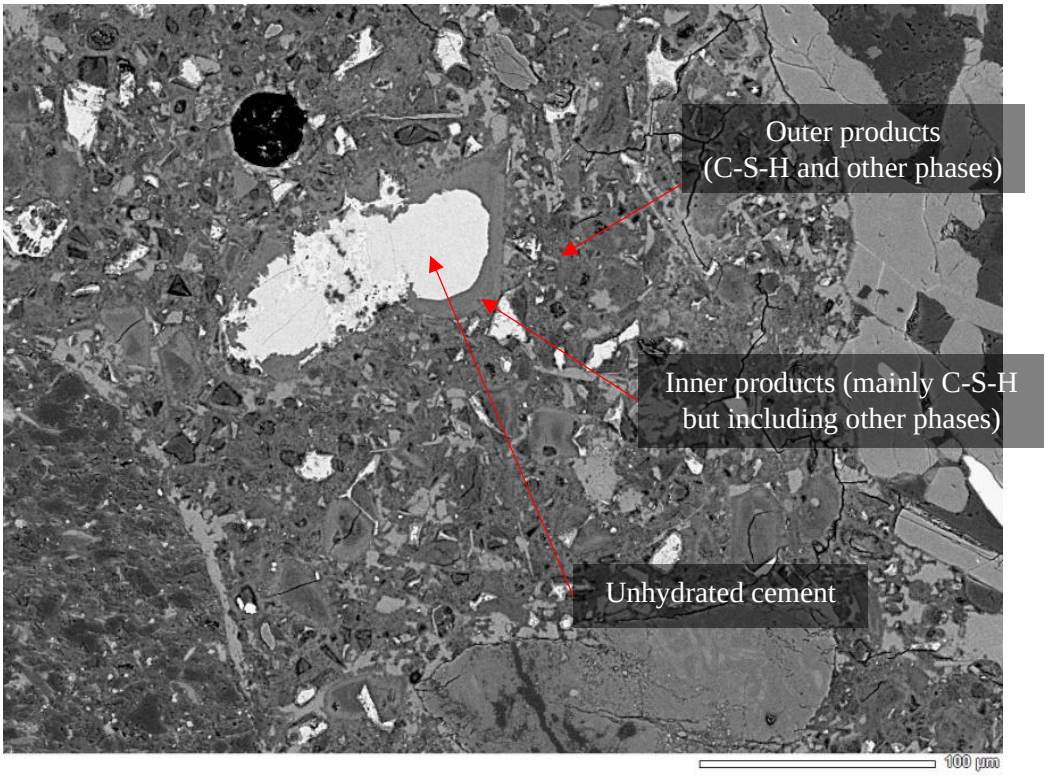

Fig. 3.35: BSE image of interface between aggregate and cement paste

3.5 CONCLUSIONS

This chapter investigated the coupling autogenous healing capacity of supplementary cementitious materials (SCMs) and superabsorbent polymer cement mortar system healed under two different environmental conditions: submerged in water or exposed to wet-dry cycles. Effects of fly ash and RHAs on self-healing performance were compared, considering the crack closure performance, the recovery of crack transportation properties and the recovery of ultrasonic pulse transition time. Microstructure changes and physicochemical processes incorporated with self-healing were studied using SEM-EDS and thermal analysis. From experimental results, the main conclusions are:

1. The use of RHAs as supplementary cementitious material (SCMs) greatly contributes to higher strength development compared to that of fly ash at all curing stages. This is due to RHAs contains a significant amount of reactive amorphous silica and effect of comprehensive internal curing.
2. Crack sealant effect of the swollen SAP is achieved instantaneously through water exposure which subsequently results in a significant initial flow reduction. The uncertainties in water flow through a crack during dry healing stage are mitigated by the existence of RHAs and SAP. This is because they act as water entraining admixture which discharge theirs absorbed moisture and liquid providing for unhydrate-particles.
3. The exterior of crack closure is found to be associated with the accumulation of calcium carbonate filling into the crack space which develops by either leaching or the reaction between dissolved $Ca(HCO_3)_2$ and either calcium hydroxide from the cement mortar or progress of carbonation. While SEM analysis shows that the interior of crack is filled with C-S-H, ettringite and calcium carbonate.
4. High calcium fly ash is characterized by a development of water-rich and pore- filling ettringite at early age which is subsequently converted to other hydrate products, generating a significant impact on self-healing performance associated with enhancing hydration, crack closure and a significant reduction of crack permeability. SEM analysis confirms that ettringite precipitated inside the healed cracks and it is generally observed at interface between the matrix and crack boundary. The formation of ettringite is found to be associated with calcite as it acted as a nucleus for the deposition of calcite. These effects are not clearly noticeable from RHAs.
5. RHAs containing specimens show slightly better transmitting time reduction compared to that of fly ash containing specimens. The better value implies to the higher degree of compressive strength recovery and microstructure changes associated with autogenous crack repair. This suggests that RHAs attribute to the formation of denser hydrated products, indicating that pozzolanic reaction in RHAs is probable greater compared to that of fly ash at later age. However, ettringite seems to be more effective than C-S-H in term of permeability reduction, considering its bulk volume.
6. Thermal analysis results at 91 days of healing confirm that RA20 and F20S4 healed either by water immersion or exposed to wet-dry conditions possess portlandite content of approximately 1% and 3% respectively. It is suggested that there is a possibility for further pozzolanic reactivity to take place. In contrast, almost 100% of portlandite is consumed in case of RB20, RA20S3 and RA20S4. The decrease in portlandite is governed by two reasons; (1) leaching and (2) being consumed by pozzolanic reactivity.
7. SEM-EDS analysis shows that hydrated products of RHAs tend to stiffer than hydrate products of fly ash, considering the lower value of Ca/Si ratio. The SEM-EDS results are in good agreement with the results of ultrasonic pulse velocity. The main hydrated product or RHAs appears to be C-S-H.

REFERENCES

[1] S.H. Kang, S.G. Hong, J. Moon, The use of rice husk ash as reactive filler in ultra-high performance concrete, Cem. Concr. Res. 115 (2019) 389–400. doi:10.1016/j.cemconres.2018.09.004.

[2] Z. He, L. Li, S. Du, Creep analysis of concrete containing rice husk ash, Cem. Concr. Compos. 80 (2017) 190–199. doi:10.1016/j.cemconcomp.2017.03.014.

[3] R.M. Ferraro, A. Nanni, Effect of off-white rice husk ash on strength, porosity, conductivity and corrosion resistance of white concrete, Constr. Build. Mater. 31 (2012) 220–225. doi:10.1016/j.conbuildmat.2011.12.010.

[4] V. Mechtcherine, E. Secrieru, C. Schröfl, Effect of superabsorbent polymers (SAPs) on rheological

properties of fresh cement-based mortars — Development of yield stress and plastic viscosity over time, Cem. Concr. Res. 67 (2015) 52–65.

[5] H.X.D. Lee, H.S. Wong, N.R. Buenfeld, Effect of alkalinity and calcium concentration of pore solution on the swelling and ionic exchange of superabsorbent polymers in cement paste, Cem. Concr. Compos. 88 (2018) 150–164. doi:10.1016/j.cemconcomp.2018.02.005.

[6] P. Chindasiriphan, H. Yokota, P. Pimpakan, Effect of fly ash and superabsorbent polymer on concrete self-healing ability, Constr. Build. Mater. 233 (2020) 116975. doi:10.1016/j.conbuildmat.2019.116975.

[7] V.G. Papadakis, Effect of fly ash on Portland cement systems. Part II. High-calcium fly ash, Cem. Concr. Res. 30 (2000) 1647–1654. doi:10.1016/S0008-8846(00)00388-4.

[8] C. Schröfl, V. Mechtcherine, M. Gorges, Relation between the molecular structure and the efficiency of superabsorbent polymers (SAP) as concrete admixture to mitigate autogenous shrinkage, Cem. Concr. Res. 42 (2012) 865–873. doi:10.1016/j.cemconres.2012.03.011.

[9] ASTM C 1437, Standard Test Method for Flow of Hydraulic Cement Mortar, ASTM International, West Conshohocken, PA.

[10] H.X.D. Lee, H.S. Wong, N.R. Buenfeld, Self-sealing of cracks in concrete using superabsorbent polymers, Cem. Concr. Res. 79 (2016) 194–208. doi:10.1016/j.cemconres.2015.09.008.

[11] H. Uchikawa, D. Sawaki, S. Hanehara, Influence of kind and added timing of organic admixture on the composition, structure and property of fresh cement paste, Cem. Concr. Res. 25 (1995) 353–364. doi:10.1016/0008-8846(95)00021-6.

[12] M.H. Zhang, K. Sisomphon, T.S. Ng, D.J. Sun, Effect of superplasticizers on workability retention and initial setting time of cement pastes, Constr. Build. Mater. 24 (2010) 1700–1707. doi:10.1016/j.conbuildmat.2010.02.021.

[13] Y. Maltais, J. Marchand, Influence of curing temperature on cement hydration and mechanical strength development of fly ash mortars, Cem. Concr. Res. 27 (1997) 1009–1020. doi:10.1016/S0008-8846(97)00098-7.

[14] P. Chindasiriphan, H. Yokota, Effect of fly asha and superabsorbent polymer on concrete carbonation, in: 16th East Asia-Pacific Conference on Structural Engineering & Construction, Brisbane, Australia, 2019.

[15] ASTM C 39, Standard test method for compressive strength of cylindricalcompressive specimens, ASTM International, West Conshohocken, PA.

[16] M. Roig-Flores, F. Pirritano, P. Serna, L. Ferrara, Effect of crystalline admixtures on the self-healing capability of early-age concrete studied by means of permeability and crack closing tests, Constr. Build. Mater. 114 (2016) 447–457. doi:10.1016/j.conbuildmat.2016.03.196.

[17] A. Colombo, M. Geiker, H. Justnes, R.A. Lauten, K. De Weerdt, The effect of calcium lignosulfonate on ettringite formation in cement paste, Cem. Concr. Res. 107 (2018) 188–205. doi:10.1016/j.cemconres.2018.02.021.

[18] L. Alarcon-Ruiz, G. Platret, E. Massieu, A. Ehrlacher, The use of thermal analysis in assessing the effect of temperature on a cement paste, Cem. Concr. Res. 35 (2005) 609–613. doi:10.1016/j.cemconres.2004.06.015.

[19] M. Henry, I.S. , Darma, T. Sugiyama, Cracking and chemical composition of cement paste subjected to heating and water re-curing, J. Adv. Concr. Technol. 14 (2016) 134–143. doi:10.3151/jact.14.134.

[20] E. Oniyama, P.G. Wahlbeck, Application of transpiration theory to TGA data : calcium carbonate and zinc chloride, Thermochim. Acta. 250 (1995) 41–53.

[21] M. Zajac, S. Hoock, C. Stabler, M. Ben Haha, Effect of hydration kinetics on properties of compositionally similar binders, Cem. Concr. Res. 101 (2017) 13–24. doi:10.1016/j.cemconres.2017.08.005.

[22] M.M. Younes, H.A. Abdel-Rahman, M.M. Khattab, Utilization of rice husk ash and waste glass in the production of ternary blended cement mortar composites, J. Build. Eng. 20 (2018) 42–50. doi:10.1016/j.jobe.2018.07.001.

[23] N. Van Tuan, G. Ye, K. Van Breugel, O. Copuroglu, Hydration and microstructure of ultra high performance concrete incorporating rice husk ash, Cem. Concr. Res. 41 (2011) 1104–1111. doi:10.1016/j.cemconres.2011.06.009.

[24] S.A. Zareei, F. Ameri, F. Dorostkar, M. Ahmadi, Rice husk ash as a partial replacement of cement in high strength concrete containing micro silica: Evaluating durability and mechanical properties, Case Stud. Constr. Mater. 7 (2017) 73–81. doi:10.1016/j.cscm.2017.05.001.

[25] H. Huang, X. Gao, H. Wang, H. Ye, Influence of rice husk ash on strength and permeability of ultra-high performance concrete, Constr. Build. Mater. 149 (2017) 621–628. doi:10.1016/j.conbuildmat.2017.05.155.

[26] A.S. Gill, R. Siddique, Durability properties of self-compacting concrete incorporating metakaolin and rice husk ash, Constr. Build. Mater. 176 (2018) 323–332. doi:10.1016/j.conbuildmat.2018.05.054.

[27] A.M. Neville, Properties of concrete, 5 ed., Pearson, London, UK, 2011.

[28] A A.M. Neville, Autogenous healing - a concrete miracle, Concr. Int. (2002) 76– 82.

[29] D. Snoeck, K. Van Tittelboom, S. Steuperaert, P. Dubruel, N. De Belie, Self-healing cementitious materials by the combination of microfibres and superabsorbent polymers, J. Intell. Mater. Syst. Struct. 25 (2014) 13–24. doi:10.1177/1045389X12438623.

[30] D. Snoeck, P. Van Den Heede, T. Van Mullem, N. De Belie, Water penetration through cracks in self-healing cementitious materials with superabsorbent polymers studied by neutron radiography, Cem. Concr. Res. 113 (2018) 86–98. doi:10.1016/j.cemconres.2018.07.002.

[31] N. Hearn, Self-sealing, autogenous healing and continued hydration: What is the difference?, Mater. Struct. 31 (1998) 563–567. doi:10.1007/BF02481539.

[32] M. Wu, B. Johannesson, M. Geiker, A review: Self-healing in cementitious materials and engineered cementitious composite as a self-healing material, Constr. Build. Mater. 28 (2012) 571–583. doi:10.1016/j.conbuildmat.2011.08.086.

[33] Y. Yang, E.H. Yang, V.C. Li, Autogenous healing of engineered cementitious composites at early age, Cem. Concr. Res. 41 (2011) 176–183. doi:10.1016/j.cemconres.2010.11.002.

[34] K. Van Tittelboom, N. De Belie, F. Lehmann, C.U. Grosse, Acoustic emission analysis for the quantification of autonomous crack healing in concrete, Constr. Build. Mater. 28 (2012) 333–341. doi:10.1016/j.conbuildmat.2011.08.079.

[35] T. Lee, J. Lee, Setting time and compressive strength prediction model of concrete by nondestructive

ultrasonic pulse velocity testing at early age, Constr. Build. Mater. 252 (2020) 119027. doi:10.1016/j.conbuildmat.2020.119027.

[36] T.P. Hills, F. Gordon, N.H. Florin, P.S. Fennell, Statistical analysis of the carbonation rate of concrete, Cem. Concr. Res. 72 (2015) 98–107. doi:10.1016/j.cemconres.2015.02.007.

[37] D. Snoeck, D. Schaubroeck, P. Dubruel, N. De Belie, Effect of high amounts of superabsorbent polymers and additional water on the workability , microstructure and strength of mortars with a water-to-cement ratio of 0 . 50, Constr. Build. Mater. 72 (2014) 148–157. doi:10.1016/j.conbuildmat.2014.09.012.

[38] M.T. Hasholt, M.H.S. Jespersen, O.M. Jensen, Mechanical Properties of Concrete with SAP Part I: Development of Compressive Strength, in: Inter. RILEM Conf. on use of superabsorbent polymer and other new additives in concrete, Copenhagen, Denmark, 2010, pp. 117 - 126.

[39] A. Hosoda, T. Higuchi, M. Eguchi, H. Yoshida, H. Aoki, Self Healing of Longitudinal Cracks in Utility Concrete Pole, J. Adv. Concr. Technol. 10 (2012) 278–284. doi:10.3151/jact.10.278.

[40] T. He, Y. Da, R. Xu, R. Yang, Effect of multiple chemical activators on mechanical property of high replacement high calcium fly ash blended system, Constr. Build. Mater. 198 (2019) 537–545. doi:10.1016/j.conbuildmat.2018.11.287.

[41] V.T.A. Van, C. Rößler, D.D. Bui, H.M. Ludwig, Rice husk ash as both pozzolanic admixture and internal curing agent in ultra-high performance concrete, Cem. Concr. Compos. 53 (2014) 270–278. doi:10.1016/j.cemconcomp.2014.07.015.

CHAPTER 4

EFEECT OF FLY ASH AND SUPERABSORBENT POLYMER ON CONCRETE CARBONATION

- General background
- Long-term risk and benefit of SAP for use in fly ash mixed concrete
- Carbonation resistance of mortar in existence of fly ash and SAP

4.1 INTRODUCTION

Concrete structures lose their integrity and durability by cracking. Cracks in concrete structures are generated through many mechanisms such as excessive stresses from the external loading, shrinkage of concrete, and physiochemical reaction of concrete constituent materials. Cracks in concrete serve as a pathway to decrease resistance to carbonation and chloride ion penetration. To prevent cracking and enhance durability of concrete, many studies have focused on using superabsorbent polymer (SAP) as an admixture. Superabsorbent polymer (SAP) is a multipurpose water-entraining agent, which is a cross-link polymer designed to absorb high amount of fluid. Therefore, SAP helps to mitigate autogenous shrinkage in concrete, including its applications to mitigate frost damage and enhance self-healing capability. In self-healing application, SAP spontaneously swells and forms a watertight gel when it is exposed to water. Swollen SAP could seal up a small crack and facilitate cement hydration in the damage areas. In contrast, SAP initial swelling generates SAP pores that potentially be a bypass allowing harmful agents to penetrate into concrete. Fly ash has been used in concrete as a cement replacement admixture which allows cement manufacturers to commit to sustainable construction strategy by lowering energy and carbon footprints in built environments. Pozzolanic reaction in fly ash greatly enhances the self-healing performance that results from the development of newly formed C-S-H products. The coupling effects of SAP and fly ash on concrete self-healing ability are well discussed in Chapter 2 and 3. However, the decline of portlandite content is generally found in fly ash concrete that is associated with the progressive of pozzolanic reaction, which inevitably results in the tendency of alkalinity reduction.

Despite their benefits, carbonation resistivity may decrease in concrete mixed with fly ash and SAP. Carbonation is a primary concern for durability of concrete structures as it reduces concrete pH, and subsequently deactivates a protective passive film on the surface of rebar. To evaluate the long-term risk and benefit of SAP for use in fly ash mixed concrete, this chapter investigates the risk of carbonation of self-healed concrete mixed with fly ash and SAP. Experimental tests were conducted in which cement mortar was cast with varying fly ash and SAP replacement ratio. A crack was induced by a mechanical load. The cracked specimens were cured in water and stored in air for 2 years. Carbonation resistance was evaluated by carbonation depth measurement and thermogravimetric/differential thermal analysis. It was found that carbonation resistivity is decreased in self-healed concrete mixed with fly ash and SAP.

4.2 METHODOLOGY

The experimental test was conducted using cement mortar specimens. The chemical compositions of cement and fly ash are presented in Table 4.1, and the specific information of the SAP is given in Table 4.2. Ordinary Portland cement (OPC) and fly ash type F according to ASTM C618 [1] were premixed along with sand and SAP for 2 minutes. The premixing was carried out to obtain a uniform distribution of materials and decrease the potential of an adhesive effects of swelling SAP. Water was then added, and continually mixed at a medium speed for 3 minutes. The SAP mixtures were designed at different replacement ratios of 1, 2, 3 and 4 % by weight of cement, and fly ash contents were 0 and 25 % by weight of cement. The designed mix proportions are given in Table 4.3. The specimens were prepared using the method explained in Chapter 2 and 3.

For the self-healing capability test, a control crack of 0.2±0.1 mm wide was induced in the specimen by a splitting tensile load. The splitting loads range of 19-30 KN were used to generate a control crack width. Then, the cracked specimens were self-healed in water for 28 days. After the evaluation of self-healing capability, the specimens were stored in dry laboratory environment for 2 years. The results of self-healing capability were reported in the work of Chinadasiriphan and Yokota [2].

Table 4.1: Chemical compositions of cement and fly ash.

Chemical composition (mass%)	Cement	Fly ash
Silicon dioxide (SiO_2)	21.2	55.4
Aluminum oxide (Al_2O_3)	5.2	25.9
Ferric oxide (Fe_2O_3)	2.8	3.7
Calcium oxide (CaO)	64.2	4.1
Magnesium oxide (MgO)	-	0.4
Sulfur trioxide (SO_3)	2.0	0.7
Alkalis (Na_2O)	0.65	-
Chlorine (Cl)	0.004	-
Sum (SiO_2+ Al_2O_3+ Fe_2O_3)	29.2	86.0

Table 4.2: Properties of SAP

Material	Apparent density (g/cm^3)	Water absorption (g/g)
SAP	0.7	417

Table 4.3: Mix proportions of mortar

Specimen	Cement (kg/m^3)	Fly ash (kg/m^3)	Water (kg/m^3)	Sand (kg/m^3)	SAP (mass% cement)
F00	525	-	237	1459	-
F00S1	525	-	237	1459	1
F25	394	131	237	1459	-
F25S1	394	131	237	1459	1
F25S2	394	131	237	1459	2
F25S3	394	131	237	1459	3
F25S4	394	131	237	1459	4

4.2.1 Carbonation depth measurement

The carbonated region is referred to the area that the concrete high alkalinity has been neutralized by CO2. The carbonation depth can be identified by using phenolphthalein solution which changes red/pink for uncarbonated concrete and remain colorless for carbonated concrete (pH < 9) (Hills et al. 2015). The self-healed specimens were cut into two pieces perpendicular to the crack. One specimen produced 2 half circular prisms. Then the phenolphthalein solution was sprayed onto the cut area at the time of the extraction. The determination of carbonation front was made using the two parameters: dc and ds, where dc and ds denote for the averaged carbonation depth from the cracked zone inside the core of healed crack

and that from the specimen surface, respectively. These measurements were done at 4 locations as presented in Fig. 4.1.

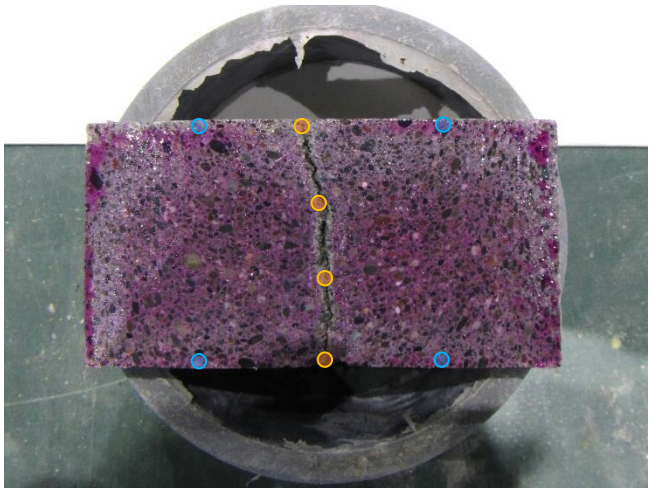

Fig. 4.1: Measurement locations of d_c (orange) and d_s (blue)

4.2.2 Service life prediction model

The carbonation depth is governed by diffusion of carbon dioxide that occurs through concrete's pore structure. The diffusion rate is influenced by many parameters such as concrete permeability, temperature, moisture content and CO_2 concentration. It was specified in the JSCE Standard Specifications for Concrete Structure (2017) that the prediction of carbonation can be made according to Fick's first law.

$$x = k\sqrt{t} \tag{1}$$

where x represents the carbonation depth (mm), t represents the period of carbonation (year) and k represents the coefficient of the rate of carbonation ($\mathrm{mm}/\sqrt{\mathrm{year}}$)

4.2.3 Thermogravimetric/Differential Thermal Analysis

The influence of fly ash and SAP on carbonation of self-healed concrete was investigated by thermogravimetric/differential thermal analysis (TG/DTA). The extracted powder sample was immersed in acetone to terminate cement hydration, before oven dried at 50 °C for 24 hours and stored in the desiccator to minimize carbonation effects. The powder sample was heated at a constant heating rate of 10 °C/min until reaching 1000 °C under a controlled nitrogen (N_2) atmosphere.

The high alkalinity of concrete is due to the presence of portlandite ($Ca(OH)_2$) produced by the solid phase of cement gel. Carbonation occurs with the reaction between the dissolved CO_2 and portlandite, which produces calcite ($CaCO_3$). Through the TG/DTA analysis, the quantity of portlandite was determined through mass change at approximately 400-500 °C while the amount of $CaCO_3$ was calculated at approximately 501-900 °C Alarcon-Ruiz et al. [4] and Harilal et al. [5] found the relation between mass lost and molecular mass of decomposed products as given in Eqs. (2) and (3).

$$\mathrm{CH}(\%) = M_1 \times \frac{M_{(\mathrm{CH})}}{M_{(\mathrm{H_2O})}} \tag{2}$$

where M_1 is the mass loss due to dehydration, $M_{(CH)}$ is the molecular mass of portlandite and $M_{(H_2O)}$ is the molecular mass of water.

$$\mathrm{CaCO_3}(\%) = M_2 \times \frac{M_{(\mathrm{CaCO_3})}}{M_{(\mathrm{CO_2})}} \quad (3)$$

where M_2 is the mass loss due to decarbonation, $M_{(\mathrm{CaCO_3})}$ is the molecular mass of $CaCO_3$ and $M_{(\mathrm{CO_2})}$ is the molecular mass of CO_2.

4.3 RESULTS AND DISCUSSIONS

4.3.1 Effect of admixtures on compressive strength of mortar

Table 4.4 presents the results of the averaged compressive strengths. It is noticeable that the main material which interfered compressive strength development is fly ash. At the 28 days of curing, F25 exhibited approximately 34.84% lower strength compared to F00, indicating that pozzolanic reaction in tested fly ash is inactive at the early age. Indeed, long-term strength under the development of pozzolanic reaction is expected to be greater than that of ordinary mortar as pozzolanic reactivity is progressive with age. Meanwhile, it was observed that SAP shows an insignificant effect on the mortar compressive strength. In presence of SAP, F00S1 is subjected to strength reduction of 1.28% compared to F00. However, a slight increase in compressive strengths was found among fly ash and SAP containing specimens (F25Sx). Hasholt et al. [6] reported that, at the right replacement ratio, SAP can enhance the compressive strength due to its ability to increase the degree of hydration and prevent microstructure's damage caused by self-desiccation. On the other hand, SAP also decreases the strength of mortar because of the formation of SAP voids.

Table 4.4: Compressive strengths at 28 days.

Specimen	Compressive strength			
	f'_c (MPa)	SD (MPa)	%CV	$\triangle f_c$ %
F00	55.4	0.35	0.63	-
F00S1	54.7	1.61	2.94	-1.28
F25	36.1	3.03	8.41	-34.84
F25S1	31.1	1.01	3.24	-43.75
F25S2	35.0	0.96	2.74	-36.76
F25S3	37.3	1.75	4.69	-32.64
F25S4	36.2	2.28	6.30	-34.69

4.3.2 Carbonation depth

The carbonation depths measured are illustrated in Fig. 4.2. The averaged carbonation depth from the surface of the specimen (d_s) was largest in F25S1, followed by F00 and F25S4. The carbonation depths of F00S1, F25, F25S2 and F25S3 were small. Therefore, mixing fly ash and SAP in mortar does not have a significant effect on the carbonation resistivity of mortar. In contrast, the averaged carbonation depth at the cracked zone (d_c) demonstrates the positive effect of fly ash and SAP on the carbonation resistivity as the carbonation depths decreased with increase in the SAP replacement ratio. This is in good agreement with the authors' previous study [2], in which they reported that concrete self-healing performance increases with increase in the SAP replacement ratio which results in the recovery of concrete permeability. It is found

that the permeability reduction is facilitated by SAP's ability to release water in the cracked area, which consequently results in crack closure and densification of concrete pore structures due to a further hydration. Therefore, it worth mentioning that crack closure due to self-healing showed a positive effect on carbonation depth mitigation.

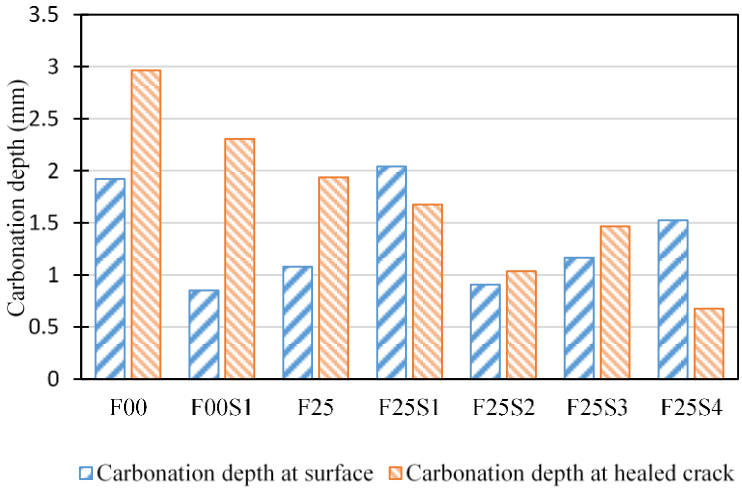

Fig. 4.2: Carbonation depth of mortar specimens

4.3.3 Service life prediction

The carbonation resistance is determined by the carbonation coefficient, k as defined in Eq. (1). *k* can be determined once the carbonation depths at the specific time are obtained. d_s and d_c for 20 years were predicted to determine the minimum concrete cover for avoiding rebar corrosion. The results are shown in Fig. 4.3. Predicted d_s at 20 years were approximately 2.7-6.0 mm, and dc reaches 9.4 mm (maximum) in F00 and 2.2 mm (minimum) in F25S4.

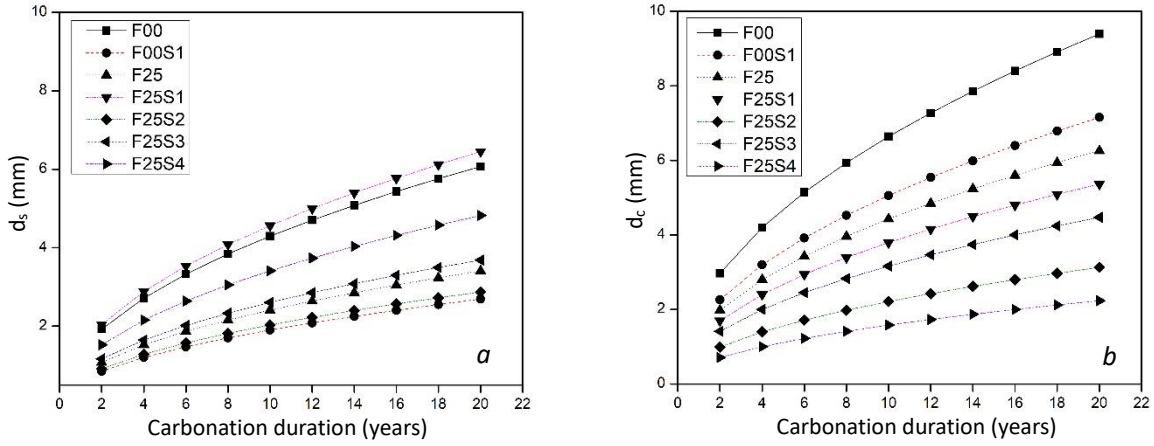

(a) d_s (b) d_c

Fig. 4.3: Carbonation depths predicted until 20 years

Although it is well known that a crack degrades concrete permeability and leads to the decrease of carbonation resistance. However, the predicted d_c at 20 years was not significantly large at the healed crack area. It was also found that d_c decreases with increase in the SAP replacement ratio. In contrast to this, SAP had no apparent effect on concrete permeability at the surface of concrete. It is predicted that SAP improves

the long-term carbonation resistance at the cracked area, whereas SAP has an insignificant effect on the long-term carbonation resistance at the uncracked area. Therefore, it is expected that SAP pores produced during an initial swelling period are not connected each other and have no significant influence on the permeability of mortar. In addition, extra water was not added to compensate the water absorbed by SAP during the fresh stage of mortar. It means that the tendency of decreasing an effective w/c ratio is found in the mortar with the higher SAP replacement ratio. As a consequence, the number of capillary pores of mortar with high SAP contents is expected to be lower than those with the low SAP contents. As a result, the potential of carbon dioxide infiltration into sound concrete is inferior. To understand the relationship between carbonation resistance and the contents of SAP and fly-ash, the information on specimens' pore structure needs to be investigated in the future.

4.3.4 Evaluation of carbonation by thermal analysis

The results of derivative thermogravimetric curve (DTG) and % weight loss are shown in Fig. 4.4. In Fig. 4.4(a), several materials can be determined by analysing mass change observed through the different peaks. This study mainly investigated the derivative of mass which occurs at approximately 450 °C and 600-800 °C as they represent dehydroxylation and decarbonation reactions. The mass change of F00 is clearly noticeable at approximately 450 °C, which denotes that the significant amount of portlandite is found. In contrast, the reduction of portlandite content is found to be associated with the presence of fly ash, which potentially results in the tendency of pH drop. It was reported by many studies that portlandite is produced due to the process within cement hydration while pozzolanic reaction from fly ash reacts to consume portlandite producing calcium silicate hydrate (C-S-H).

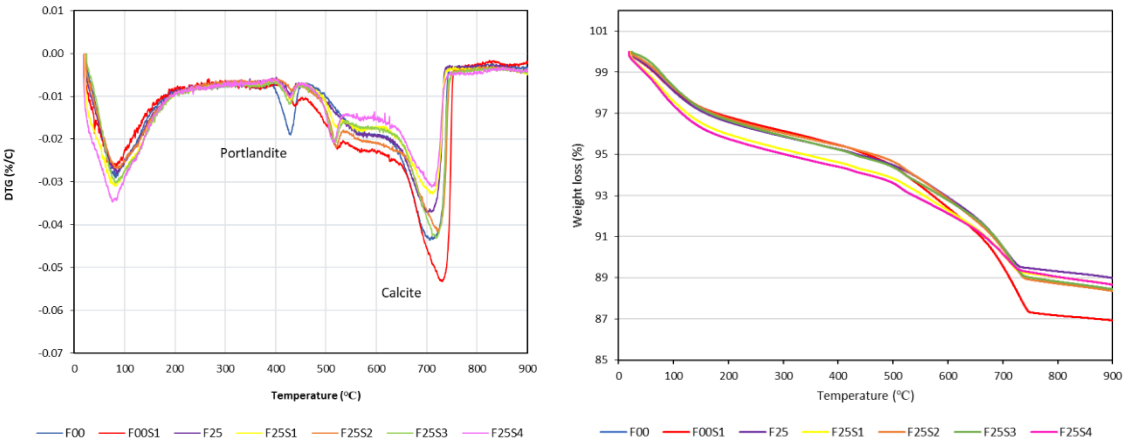

(a) DTG curves for portlandite and calcite (b) TGA curves for powder fired to various temperature regimes

Fig. 4.4: Result of TG/DTA.

It is interesting to note that the portlandite content of F00S1 is lower than that of the reference specimen (F00), and the calcite content of F00S1 was considerably higher than that of F00. As shown in Fig. 4.4(b), F00S1 shows a great mass loss at the temperature range of 650-750 °C which was caused by the decomposition of calcite. This draws an attention to the influence of SAP on carbonation acceleration. In contrast, specimens in F25Sx series show no significant gain in calcite content compared with F00S1. In F25Sx series, it is assumed that portlandite is the control reactant. Once portlandite is consumed by fly ash, carbonation progress is restrained due to absent of coupling substrate. However, specimens are encountered with pH reduction through the pozzolanic reaction of fly ash.

The results of quantitative analysis on portlandite and calcite contents are shown in Fig. 4.5(a), whereas the amount of chemically bound water is shown in Fig. 4.5(b). The chemically bound water is recognised as the water that chemically bonded into the structure of hydrates. The chemically bound water can be used to

determine the degree of hydration. The results show that the change in chemically bound water is related to the fly ash and SAP contents that lead to a higher value of chemically bound water.

(a) Contents of portlandite and calcite (b) Contents of chemically bound water

Fig. 4.5. Quantitative analysis results of cement powder

In consideration of the pozzolanic reaction, the reduction of portlandite in fly ash containing specimens is reflected with increase in bound water, which indicates that the main hydrated product is expected to be C-S-H. In case of SAP mortar, there is no clear evidence that shows any chemical reaction related to SAP and the increase of bound water. However, the effect of SAP on promoting internal curing which further improves the degree of hydration is profound. The change in chemically bound water gives a brief overview on phase transformation among hydrate products which tentatively shows the increase in the C-S-H content.

4.4 CONCLUSIONS

In this chapter, the effect fly ash and SAP on carbonation of self-healed mortar was focused using phenolphthalein indicator and thermal analysis technique. The progress of carbonation within 20 years was predicted in terms of the carbonation depth. The thermal analysis allows to quantify portlandite and calcite contents through materials decomposition which occurs at the elevated temperatures. The conclusions are summarized as follows:

1. The compressive strength development of mortar at 28 days was interfered by fly ash which resulted in approximately 34.8% lower than that of non-fly ash containing mortar. In contrast SAP had an insignificant effect on compressive strength.
2. There is no noteworthy systematic difference in the averaged surface carbonation depths between specimens mixed with fly ash and SAP.
3. The carbonation depth at the cracked area showed the evidence that durability of specimens is enhanced as increase in the SAP replacement ratio.
4. Mortar containing fly ash shows the limited potential for mitigating carbonation due to absent of portlandite but is inevitably encountered with alkalinity reduction as portlandite is consumed by pozzolanic activities.
5. The rate of carbonation is increased with the presence of SAP.

REFERENCES

[1] American Coal Ash Association, Fly Ash Facts for Highway Engineers, (2003). https://www.fhwa.dot.gov/pavement/recycling/fach00.cfm (accessed April 8, 2020).

[2] P. Chindasiriphan, H. Yokota, Self-healing ability of concrete made with fly ash and superabsorbent polymer, in: 2nd ACF Symp. 2017 Innovation of Sustainable Concrete Structures, Chiang Mai, Thailand, 2017.

[3] Japan Society of Civil Engineers, Standard specifications for concrete structures - "Maintenance", Japan Society of Civil Engineers (JSCE), Tokyo, Japan, 2007.

[4] L. Alarcon-Ruiz, G. Platret, E. Massieu, A. Ehrlacher, The use of thermal analysis in assessing the effect of temperature on a cement paste, Cem. Concr. Res. 35 (2005) 609–613. doi:10.1016/j.cemconres.2004.06.015.

[5] M. Harilal, V.R. Rathish, B. Anandkumar, R.P. George, M.S.H.S. Mohammed, J. Philip, G. Amarendra, High performance green concrete (HPGC) with improved strength and chloride ion penetration resistance by synergistic action of fly ash, nanoparticles and corrosion inhibitor, Constr. Build. Mater. 198 (2019) 299–312. doi:10.1016/j.conbuildmat.2018.11.266.

[6] M.T. Hasholt, M.H.S. Jespersen, O.M. Jensen, Mechanical Properties of Concrete with SAP Part I: Development of Compressive Strength, in: Inter. RILEM Conf. on use of superabsorbent polymer and other new additives in concrete, Copenhagen, Denmark, 2010, pp. 117 - 126.

CHAPTER 5

CONCLUSIONS AND FUTURE WORKS

5.1 CONCLUSIONS

This chapter summarizes the conclusions on how supplementary cementitious materials (SCMs) and SAP contribute to the self-healing ability of concrete. The benefits of both materials were discussed on the mechanical properties, the crack closure performance, the recovery of concrete permeability and the microstructure changes associated with the progressive of self-healing. Drawbacks and limitations of self-healing additives on physical properties and microstructure developments were assessed, considering rheological behavior, compressive strength and carbonation resistivity. The following conclusions can be drawn.

1. The use of RHAs as supplementary cementitious material (SCMs) develops the higher degree of strength development compared to that of fly ash at all curing stages. This is due to RHAs contain significant amount of reactive amorphous silica and the effect of comprehensive internal curing.

2. RHAs and SAP reduce workability because of the absorption of free water in the concrete system. The adhesive effect is found to be associated with swollen SAP which further degenerates the rheological properties. The initial absorbency of SAP can be suppressed by adding concentrated Ca^{2+} to the concrete mixing solution, as it binds to the carboxylic groups in acrylate chains of SAP which leads to the desorption of stored liquid.

3. The initial water discharge is significantly lower for the SAP-containing specimens than that for the non-SAP specimens. The crack sealing mechanism for the SAP-containing specimens is promoted by the formation of an impermeable gel that expands to seal an opening crack which occurs instantaneously after the SAP is exposed to water.

4. In dry healing stage, the RHAs and SAP function as water reservoir which facilitates self-healing activities by discharging theirs absorbed moisture and liquid providing for unhydrate-particles.

5. Increasing the SAP replacement ratio improves the crack sealing performance, as characterized by greater crack-widening mitigation and water discharge reduction resulting from extensive moisture supply from the SAP. Although, the SAP greatly accelerates carbonation activities which enhances self-healing performance by introducing a higher degree of calcium carbonate deposition along the open crack compared to non-SAP containing specimens. The carbonation depth at the cracked interface is found to decrease with increase crack closure performance.

6. Fly ash with a high calcium content shows the potential to achieve the higher SAP replacement ratio in mix proportions. In addition, high calcium fly ash significantly decreases crack water tightness by producing high bulk volume products such as pore- filling ettringite at early age, which is subsequently converted to other hydrate products, generating a significant impact on self-healing performance associated with enhancing hydration, crack closure and a significant reduction of crack permeability. The formation of ettringite further induces calcite formation as it acts as a nucleus for the deposition of calcite. These effects are not clearly noticeable from RHAs.

8. Long-term self-healing ability of concrete is enhanced through the crack closure which is found to be associated with the development of permanent self-healing products. Calcium carbonate is found in significant amounts around the surface and outer region of the healed specimens. The crack interior of cast-in fly ash specimens is filled with high amount of ettringite, calcium carbonate and lower amounts of C-S-H whereas the crack of cast-in RHAs specimens is filled with significant amounts of C-S-H. This is confirmed by the results of Ca/Si ratio and the recovery of ultrasonic pulse velocity suggested that RHAs attribute to the formation of denser hydrated products. It is implied that self-healing associated with RHAs

are superior than fly ash in terms of strength recovery, while fly ash shows better performance in permeability recovery.

5.2 FUTURE WORK

As stated in the research motivations, this study attempts to embrace sustainability goals by developing concretes in possession of environmentally responsible and resource-efficient throughout a structure's lifecycle considering engineering, social and economic aspects. The concept of applying self-healing capabilities that can reduce maintenance cost and time is still novel but has enormous potential. Therefore, the following extension work should be considered.

Economic aspects

To tackle budgetary constraints and reduce life cycle cost of concrete structures, it would be interesting to further evaluate on cost-benefit analysis of self-healing concrete made with supplementary cementitious materials (SCMs) and SAP in the future which should be carried out along the evaluation of self-healing performance on the real environmental exposure conditions.

Engineering aspects

Despite versatility and performance, without a proper mix proportion design, the usage of either RHA or SAP as supplementary self-healing materials can generate enormous negative effects toward concrete properties. For examples, the usage of SAP in the RHA mixed concrete generally found to be associated with a significant rheological behavior variation as both materials withdraw free water from the mix. The effects of initial swelling and the absorbency of SAP during mixing stage are the weakest points in the cementitious matrix which will strongly decrease both rheological and hardening properties of concrete such as; accounting for an increase in the total porosity. Initially the workability issues are solved by adding extra water to compensate the amount of uptake water, still, it inevitably results in the increasing in the water-to-binder ratio and subsequently lead to the decrease in compressive strength and concrete density. Although, the method of using high calcium oxide content fly ash to restrain the initial absorbency of SAP was proposed in chapter 2, it is moderately effective to enhance rheological and hardening properties of cement mortar and enable mix proportions to achieve higher SAP replacement ratios. However, it is reasonable to believe that the initial swelling of SAP should be minimized at greatest degree possible throughout the mortar fresh stage. This potentially allows the mix proportion to achieve higher self-healing performance without disadvantages in hardening properties. Also, this leads to our proposal to investigate for the more effective method to suppress the initial swelling of SAP such as applying a temporary water-repellent coating for the SAP in the future works.

Social and Environmental aspects

In the recent year, sustainability issues are becoming more and more relevant to any human activities. For the long-term goals, sustainable development indicators incorporated with a relevant multicriteria analytical framework should be established to evaluate, monitor and report on future progress of self-healing concrete structures. This idea would enable the structure stakeholders to make decision on how self-healing concrete structures perform in accordance with UN 17 sustainable development goals (SDGs). This area has a great potential to be investigated in order to resolve challenges of construction and its related industries, reducing negative impacts toward the environment. Although this area of research is not directly related to the area of the current study, the authors are more than happy to seek for a collaboration and provide data relevant to the engineering aspects.